# Dielectric Relaxation Analysis to Assess the Integrity of High Voltage DC Cables of the Mass Impregnated Type

Barry Lennon
1293923

**Master of Science Thesis, 2009**
**HV Components and Power Systems**
**TU Delft, The Netherlands**

# Abstract

This thesis is an in-depth resource for information concerning *High Voltage Direct Current (HVDC)* power transmission. The far reaching effects from faults arising in HVDC cable systems are noteworthy and from this perspective a broad literature review is dedicated to insulation monitoring techniques. The analysis is further subcategorised into *on-site* and *off-site* solutions and some existing, operational systems are discussed.

Furthermore, the experimental aspect to this work uses *dielectric relaxation analysis* to assess the integrity of *Mass Impregnated* HVDC cables. This off-site analysis technique investigates insulation samples using *broadband dielectric spectroscopy*. It is here proposed that the resulting dielectric relaxation characteristics can be compared to a database of pre-existing spectra as a means to determining the condition of the insulation under investigation.

The introductory chapter to this thesis work begins with an account of direct current power transmission in a historical context, from its foundations in the 1880's to the present day, where HVDC transmission systems are dotted throughout the globe.

The pioneering research which sparked this *renaissance* has its foundations in Sweden in the 1930's. This very work heralded the first HVDC transmission line between the island of Gotland and the Swedish mainland in the 1950's. A milestone in electrical energy transmission, this was evidently the harbinger for a technology that is now growing from strength to strength.

In the same chapter, electrical insulation is discussed with respect to the integrity of operational cable systems. This analysis explores the behavior of insulation under operational stress and relates observable phenomena to the material physics of the insulation.

Furthermore, the principles of dielectric relaxation analysis are introduced as a sophisticated approach to assess the integrity of cable insulation. This is an important focal point in this work as mentioned above since broadband dielectric spectroscopy is used within the experimental framework of this thesis to investigate the integrity of Mass Impregnated paper insulation.

The remainder of this first chapter discusses the impact of deregulation and privatisation on relevant energy trade market trends and the chapter concludes with a concise overview of system configurations and cable systems.

The second chapter introduces testing procedures for HVDC cables as recommended by CIGRE based on lifetime curve considerations. This is followed by an inventory of on-site and off-site techniques to monitor the condition of cable insulation. A concluding section mentions some HVDC cable fault location techniques which were found in literature

The focus of the experimental work in this thesis is on Mass Impregnated paper insulation and with this in mind the production process behind the Kraft electrical grade paper insulation is mentioned in chapter three. Following this, the degradation kinetics of cellulose papers and cellulose-oil composites are introduced. Furthermore, the way this degradation might be reflected in the dielectric relaxation characteristic is discussed.

The Novocontrol dielectric spectroscopy test equipment is introduced in chapter four together with two experimental methods for moisture determination in insulation samples.

This is followed by the results chapter, divided into three sections. The first section analyses the dielectric spectroscopy results for artificially thermally aged Mass Impregnated insulation samples and compares these to the results for an unaged reference sample. The changes to the dielectric relaxation for the thermally aged samples are noted and the observed relaxation characteristic is explained in terms of the underlying processes of this thermal degradation

Part two of the results chapter investigates two samples which exhibit some unusual dielectric relaxation characteristics in the dielectric spectroscopy results. The origins of these effects are investigated and the findings are justified based on the properties of the materials. The remaining part 3 to this chapter investigates the dielectric spectroscopy results for Non-Impregnated Kraft insulation paper. Some concluding remarks to this chapter compare this last result with those from the dielectric spectroscopy test on the unaged Mass Impregnated reference sample.

In conclusion, the sixth and final chapter in this thesis reflects on the literary and experimental findings in this work, focusing in particular on the underlying causes of the characteristic dielectric relaxations which were observed.

# Table of contents

# 1. Introduction

## 1.1. Introduction to HVDC

Since the '*The Battle of the Currents*', *circa* 1880, the rivalry between *alternating current (ac)* and *direct current (dc)* technology has been endemic to the field of electricity distribution and generation. Thomas Edison and Nikola Tesla, once esteemed colleagues, quickly became adversaries in the promotion of their respective dc and ac systems.

This juncture in time saw the prevalence of the ac system of Nikola Tesla, much to the dissatisfaction of Edison who had a vested financial interest in overseeing the success of his dc system. The advantages of ac over dc were obvious at the time. Power transformers allowed ac to reach high voltages and in doing so the resulting low currents helped reduce the ohmic losses in the transmission lines. The adoption of ac generation and distribution helped remove the need for the *distributed generation* network typology of the dc system.

Since this era, *High Voltage Alternating Current (HVAC)* has had the leading role in energy distribution and now there is evidence of a growing resurgence in *High Voltage Direct Current (HVDC)* distribution; a technology traditionally associated with *non-energy* applications such as the television, x-ray medical equipment, the radar, electron microscopes and satellite broadcasting. With this emergence it would appear *the battle of the currents* rages on, and for good reason.

Many of the advantages of HVDC are inherent in the shortcomings of HVAC technology in some respects. As is well documented, the capacitive elements of an energy transmission cable limit HVAC transmission to relatively short distances. For longer distances intermediate switching stations and reactive power compensation is necessary [1].

HVDC technology is an important tool in connecting electricity grids that are operating unsynchronised or at different frequencies, with the additional benefit of active power flow control. These connections are often back-to-back where no transmission lines are necessary. The asynchronous link acts as a firewall against cascading outages between interconnected grids [2]. Furthermore, HVAC connections may not be possible due to stability issues and because of the potential increase in short circuit current levels when making interconnections.

Insulation and conductor sizes for specified power ratings are also smaller in HVDC cables leading to further savings [3]. Typical transmission distances of 40 to 100 km are feasible solutions with todays HVAC technologies. However, the break even point when choosing a HVDC solution occurs when the savings in line losses coupled to the capitalised cost of the losses offsets the expense of the converter stations [4].

Furthermore, for long transmission distances, typically greater than 40 km, in most cases HVDC transmission is the only technical solution because of the high charging current of an AC cable. [5].

Modern HVDC technology holds an interesting past and its foundations were developed extensively during the 1930's. During the 1940's a 60 MW, 115 km subterranean cable was commissioned in Berlin but never saw completion. This line was proposed as an alternative to traditional overhead lines which could pose as targets for an intruding enemy force during times of strife. As it transpired the line was moved to Russia and put into service there following the dissolution of the German government in 1945 [6].

The understanding of HVDC installation stresses remains far behind those of their HVAC counterpart. The reason for this lies in the economics of running predominantly AC power grids. Failures in electricity grids often result in huge financial expenses to grid operators and for this reason the life-times and reliabilities were important design aspects of AC components over the years. The follow on effect from this is a greater understanding of HVAC dielectrics.

The dawn of a new era saw the commissioning of the first submarine HVDC installation connecting Gotland Island to the Swedish mainland in 1954. Since then similar interconnections to *Gotland I* have become commonplace and, to date, the longest HVDC interconnector in operation is the 600MW, 1700 km interconnector between the Inga Dam and the Shaba copper mine in the Democratic Republic of Congo.

## 1.2. Breakdown Mechanisms in HVDC Cables

The breakdown mechanisms inherent to HVDC cables [7] are;

- A thermal runaway effect caused by the heat generated in the insulation due to the leakage current $I_0$ and
- Electrical stresses due to localised field enhancements that result from the accumulation of space charge inside the dielectric.

Critical instances of the above must be avoided to ensure normal operation of a HVDC cable. The electric field calculations in HVDC cables are more complicated than in HVAC cables where the permittivity $\varepsilon_r$, the cable geometry and the applied field fully describe its electrical behavior. In HVAC cables the permittivity $\varepsilon_r$ changes very little under service conditions, further simplifying field calculations [8].

Furthermore, the field calculations for HVDC depend on the geometry of the cable, the permittivity $\varepsilon_r$, the applied electric field and the conductivity $\sigma$ which itself shows a strong electric field and temperature dependency. This complexity gives rise to field distributions that exhibit capacitive, intermediate time-dependent or resistive behavior. [8].

However, the field in a HVDC cable is never purely resistive and only approaches this behavior. For this reason it is said that pure dc does not exist [9]. This resistive stage is referred to as the stable dc field situation.

In literature many empirical formulas exist that describe the behavior of the insulation conductivity. All acknowledge the conductivities dependency on the temperature and the electric field as follows;

$$\sigma = \sigma_0 \exp(\alpha T) \exp(\gamma E) \qquad [8]$$

$$\sigma = \sigma_{ref} \left( \frac{E}{E_{ref}} \right)^{\nu} \exp\left[\alpha (T - T_{ref})\right] \qquad [10]$$

$$\sigma = A.\exp\left( -\frac{E_a}{K_B T} \right) \frac{\sinh(B|E|)}{|E|} \qquad [10]$$

Stable dc fields under no-load conditions exhibit higher electric fields at the insulation in the vicinity of the conductor core. Conversely, when the cable is loaded, current is flowing and a temperature gradient exists. This causes an increase in the electric field at the outer conductor and a decrease close to the inner core.

This demonstrates the effect of the temperature on the conductivity in the insulation and this behavior is referred to as field inversion. The field dependency of the conductivity causes a leveling-off effect of this inverted field. These field inversion and leveling-off processes are both due to a phenomenon known as space charge and its effects on the field distribution are shown graphically in figure 1.1 below.

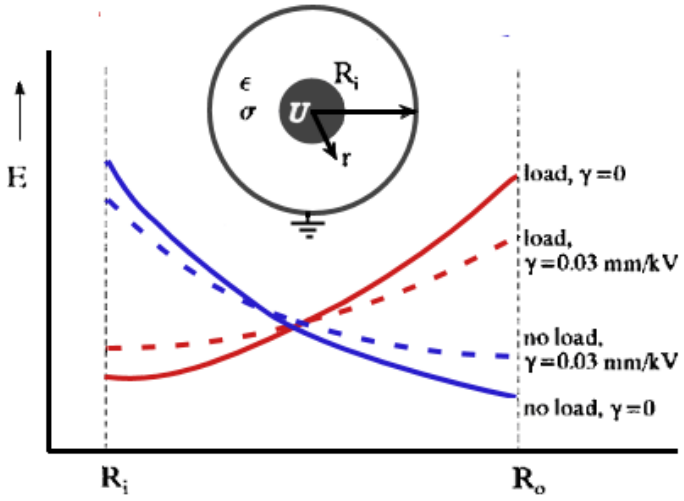


***Figure 1.1.*** *Electric Field in HVDC Cable Insulation*

The effects of space charge are most dangerous during a polarity reversal. A superposition of the charge induced field and the external field, now reversed, can cause very high electrical stresses on the insulation. Furthermore, switching and lightning operations can produce transients that are also superimposed on the dc voltage.

In situations where the cable is exposed to high ambient temperatures or significant electrical stresses the effects of the ohmic insulation losses must be carefully considered. In this case the leakage current $I_0$ can increase considerably.

This can lead to a higher insulation temperature and therefore the conductivity also increases. The leakage current then increases again since the conductivity has changed. This process continues until a balance is reached or an instable situation arises culminating in the breakdown of the insulation by thermal runaway [8].

## 1.2.1. Space Charge

Space charge is an intrinsic property of dc insulation, the dynamics of which demand careful attention during the design process of HVDC equipment. Analysis of space charge under different operating conditions is an important consideration when designing dc equipment; its presence can cause increased material stresses in dc electrical equipment.

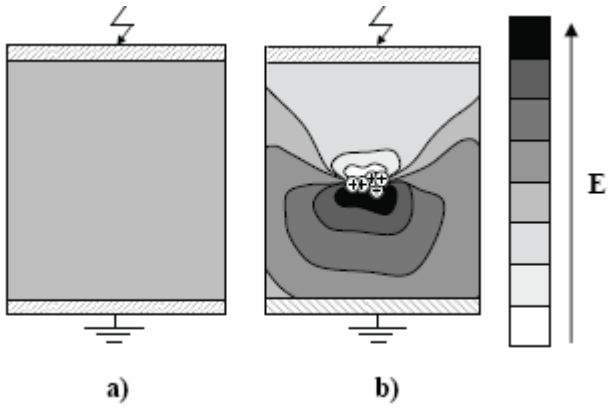


***Figure 1.2.*** *Depiction of a) a Laplacian field in a homogenous dielectric and b) a field distorted by the presence of space charge [10]*

Figure 1.2 illustrates the increased electrical field stress in the dielectric resulting from the accumulation of space charge.

In general, space charge forms due to the inhomogeneities present in a dielectric, giving rise to a non-uniform leakage current $I_0$. The conductivity of the insulation relating to this leakage current shows a dependency on the temperature and the electric field [3].

From a macroscopic point of view; when an inequality exists between the flow of charge into a material and the flow of charge out of a material there is a divergence from ohmic conduction. This is a result of the space charge present. The following is a mathematical explanation of how this space charge arises;

$$\vec{J} = \sigma.\vec{E} \quad \text{----} \quad \vec{E} = \frac{\vec{J}}{\sigma} \qquad\qquad \nabla.\vec{J} + \frac{\partial \rho}{\partial t} = 0 \quad \text{----} \quad \nabla.\vec{J} = -\frac{\partial \rho}{\partial t}$$

$$\rho = \nabla(\varepsilon_0.\varepsilon_r.E)$$

$$\vdots \text{---} \quad \rho = \nabla(\varepsilon_0.\varepsilon_r.\frac{\vec{J}}{\sigma})$$

$$\vdots \text{---} \quad \rho = \frac{\varepsilon_0.\vec{\varepsilon_r}}{\sigma}\ \nabla.\vec{J} + \vec{J}.\nabla(\frac{\varepsilon_0.\vec{\varepsilon_r}}{\sigma})$$

$$\vdots \text{---} \quad \rho = -\frac{\varepsilon_0.\vec{\varepsilon_r}}{\sigma}\ \frac{\partial \rho}{\partial t} + \vec{J}.\nabla(\frac{\varepsilon_0.\varepsilon_r}{\sigma})$$

$$---- \quad \rho + \frac{\vec{\varepsilon_0 . \varepsilon_r}}{\sigma} \frac{\partial \rho}{\partial t} = \vec{J} . \nabla \left( \frac{\varepsilon_0 . \varepsilon_r}{\sigma} \right)$$

Therefore when $\vec{J} \neq 0$ and the ratio between the relative permittivity $\varepsilon_r$ and the conductivity $\sigma$ are not spatially uniform across the insulation a space charge $\rho$ develops over time.

The important mechanisms governing the accumulation of this space charge and its dynamical behavior are the following [11][12];

- Charge injection/extraction at electrode-dielectric interfaces which is then trapped in the bulk of the insulation.
- Charge transportation throughout the bulk.
- Field assisted thermal ionisation of impurities creating donor/acceptor trapping sites.
- Recombination and generation centres of charge carriers.
- Non-uniform concentrations of dipoles in the bulk.

In the majority of cases *homo-charge* is responsible for the increases in electrical stresses of HVDC equipment [11]. In essence, homo-charge refers to the charge that accumulates in the dielectric in the vicinity of the electrode, having the same polarity as that of the electrode charge. This phenomenon arises when the bulk of the dielectric is unable to transport the charges at the same rate as the charges are supplied or injected. The outcome of this is a reduced field at the electrode-dielectric interface and a field enhancement in the bulk of the dielectric.

In literature, tests on Mass Impregnated HVDC cables revealed the presence of homo-charge for various combinations of different oils, papers and electrode materials subject to electrical field strengths ranging from 20kV/mm to 80kV/mm [8]. Negative and positive charge injection occurred at the cathode and anode respectively. The air impermeability, thickness, kinematic viscosity and electric resistance of the oil-paper insulation are deemed important characteristics in determining the space charge build up and the subsequent field enhancement.

A less frequently observed phenomenon is known as *hetero-charge* and refers to the charge that accumulates in the dielectric next to the electrode, having the opposite polarity to that of the electrode charge. Hetero-charge occurs when the bulk of the dielectric material transports charge faster than the electrodes can supply it and in a similar fashion the result is a reduced electrical stress throughout the bulk of the dielectric medium and an increase in electrical stress in the dielectric close to the electrode.

Both hetero-charge and homo-charge are illustrated in figure 1.3.

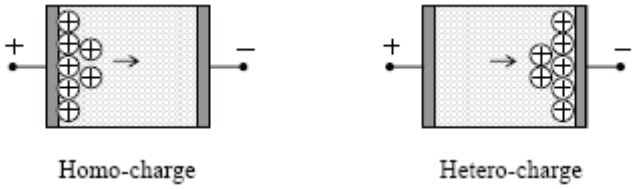


***Figure 1.3.*** *Illustration of homo and hetero-charge accumulation in the anode and cathode regions of a specimen [11]*

Space charge is a design constraint unique to dc technology. In ac applications the voltage alternates too quickly for space charge to accumulate or else its effects are negligible. Electricity distribution networks are typically ac, operating at frequencies of 50Hz or 60Hz, and the high voltage assets they employ are often designed to have life expectancies of 40 years or more.

The prevalence of ac technology in the energy sector has led to a much greater understanding of dielectric behaviors at ac voltages. DC systems can experience combinations of dc voltages, polarity reversals, superimposed ac voltages, impulse and switching surges creating complicated dynamical electrical fields. For this reason the understanding of the more complex dc dielectric behavior lags far behind that of its ac counterpart. A result of this is the limited use in dc applications of some proven ac dielectrics over the years.

An example of this is the accumulation of space charge in extruded polymeric cables, a widely used dielectric in ac technology. In extruded polymer cables the effects of the space charges are slow to dissipate. This creates a stress in the dielectric in the form of a charge induced field which can be detrimental to the insulation during operation, especially after a polarity reversal.

$$E_{insulation} = E_{external} + E_{charge\_induced}$$

The contribution made by the charge induced field to the electrical stress of the insulation is evident in the above equation. Together with the external field, also referred to as the Laplacian field the result can cause high insulation stresses.

In research studies on extruded polymer insulation for HVDC applications space charge was identified early on as a major problem. The development work on a bipolar 250kV HVDC cable in Japan showed the early failures to be a result of space charge accumulation.

Furthermore, the decision not to use the extruded polymer insulation for the submarine HVDC cable between Hokaido and Honshu, Japan was due to a reduction in the breakdown strength upon polarity reversal, a direct result of space charge accumulation [3]. This is also the reason why extruded polymer technology was not used in the

Australian Bass-link project [3]. Polarity reversal is thought to reduce the breakdown resistance of a cable by approximately 10% [3].

In spite of this, following extensive research efforts, extruded polymeric HVDC cables are now an available alternative to the traditional MI cables used in some applications. This advance is the result of Voltage Source Converter (VSC) technology. However, these developments are restricted to unipolar operation and challenges still exist at voltages above 250kV where ageing mechanisms need further attention [3].

Furthermore, the current flow then dictates the direction of the power flow and polarity reversals don't occur. The commissioning of the first extruded polymer insulation HVDC cable was in 1999 between Sweden and an island off its coast, Gotland. [3]. It is interesting to note that the first submarine line commissioned in 1953 was also at this location.

As a side note, Furakawa have developed a 500kV DC XLPE system which has passed pre-qualification tests conforming to CIGRE recommendations. [7] To date and to the best of this author's knowledge there is no such line yet in operation. The electrical field caused by the space charge can be calculated by Gauss' Law;

$$\rho = \nabla(\varepsilon_0.\varepsilon_r.E_{charge\_induced})$$

Furthermore, after analysing the distribution of the space charge, $\rho$, the electrical stress of the insulation can be calculated, combining the following equations;

$$\nabla^2 U = -\frac{\rho}{\varepsilon_0.\varepsilon_r} \quad \text{, and} \quad \vec{E} = -\nabla.V$$

Methods to detect space charge and analyse its effect will be further discussed in chapter 2.

### 1.2.2. Partial Discharges

The partial discharge is a phenomenon whereby insulation suffers a localised breakdown that does not bridge the full distance between the electrodes [14]. This process is the result of concentrated ionisations occurring in voids or in other low-density areas within the insulation.

Partial discharges produce low amplitude, high frequency transient current pulses of nano-to-micro-second duration and the damage sustained to insulation due to partial discharges is often attributed to the following mechanisms [14];

- Heating effects due to high energy electron and ion bombardment.
- UV-light from the discharges causing stress-cracking.
- Chain scission and chemical processes that reduce the longevity of the insulations lifespan.

The bipolar partial discharges observed in ac systems do not occur in a dc system. There is no phase information contained in the unipolar partial discharges resulting from a dc excitation. For this reason the magnitude of unipolar discharges and the times of occurrence are recorded giving valuable information on the time between consecutive discharges [8].

The most common source of partial discharge is internal, surface and corona discharges. For internal and surface discharges the electrical field strength determines the inception voltage of the partial discharges whereas the absolute voltage determines the onset of corona discharges.

Surface discharges are common along dielectric interfaces where a high tangential field exists and corona discharges usually occur at sharp metallic points. In an ac cable, protrusions at the inner and outer semiconducting screens can result in harmful partial discharges when the electrical field reaches the partial discharge inception value. In a dc system partial discharges can indicate a weakness in the insulation where a future breakdown may begin [8].

Operational HVDC cables are no exception to partial discharge activity. The use of HVDC lines for the interconnection of electricity grids involves frequent load changes during the trade of electricity between operators. Loading a HVDC cable can be accompanied by an increase in the repetition rate of partial discharges, a result of the insulation conductivity rising with the increasing temperatures.

Furthermore, for a Mass Impregnated HVDC cable, when the cable load is decreasing the temperature also decreases and partial discharge activity with an enhanced repetition rate can occur. The insulation in this case is contracting with the decrease in temperature. The enhanced partial discharge activity could be due to cavitation during the cooling process. Interfaces such as joints and semicon screens are possible weak points in HVDC systems where discharge activity is more likely. Localised high partial discharge activity in these areas might be the first indicators of cable degradation or the onset of breakdown.

On-site diagnostic equipment for partial discharges are popular tools available to power utilities in assessing the condition of their power cable networks [15]. This equipment ignites partial discharges in the circuit of interest using a special test voltage such as a Damped Alternating Current, DAC. Analysis software of the partial discharges gives valuable information about the condition of the circuit and where potential weakpoints may be [16]. Diagnostic tools such as these are further discussed in chapter 2.

When upgrading the 400kV Fenno-Skan submarine cable in 1998 the partial discharge behavior was used in an extensive study of the cables load capabilities [17]. In load cycle laboratory experiments on a cable sample the partial discharge current was measured by integrating the recorded discharges over time.

In this work the authors calculated the expected partial discharge current for the range of test voltages used in the test set-up. During load cycles the voltage was stepped up until breakdown occurred. It was discovered that the partial discharge current before breakdown was greater than the value expected from calculations. The findings from this experiment are three-fold; the partial discharge current is a good indication of the insulation quality; it gives an indication of the power transmission capabilities of a cable and; high partial discharge current is a precursor to breakdown

The breakdown behavior in a layered insulation is quite complex. In a study by Evenset [19] focusing on the breakdown mechanism of HVDC Mass-Impregnated cables the effects of cavitation were analysed. The findings of this study show the temperature dependence of the dc breakdown.
This was attributed to the formation of cavities in the mass during the cooling period of the thermal cycle resulting from the differences in the thermal contraction of the mass and the paper. This situation closely mimics the situation where a load is turned off or reduced in a dc transmission line.

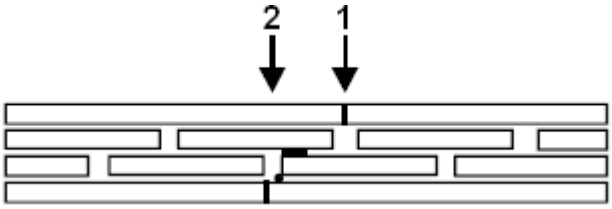


***Figure 1.4.*** *Breakdown of MI Paper Insulation [17]*

During the thermal cycles the magnitude of the discharges in the cavity at the first butt-gap increased considerably. This butt-gap is marked number 1 in figure 1.4 above. The author concludes that this occurs after paper layer adjacent to the top electrode breaks down, causing a transfer of the electrode potential to this first cavity.

The cavity grows in an axial direction under the influence of this transferred potential. The cavity extends between the paper layers to the second butt-gap. This resulted in a carbonised breakdown path between the paper layers and a further growth in the cavity

size at the second butt-gap. The growth in the second cavity then progressed to breakdown the paper layer adjacent to the lower electrode creating the full breakdown path.

The authors conclude that the electrical strength of MI paper insulation is dependent on cavitation, citing partial discharges and the transfer of electrode potentials as the propagating factors contributing to breakdown.

In general, the magnitude of a partial discharge is a good indication of the energy stored and the volume of a discharge source and its intensity is an indication of the degree of ageing of the insulation [19]. The analysis of partial discharges using different detection circuits is an important diagnosis and monitoring technique of insulation that will be further elaborated upon in chapter 2.

# 1.3. Dielectric Relaxation Analysis

Dielectric Relaxation Analysis is an important tool at the disposal of electrical engineers that gives valuable information about the loss mechanisms and electrical strengths of insulating materials.

In introducing this technique of relaxation analysis it is first necessary to explain the principle of polarisation in a dielectric material whereby neighboring charges are aligned relative to one another under the application of an external electric field, a result of the following processes but not necessarily them all [20];

- Electronic polarisation.
- Molecular/Ionic polarisation.
- Dipole/Orientational polarisation.
- Hopping charge carriers.

A polarised material gives rise to an internal electric field that interacts with the externally applied field and the effect can be interpreted as the finite displacement of charges in a steady electric field [20]. Power engineering dielectrics are isotropic and their linearity [11] implies the superposition principle is applicable to the different polarisation mechanisms present.

In essence, dielectric relaxation is the recovery in strain of a material when the external stress is removed. In the case of Dielectric Spectroscopy this external stress can have two forms, an electrostatic field or a time varying harmonic field of angular frequency $\omega$. These external stresses are used in TDS (Time Domain Spectroscopy) and Frequency Domain Spectroscopy (FDS) respectively. For a linear dielectric, the information from TDS is equivalent to that obtained from FDS and the two are inter-related by the Fourier transform.

The dielectric susceptibility $\chi$ of a material measures the extent of polarisation P within the dielectric in response to an external electric field E. This relationship is represented her in vector form as follows;

$$P = \chi \varepsilon_0 E$$

, where $\varepsilon_0$ is the permittivity of free space.

Polarisation processes are time and frequency dependent. Assuming a time varying external field $E_m e^{i\omega t_0}$, the resultant electric displacement field D(t), consists of the field contribution of free space together with the convolution integral of the dielectric response function f(t) and the external field $E_m e^{i\omega t_0}$ [21];

$$D(t) = \varepsilon_0 \varepsilon_\infty E_m e^{i\omega t_0} + \varepsilon_0 \int_{-\infty}^{0} f(t - t_0) E_m e^{i\omega t_0} dt_0$$

After some manipulation of this formula the result is,

$$D(t) = \varepsilon_0 \left[ \varepsilon_\infty + \int_0^\infty f(t) e^{i\omega t} dt \right] . E_m e^{i\omega t}$$

, where $\int_0^\infty f(t) e^{i\omega t} dt.$, the Fourier transform of the dielectric response is equivalent to the complex susceptibility $\chi(\omega)$

As mentioned already the time domain and frequency domain responses of a linear dielectric contain the same information and are inter-related by the Fourier transform thus giving the following;

$$\chi'(\omega) = \int_0^\infty f(t) \cos(\omega t) dt$$

$$\chi''(\omega) = \int_0^\infty f(t) \sin(\omega t) dt$$

, and

$$f(t) = \int_0^\infty \chi'(\omega) \cos(\omega t) d\omega$$

$$= \int_0^\infty \chi''(\omega) \sin(\omega t) d\omega$$

In this thesis the behavior of the complex permittivity components representing the dielectric energy storage and losses together with $\tan(\delta)$ are analysed; the $\tan(\delta)$ spectra giving a more clear indication of the relaxation processes at work. The relationships to the complex susceptibility are as follows;

$$\varepsilon'(\omega) = \varepsilon_\infty + \chi'(\omega)$$

$$\varepsilon''(\omega) = \frac{\sigma_{dc}}{\varepsilon_0 \omega} + \chi''(\omega)$$

$$\tan(\delta) = \frac{\varepsilon''}{\varepsilon'}$$

, where $\varepsilon_\infty$ is the high frequency value of the permittivity. The first term on the right hand side of the equation for the imaginary component of the permittivity shows the contribution of the dc conductivity to the frequency spectrum.

The concept of dipoles giving rise to a dielectric polarisation was introduced first by Debye in 1912 and in 1945 Debye formulated a derivation describing this behavior [22]. This model is accurate for materials having low molecular contents such as liquids and gases. In the Debye model the assumption is that one polar group only contributes to the dielectric polarisation. The response is formulated in a relationship between the dielectric permittivity $\varepsilon$, the angular frequency $\omega$ and the temperature T as follows [11];

$$\varepsilon(\omega,T) - \varepsilon_\infty = \frac{\varepsilon_s - \varepsilon_\infty}{1 + i\omega\tau(T)}$$

Variations of the Debye model such as the Cole-Cole and Havriliak and Negami modifications account for materials containing interacting polar groups resulting in more then one relaxation time. This is the result of superimposed relaxation processes and is observed as a group of relaxation times grouped around a mean relaxation time [11]. The different models give close approximations to the observed results yet they fail to pinpoint the underlying mechanisms at play relating to physical chemical and the structural properties of the materials [22]

The different relaxation processes commonly fall into one of three categories;

$\alpha$-relaxation is usually characterised by a narrow loss peak of large magnitude. The response is related to the glass to crystalline transition point in a material, occurring at the glass transition temperature $T_g$. The relaxation mechanism is thought to derive from the motion of polar segments of the main molecular chain [11]. This relaxation is not so common in cellulose materials containing low moisture contents [23]

$\beta$-relaxation has a broad relaxation peak usually extending over several decades in the frequency spectrum. This response is observed below the glass transition temperature of a material and has an Arrhenius type temperature dependence. It has been suggested that this process results from side-chain motion of the molecular chain [11]. An alternative theory proposed by [23][24] when testing cellulose is that this relaxation process is again due to segmental motion of the main molecular chain. .

$\gamma$-relaxation is often masked by the broad spectrum of the $\beta$ relaxation in pure celluloses and is associated with the side-group motion of molecules [23].

$\sigma$-relaxation relating to proton migration or ion hopping at high temperatures in amorphous polymers [24]

The frequency domain spectrum can consist of combinations of these processes making it difficult to identify the individual relaxation processes. This thesis focuses on the dielectric spectra of Mass Impregnated paper insulation in the low frequency range characterised by either dc conduction, or Low Frequency Dispersion (LFD) behavior and other loss mechanisms that may be present.

## 1.4. Renewable Energies and the Environment

In a report to the United Nations general assembly, the World Commission on Environment and Development states that the principal goal of sustainable development is structured around meeting '*the needs of the present without compromising the ability of future generations to meet their own needs*' [25].

This directive is intended to be the central building block for governments, private institutions, organisations and enterprises and in recent years, in view of the negative environmental impacts witnessed globally these policies are intended to promote sustainable development without repercussions for the environment.

In saying this, a sustainable supply of cost effective energy resources and their efficiency and effectiveness in use are critical elements in achieving these goals. In this regard, the inextricable link between renewable energy resources and sustainable development is apparent.

Solar radiation, tidal energy from earth-moon gravitational forces and geothermal energy from the earth's core are all sources of renewable energies. The technologies to tap these vast reservoirs of energy are still in their infancy and it is hoped that future developments should remove the dependencies on fossil fuels and help alleviate environmental stresses.

The role that *HVDC* technology plays in the afore mentioned policies is becoming more and more substantial through the interconnection of power grids and through the connection of wind farms and other decentralised renewable energy sources to the electricity grid.

For instance, wind power generation is a fast growing renewable energy market in the electricity generation sector with an estimated world capacity of 100GW and an annual growth rate of 30 percent [26]. Typical locations for windfarms are high altitude land areas or remote offshore sea areas where the wind speeds higher than for land installations. The largest wind farm to date is located in Texas, supplying circa 740 MWs of electricity.

The interconnection of power grids via *HVDC* lines creates a flexible transmission infrastructure, improving the efficiency of existing power plants in the process. Assistance from neighboring power grids can defer, and often make the building of new power stations unnecessary. The reduction in the number of stations is a first step in improving the environment.

Furthermore, the narrower tower construction for *HVDC* lines leads to a reduced visual impact on its surroundings. Subterranean *HVDC* lines using extruded polymer insulation are new alternatives for long distance power transmission without the visual impact of overhead lines [4].

## 1.3.1. Market Liberalisation

Liberalisation of the electricity sector involves processes of deregulation and privatisation and aims to limit any widespread commercial or institutional dominance within the market. This is a functioning directive in Europe, Australia, South America and in the USA and is expected to become more widespread [27]. Liberalisation gives rise to a more competitive market and provides a higher quality of service to the customer. With this there is then an onus on power utilities from an economical and from a societal point of view.

The advantages expected to arise from the liberisation of electricity markets are numerous. The economics of supply are more focused. Maintenance issues have received a lot of attention for this reason and terms such as Time Based Maintenance (TBM) and Condition Based Maintenance (CBM) are common benchmarks. For example, when a grid operator removes a high voltage asset from service before a potential failure occurs, this in theory leads to a more reliable customer service where the chances of a propagating fault in the future become less likely.

In Europe the trade of electricity between neighboring networks is common and new connections between existing grids are frequently commissioned. These connections are often HVDC interconnections providing;

- Bulk power transfer between grids.
- A firewalling effect, reducing the chances of cascading outages.
- A mechanism for the trade of electricity.
- Support for grids that cannot meet their load demands.
- No increase in the short circuit current capacity.
- Diversity in generation sources. i.e wind, hydro, fossil etc
- Reduction in installed generation reserves.
- Share of spinning reserve.

The trade of electricity between grid operators should provide equal savings for those involved. For instance, The Netherlands (a primarily fossil based electricity generator) may choose to buy electricity from Norway (primarily hydro-electric generation) when Norway can produce electricity at less expense.

This could also be the reversed situation at a point in time when The Netherlands can produce at a cheaper rate. This is the reason why the NorNed HVDC submarine cable was commissioned in 2008.

In the near future global transmission grids could be realised where HVDC interconnections will ultimately play an important role.

# 1.5. HVDC Systems

The main features of a HVDC system are the converter stations, the earthing electrodes and a HVDC cable which is omitted in the case of back-to-back conversion. Both arrangements are depicted in figure 1.5 and 1.6.

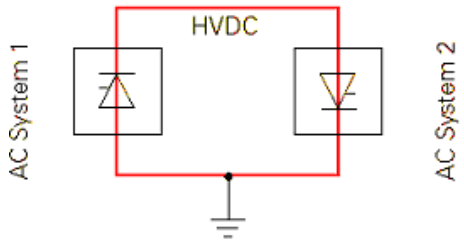


***Figure 1.5.*** *Back-To-Back system*

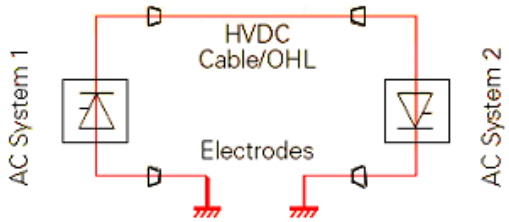


***Figure 1.6.*** *HVDC transmission system*

## 1.5.1. Converter Stations

The converter stations are very complex electrical systems consisting of filter banks, switching yards, transformers, converter bridges, smoothing reactance and bushings with dedicated control and protection systems in place to ensure safe operation The sole purpose of a converter station is in rectification (ac-to-dc) at the transmission end and inversion (dc-to-ac) at the receiving end of the transmission line. The arrangement in figure 1.7 shows the general layout of the converter station.

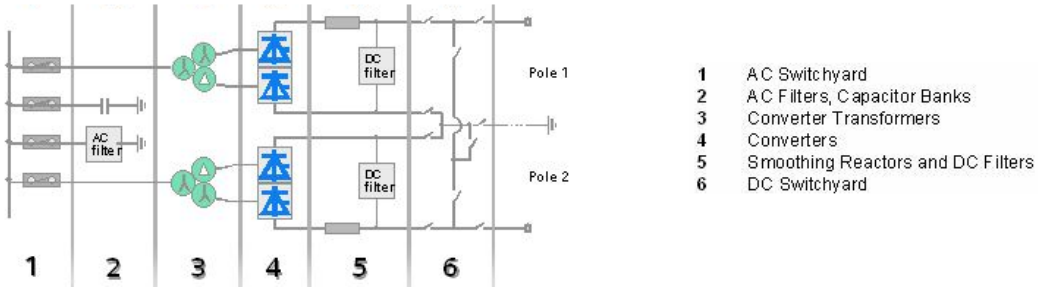


***Figure 1.7.*** *Converter station layout*

### 1.5.2. Classical HVDC Systems

The classic HVDC transmission system combine Mass Impregnated cable technology with converter stations incorporating natural or capacitor based power electronics for commutation. Mass Impregnated cables have no limit to their lengths and they can operate at depths of 1000m. Today the classic system is the only choice for HVDC systems where individual cable voltage levels exceed 250kV. Alternative systems such as *HVDC Light* (ABB) and *HVDC PLUS* (Siemens) technologies are somewhat limited above these voltage levels.

Naturally Commutated Converters are based on thyristor banks consisting of many individual elements connected in series. Todays thyristors are core power electronic devices with current ratings of 4000 Amps, capable of blocking voltages up to 10kV. The thyristor banks are therefore capable of operating at very high voltages. Thyristor valves are operated at the ac grid frequency and a special control signal adjusts the voltage level across the dc bridge, dictating the control of power flow. Capacitor Commutated Converters (CCC) adds an improvement in performance to this technique. The Capacitors are inserted between the thyristor valves and the conversion transformers and help improve the commutation failure performance of the system.

The drawback to this system is that it can only transfer power between two (or more) active grids. In the case of connecting an offshore marine farm for instance, an auxiliary start-up system would be necessary.

### 1.5.3. HVDC Light and HVDC PLUS Systems

The *HVDC Light* (ABB) and *HVDC PLUS* (Siemens) systems are more recent innovations in the HVDC electricity transmission market. These systems combine extruded polymeric cable insulation technology together with Forced Commutator Converter (FCC) stations. Extruded polymeric cables are lighter, are easily produced and are less expensive than MI cables.

The valves in the converter stations are made from Voltage Source Converters (VSCs) based on Gate Turn-Off (GTO) thyristor or Inverse Gate Bipolar Transistor (IGBT) power electronics. A high frequency Pulse Width Modulation (PWM) control signal is used in VSC conversion. VSCs have turn-on turn-off capabilities adding a further dimension of flexibility to the system where individual control of active and reactive power and control of the power quality is possible. The PWM control enables rapid independent control of the active and reactive power acting as an inertia free motor or generator within the system

The converter stations in *HVDC Light* and *HVDC PLUS* projects take approximately 1 year to commission after the contract is agreed upon. This is in stark contrast to the classic system, taking 2 and 3 years naturally commutated converters and capacitor commuted converter respectively. The more compact design together with the fast construction make the *Light* and *PLUS* systems appealing choices of technology for power ratings in the region of 250MW.

## 1.5.4. System Configurations

A monopole system is one of the simplest and more economic systems available and is often the chosen technology for moderate power transfers.

***Figure 1.8.*** *Monopole, ground return*

A slight variation on this topology is the Moyle inter-connector, a dual monopole system which connects the Northern Irish and Scottish electricity grids via a submarine Mass Impregnated HVDC cable. The twin 250kV lines have a combined power rating of 500MW with individual Integrated Return Paths (IRCs) for the return currents. This metallic coaxial layer improves the torsional strength and screens the surrounding environment from the cables magnetic field.

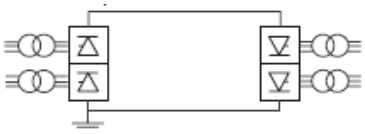

***Figure 1.9.*** *Monopole, metallic return*

Monopole systems commonly use sea electrode return paths. However, in instances where high resistivity is encountered, dedicated low voltage return lines (figure 1.9) are added which are often a variation on the IRC just mentioned. In this case a local earthing at the converter station is used for reference purposes only.

When considering back-to-back conversion (figure 1.10) the power transfer capabilities are limited by the relative capacities of the adjacent grids at the point of connection. This arrangement is used for connecting asynchronous grids, out of phase grids and in other situations as a stability measure.

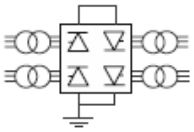

***Figure 1.10.*** *back-to-back conversion*

*HVDC Light* and *HVDC PLUS* systems use a topology where the midpoint of a single 12-pulse converter is chosen as the dc reference point; a slight variation on the arrangement in figure 1.11. In these systems the midpoint is connected to earth through high impedance that ensures no earth current under balanced operation. Two extruded polymeric cables with individual ratings in the region of 250kV are then used at opposite polarities, connected to either pole.

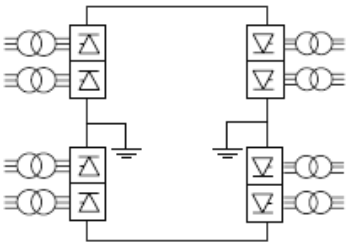

***Figure 1.11.*** *Bipole*

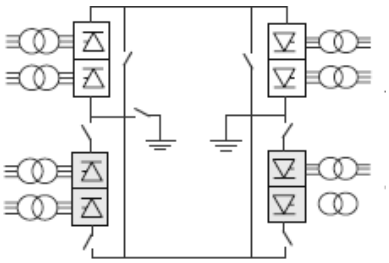

***Figure 1.12.*** *Bipole, metallic return*

The bipole arrangement in figure 1.11 is often the system of choice for HVDC overhead line transmission. Each converter station has two 12-pulse converters giving 2 independent lines, adding redundancy to the system in the case of a fault on one line. Alternatively, figure 1.12 shows how a line can be used as a low voltage return path when a converter station or some other variable is out of operation at that pole. A flexible design allows the functional pole to operate at a higher transmission level under these circumstances.

The series connected system in figure 1.13 is for high power HVDC applications above 500kV. This topology offers many switching operations adding more redundancy to the transmission system. For instance, when one converter bridge is down this can be bypassed and one pole can still operate at a reduced capacity.

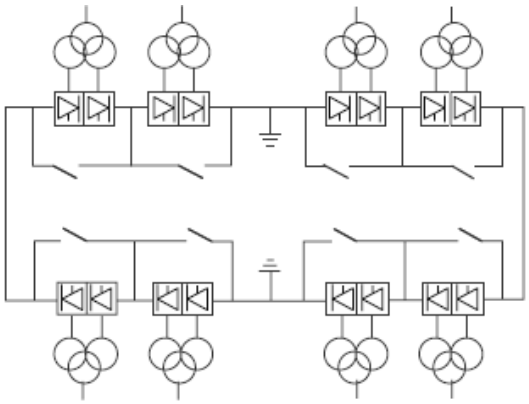

***Figure 1.13.*** *Bipole, series connected converter bridges*

NorNed is a HVDC system and submarine cable connecting the electricity grids between Norway and The Netherlands. This is a bipolar system with an effective transmission voltage of 900kV. Its configuration however is a slight variation from the series connected system mentioned for high power transmission. Each station has one single 12-pulse pulse converter where the midpoint is grounded. Two HVDC MI cables are then connected to each converter pole at ± 450kV respectively, and an effective voltage of 900kV can be reached. The topology of this system is suitable for long distance power transfer considering the low current and therefore low losses in the line.

## 1.5.5. HVDC Transmission Lines (Cables)

Mass Impregnated HVDC cables are manufactured in continuous factory lengths. These cable sections can be 10km long and when connected by factory joints the overall delivery length can reach 100km depending on the cable laying vessel. The delivery lengths are joined by field joints enabling the full submarine crossing. Transition joints then connect the submarine cable with the shore cable that connects to the converter station.

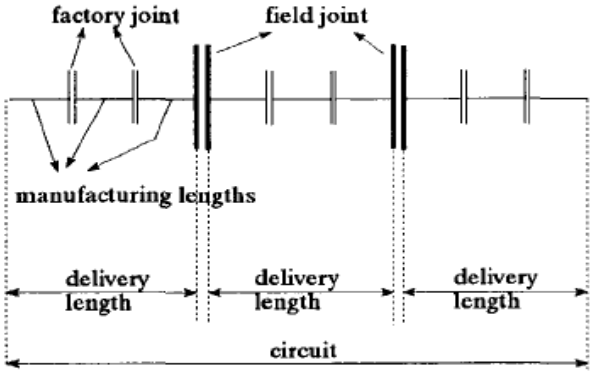


***Figure 1.14.*** *Submarine MI HVDC cable section [8]*

Knowledge of the land-to-sea profile of a HVDC system is indispensable in determining the possible weak points in a system. This should include cable depths, the number and location of transition joints and field joints, the service temperatures throughout the system and mechanical stresses along the cable such as water pressure and torsional forces. A good knowledge of these will help identify key locations in system monitoring.

One such profile is that for The Moyle Interconnector between Northern Ireland and Scotland. This system includes 8.5km of underground shore lines consisting of jointed cables, each 1.5km in length entrenched at a depth of 1.2m. A transition joint connects the shore cables to the 2 submarine cables, each 55km in length, laid in continuous delivery lengths. The cable is also equipped with a single point temperature measurement system. The vertical depth profile is shown in figure 1.15.

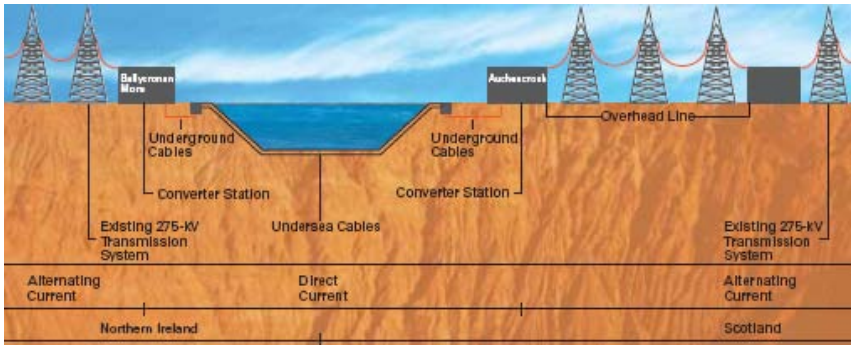


***Figure 1.15.*** *The Moyle Interconnector*

Another well documented system is The Baltic cable, a 600MW 250km submarine cable connecting the German and Swedish electricity grids. The profile of this system is quite complex. The overall cable length consists of 5.5km of shore cable in Sweden, 231km of submarine Baltic Sea cable and 12km of cable running through the river Trave, Germany.

The shore cable in Sweden was layed in one continuous factory length and the 12km river cable at Germany passes under a channel crossing for over 300m at 7 metres below the river base. The maximum water depth of the 231km sea cable is 45 metres. Sea electrodes are 20km into the Baltic Sea on the German side, 12km in the river Trave at a distance of 2.5 metre from the cable and twice times 23km on the land in Sweden. Careful analysis of this information can lead to a detailed profile of the overall system.

Polymeric cables which have replaced Mass Impregnated cables in ac applications are widely expected to do the same in future HVDC systems. In 1999, Gotland became the stage for the pioneering HVDC Light system developed by ABB as mentioned earlier. This system was commissioned to link a wind farm on the southern tip of the island to the town of Visby, 70km to the north. This new system is the fourth HVDC project commissioned on the Island of Gotland to date.

The push towards polymeric solutions in HVDC transmission systems is directly related to the extrusion production processes, the costs involved and the advantages polymeric systems have over alternative Mass Impregnated technologies. The extrusion process used to produce polymeric cables is cheaper and simpler than the process used in the production of Mass Impregnated cables. The inherent advantage of polymeric systems over Mass Impregnated systems are as follows [10];

- Absence of any oil or impregnants.
- Extruded polymer insulations have a higher thermal operating limit.
- Cable armoring is reduced due to increased mechanical rigidity of the insulation.
- Easier cable maintenance and component replacements.
- Easier preparation and mounting of the cable joints.

The advantages in polymeric cable systems are clear yet the prevailing issue of space charge continues to affect their reliability. The phenomena of space charge accumulation has been addressed but the problem is still only partially solved. For this reason Mass Impregnated insulation remains the dominant technology in HVDC cable systems to date.

# 2. Insulation Monitoring and Fault Location

In this chapter, the testing procedures for HVDC cables are introduced in sections 2.1 and 2.2. Those mentioned are test recommendations for paper and extruded polymer cables respectively. The electrical life of cable insulation, different insulation stress factors and the negative consequences of faults are discussed in section 2.3.

Furthermore, different systems used to monitor cable insulation are discussed in section 2.4. These systems are generally catagorised into on-site and off-site test techniques. The remaining discussion in section 2.5 investigates fault location techniques available for HVDC cable systems.

## 2.1. HVDC Paper Insulated Cable Tests

In the Electra 72 document, recommendations by CIGRE working group 21 are made for tests on power transmission dc cables up to rated voltages of 800kV [28]. This document covers the routine tests, type tests and after laying tests for all submarine and subterranean HVDC cables. These tests are specifically for paper insulated cables, the predominant HVDC cable in use today.

### 2.1.1. Routine Tests

- The conductor resistance test - The dc resistance of the conductor is measured and is subsequently corrected to a temperature of $20^{\circ}C$ and to a length of 1km using IEC 228 directives. The corrected resistance should not exceed the specified value in the directive.
- The capacitance test - The capacitance is measured at the power frequency using an ac bridge. The value should not diverge more than 8% from the originally stated value.
- High voltage test at works - Each length of cable is subject to a negative direct current voltage of $2U_0$ between conductor and sheath for 15 minutes.
- Power factor tests - A power factor test at ambient temperature is carried out on each core of every length of cable. This is a quality control measure during cable production.

## 2.1.2. Type Tests

- Mechanical handling - Land cables are subjected to a bending operation in accordance with IEC recommendations for an ac cable with the same insulation. In the case of a submarine cable, bending tests are in accordance with the latest CIGRE recommendations for the mechanical tests on submarine cables.

- Loading cycles and polarity reversals - This test is made on a test length cable fitted with one component of all accessories, intended for the final cable i.e. at least one field joint, one factory joint etc. The total test length of cable and accessories must be at least 30m.

  Furthermore, the test length is then subjected to a total of 30 daily loading cycles each consisting of 8 hours heating followed by a further 16 hours of cooling. The general idea is to mimic the conditions a cable will experience when in service and check that it operates within its design parameters. For the submarine cable test, the water pressure the cable will experience when in service is also taken into account.

  The first 10 of the 30 loading cycles are made with a positive direct current voltage of $2U_0$ between conductor and sheath. This is followed by a rest period for 8 hours when no voltage or current is applied and the conductor is connected to the sheath.

  The second 10 loading cycles are made with a negative direct current voltage of $2U_0$ between conductor and sheath. This is again followed by a rest period for 8 hours when no voltage or current is applied and the conductor is connected to the sheath.

  The final 10 loading cycles are at a direct current voltage of $1.5U_0$ applied between the conductor and sheath. Starting with positive voltage, the voltage polarity is reversed every 4 hours and one reversal shall coincide with the cessation of loading current in every loading cycle

- Impulse withstand test - These tests are carried out on installations that are subject to overvoltages arising from lightning impulses or from rapid transient of internal origin. Loading currents are again used to bring the cable to its maximum temperature design value after which a negative voltage equal to $U_0$ is applied between conductor and sheath for at least 3 hours. Following this, 10 positive lightning pulses are superimposed on the - $U_0$ test voltage. A reverse test of the previous test is then made on the cable. $U_0$ is applied for a minimum of 2 hours and then 10 negative lightning pulses are superimposed. The cable should not break down during any of these tests.

### 2.1.3. After Laying Tests

- The installed HVDC cable is subjected to a negative polarity direct current voltage of 1.8 or to a direct current voltage 50% of the earlier specified impulse voltage. This test lasts for 15 minutes.

## 2.2. HVDC Extruded Cable Tests

For testing dc extruded cable systems at power transmission voltages up to rated values of 250kV the general consensus throughout the same working group as before was that established test practices such as those described in paper insulation cables should be used to the largest extent possible for extruded HVDC cables. The details of relevant changes to test procedures are outlined by the same working group. However, decisions on some aspects of the testing were made, taking into consideration the converter technologies used with these cables, the long time constants in extruded polymer insulation, routine tests and return cables.

In consideration of the voltage source converters used with extruded polymers cables it is considered that the polarity reversal tests are not necessary in this case. It is also known that extruded insulations have larger dielectric time constants. This is addressed in the recommendations for a longer voltage test in the prequalification test, essentially 120 days with no load. Furthermore, long load cycles are also introduced to the type test. These are typically 24 and 24 hour load cycles. Lastly, to verify the quality of the extrusion process during the routine test the working group advises an ac test is considered on extrusion lengths when technically possible.

## 2.3. Insulation Life

It is common practice to model the electrical ageing of insulation by an inverse power law describing the *life-line* of a cable. This shows the lifetime $L$ to vary inversely with the applied voltage $V$.

$$L = c.V^{-n}$$

From this relation it is understood that the complete lifetime of a cable can be consumed over a short period of time by applying test voltages higher than the rated voltage of the cable. This concept is used as a guideline in the procedures proposed under CIGRE's Electra 72 standard for the testing of submarine HVDC cables up to rated voltages of 800kV [28]

For existing HVDC Mass Impregnated cables a minimum operational lifetime of 30 years is a design requisite. Therefore, the *life-line* is assumed to have a slope *n=8.5, cf.* figure 2.1. However, evidence suggests that the *life-line* differs from this and that the current generation of HVDC MI cables have a longer operational lifetime. Recent findings support this idea such as the after service analysis of the 32-year-old *Gotland 1* cable [29].

Including 30 years of operational service the Gotland submarine cable withstood an accelerated ageing test as outlined in the Electra 72 type test specifications. The conclusion from this is that the *life-line* of current generation MI cables have a slope *n* equal to 9.5 or perhaps even higher (see figure 2.1), suggesting lifetimes of 60 years or more are reasonable.

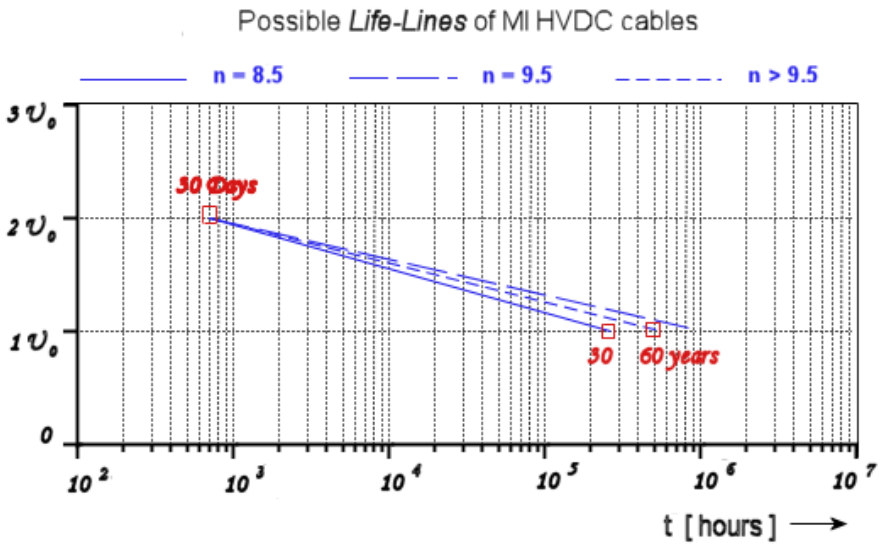


***Figure 2.1.*** *Life-Curves (MI paper insulation) [8]*

In spite of this and keeping in mind the privatisation and deregulation of electricity markets world wide it is important for operators to monitor closely these HVDC systems and try to identify any problems that arise during operation. When a potential risk is discovered in advance, procedural actions can avert damage, helping alleviate the costs of down-time and repairs in the process. From this perspective some of the on- and off-site diagnosis and analysis technologies available are presented further in this chapter.

### 2.3.1. Submarine Cable Faults

From industry data the main source of outages in a HVDC submarine cable system are found to arise from ships dropping anchor on the cables. An advisory group for CIGRE for HVDC and Power Electronics (B4.04) was established to publish reliability data on HVDC systems in service throughout the world. In 2006 the group published a report on the reliability of operational HVDC systems for the years 2003 and 2004 [30].

Utilities operating HVDC systems are asked to gather operational data in accordance with the protocols from the study committee and to submit a yearly report under these guidelines. The longest outages reported in 2003 occurred on the Fenno-Skan submarine cable between Finland and Sweden. The inter-connector was inoperable for 1692.5 continuous hours in 2003 due to a ship dropping anchor on the submarine cable. Other utilities reported line outages during the same years with many also attributed to anchor damage.

The immediate location and repair of faults is essential for any electrical system where economic implications of a fault occurring in a HVDC submarine system stems from the loss in tradable power between electricity grids that ensues. Furthermore, there is an onus on utilities to meet service standards concerning the quality of the electricity supply to customers. When a fault occurs, the quality of that supply can be jeopardised. Some of the techniques to detect and locate faults in a HVDC submarine system will be discussed in this chapter.

### 2.3.2. Stress Factors in a HVDC Cable System

To assess the integrity of a HVDC submarine cable system various stress factors must be considered. During its operational lifetime the cable and accessories are subject to a range of electrical, mechanical, chemical and thermal stresses.

Furthermore, the concept of localised degradation and system-wide (integral) degradation are important factors when considering approaches to monitor or evaluate the reliability of a cable system.

Regarding the **electrical stress**, space charge is known to directly influence the electrical field strength of insulation and its distribution. Furthermore, when field inversion occurs due to a temperature gradient across the insulation, the resulting inhomogeneous conductivity can cause the electrical stress to increase considerably at certain points in the insulation. In this case the insulation is at greater risk of breakdown.

Furthermore, an impulse voltage may arise on a HVDC line due to a flashover at a sealing end or due to a switching surge. The most dangerous situation in this case is when the impulse is opposite in polarity to the cable charging voltage. The insulation is then stressed by the whole voltage variation and the cable insulation may be at risk from high electrical field stresses.

Space charge is considered a system-wide (integral) phenomena and the technology to monitor its behavior on-site when a system is on-line does not currently exist. However, an on-line, on-site integrated measurement system has been proposed by R.Bodega for HVDC cables.

In literature, high partial discharge activity is noted to precede breakdown. Therefore, monitoring the pd activity can give insight concerning the condition of an insulation system. Dielectric interfaces are highly susceptible to partial discharge activity and from this point of view the phenomena is considered localised. Furthermore, field joints, factory joints and transition joints between land and submarine cables may all be considered as weak-points within a HVDC cable system in this respect. Test systems available to record the partial discharge activity in a cable system and the limitations of these technologies will be discussed at a later point in this chapter.

Insulation in HVDC cable systems also experience a **thermal stress**. As noted in [8] the leakage current $I_0$ of HVDC cables has a dielectric heating effect on mass impregnated insulation. At elevated ambient temperatures or electrical stress levels the leakage current increases throughout the insulation due to a rise in the conductivity. In turn, the leakage current heats the insulation further and the conductivity again rises due to its temperature dependency. This behavior continues until a balance is reached or until a thermal breakdown occurs in the insulation.

Again, a system to monitor the leakage current $I_0$ throughout the insulation could avoid a thermal runaway situation. Alternatively, technologies such as Distributed Temperature Sensing (DTS) can be used to monitor the cable temperature. This technology is already used in the NorNed HVDC interconnector between Norway and The Netherlands and will be further discussed later in this chapter.

The **mechanical stresses** on a submarine HVDC cable include mainly tensile forces and the effects of water pressure at different sea depths throughout the cable system. During the laying and operation of a HVDC submarine cable the system experiences tensile bending stresses. Furthermore, a normal recovery occurs when a HVDC cable is exposed on the seabed floor and is no longer in its trench. In this case high normal recovery tensile stresses arise when the cable is been replaced. Different calculations to determine typical tensile stresses above and below 500m are outlined in Electra 72.

**Chemical stresses** manifest during processes of dielectric ageing and via corrosion effects. In Mass impregnated paper the degradation of cellulose weakens the mechanical (tensile) strength of the insulation creating by products such as moisture, furfurals and acids in the process thereby decreasing its electrical strength at the same time. In this thesis Dielectric Spectroscopy measurements in the frequency domain are used to analyse the degradation of mass impregnated (cellulose) insulation. This technique is discussed further on in this chapter and a closer examination of the molecular dynamics of mass impregnated paper is given in chapter 3

# 2.4. Insulation Monitoring in HVDC Cable Systems

This section introduces systems used to monitor the integrity of cable insulation. The test systems are subcategorised into on-site and off-site solutions. Some of the systems described have been used primarily in the past to monitor ac cable systems. However, the application of these techniques to dc systems is equally valid in consideration of the various insulation stresses described in section 2.3.2. Furthermore, the systems introduced here have some limitations which are discussed on a case by case basis.

## 2.4.1. On-Site Insulation Monitoring

### 2.4.1.1. On-Site off-line Dielectric Spectroscopy Measurement System

This system was developed at The Technical University of Stockholm, Sweden. It was originally designed to investigate medium voltage XLPE power cables, especially those degraded by water treeing. The high voltage field system is based on a laboratory system that is capable of high voltage and low voltage dielectric spectroscopy measurements also.

The field system is modified to measure both earthed and non-earthed long cables having large capacitances. For large capacitance cable test objects the upper test frequency is limited by the current limit of the high voltage amplifier shown in figure 2.2. The voltage range for this test system is between 0 and 14*kV* or 20 $k\hat{V}$ with a frequency range between 10mHz and 100Hz. This system is capable of resolving $\tan(\delta)$ losses as low as $1 \cdot 10^{-4}$

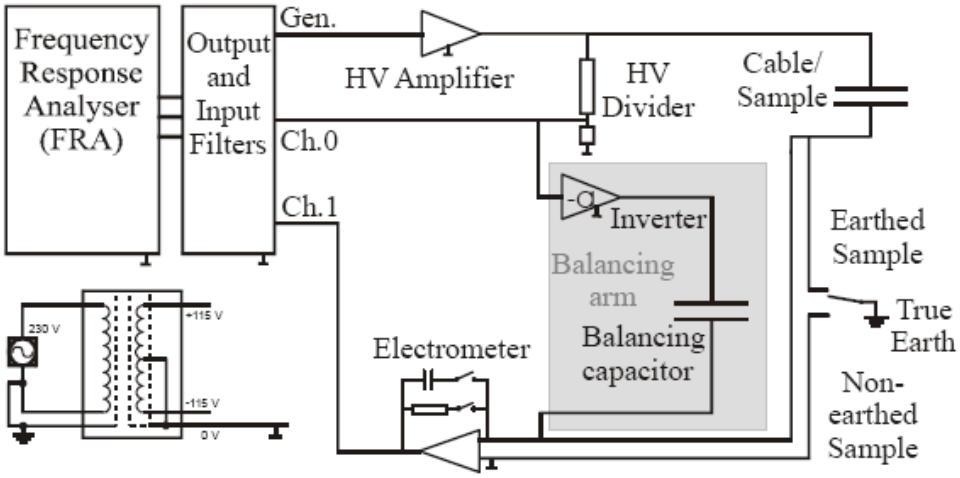


***Figure 2.2.*** *on-site off-line dielectric spectroscopy measurement system*

The system operates whereby the frequency response analyser generates a sinusoidal signal that is amplified in the high voltage generator. For low voltage tests the output from the frequency response analyser can be applied directly to the test object.

The low voltage arm or the voltage divider is fed to the balancing arm where it is inverted, adjusted and applied to the balancing capacitor. The balancing capacitor has the effect of reducing the major part of the sample displacement current. The sum of the currents from the sample and the balancing arm is then passed to channel 1 of the frequency response analyser through an electrometer.

The recorded signals are then used to calculate the dielectric response at the measurement frequency. The balancing arm reduces the current entering the electrometer. This enables the measurement of small change in the loss and capacitive components of the permittivity.

For earthed samples such as an on-site cable, the electrometer input, the ammeter, is connected to earth and the system-signal earth is left floating. This system was designed to be insensitive to noise and hum where the set-up is connected to true earth at one single point and the lead loop areas are kept as small as possible.

### 2.4.1.2. Baur Cable Test and Diagnostic TD – VLF System

The Baur programmable high voltage generator is a very low frequency (VLF) on-site test system. Additional $\tan(\delta)$ (TD) dissipation factor and partial discharge measurement upgrades are available for this system. The partial discharge measurement can localize the source of the measured discharges in a cable system.

The test system measures at a test voltage of $57\,kV_{rms}$ at a fixed frequency between 0.01Hz and 1Hz. Furthermore, square wave and DC test voltages up to $80kV$ / 0.1Hz and $\pm$ 80kV respectively are possible. The limitation to this system is the maximum load capacity. The load diagrams are depicted in figure 2.3.

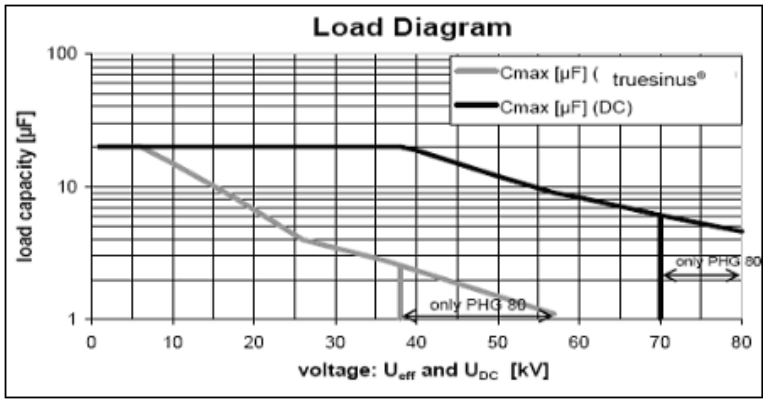


***Figure 2.3.*** *Baur system load diagram*

### 2.4.1.3. Damped sinusoidal Alternating Current (DAC) Test Voltage

Damped sinusoidal AC (DAC) test equipment is used for on-site off-line testing and diagnosis of AC power cables. This test system can detect and localise partial discharges, record dielectric losses and perform voltage withstand tests. The technique is referred to as Complex Discharge Analysis (CDA) or by the acronym OWTS (Oscillating Wave Test Voltage) [32].

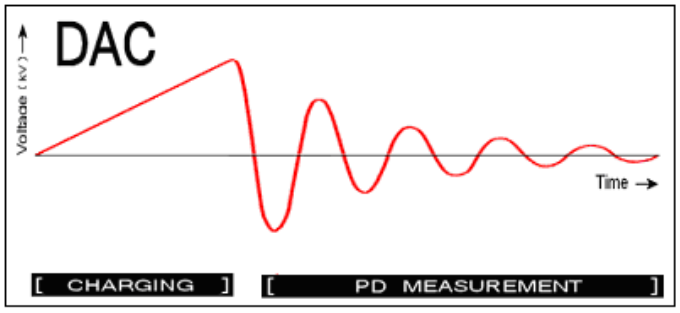


***Figure 2.4.*** *Damped AC (DAC) test voltage*

DAC test equipment is already used for AC applications and the measurement principle is applicable to on-site HVDC cable systems. During testing, both ends of the cable are first disconnected and the cable is then energised by the test unit. A linear DC charging current energises the cable to a selected test voltage and the voltage source is then switched off. This process is depicted in figure 2.4.

After the switching operation the RLC circuit loop creates a damped AC test voltage. Traveling wave analysis involving statistical evaluation methods is then used to localise the partial discharge activity in the cable system. Figure 2.5 shows an example of recorded partial discharges and some statistical mappings.

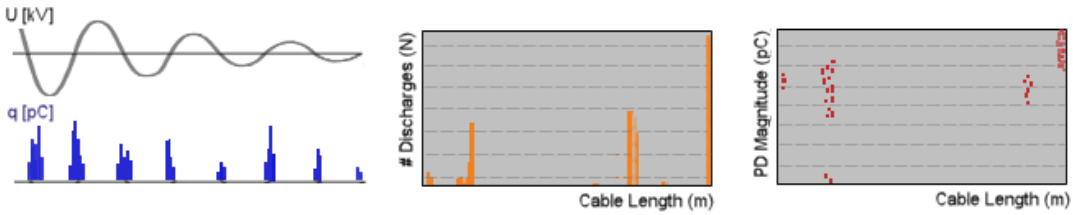


***Figure 2.5.*** *Partial discharge measurement and analysis*

When testing a HVDC submarine cable the excitation voltage should ignite partial discharges in the cable, transition joints and field joints which are present during normal operation. The OWTS has a maximum test voltage of $150\,k\hat{V}$ . The frequency range of the damped ac test voltage is between 20Hz and 500Hz. The capacitive range for the HVDC cable system under test is between $0.025\,\mu F$ and $13\,\mu F$ . The power limitations of this system permit only a selected part of the HVDC cable to be interrogated within a

specified timeframe. The exact length is determined by the capacitance per meter of the cable system. Furthermore, the badwidth for PD localization is 150kHz to 45MHZ.

#### 2.4.1.4. UHF and Acoustic Emission sensors for Partial Discharge Measurement

Fast displacements of partial discharges in insulation introduce propagating electromagnetic waves that are measurable by Ultra High Frequency (UHF) wideband probes. This measurement technique is already widely used for partial discharge detection. Furthermore, it also has application for the condition assessment of Gas Insulated Switchgear (GIS) and transformers where direct current Gas Insulated Switchgear (dcGIS) rated at $\pm 500$kV have been in development since 1995. The technology is already in use for HVDC switchgear (dcGIS) in the converter stations for the Kii Channel HVDC system in Japan. This system has the highest power transfer capability to date of any submarine line.

UHF detectors have a high sensitivity over a broad frequency range and they are screened from external interference. However, various drawbacks exist. In dcGIS for instance, there is still not a clear understanding of the propagation characteristics of the electro-magnetic waves arising from the structure of the equipment. Furthermore, the equipment must be earthscreen free or the probe must be integrated into the system in an intrusive manner, increasing the possibility of partial discharge ignition.

Therefore it is infeasible to envisage a network of UHF probes throughout a HVDC cable. However, if the transition joint between the land and submarine cable is accessible then UHF sensors could be used to monitor this localised point.

An alternative system to the UHF probes for partial discharge measurement in a HVDC system is an acoustic probe. This technology uses Acoustic Emission (AE) sensors to detect discharges. AE sensors are not prone to external noise and are highly sensitive. The sensors are non-intrusive with external mounting and are capable of locating the source of discharges during operation.

Again, a network of AE probes throughout a HVDC line is impractical, especially over long distances. However, this author proposes that these sensors are integrated to a HVDC cable over one delivery length for the land cable, over one delivery length of submarine cable in shallow water and over one delivery length of deep sea cable. In doing so this should give an integral assessment of the HVDC cable insulation system.

Furthermore, a second system of sensors, strategically placed at field joints, factory joints and transition joints will give a localised assessment of the cable system Joints are regarded as weak points in any cable system. Monitoring the behavior at the joints might therefore help identify potential problems somewhere in the HVDC cable system.

### 2.4.1.5. On-Site on-line Space Charge Detection

An on-site on-line space charge detection system is proposed by R.Bodega [10]. In theory, the pulsed electroacoustic space charge detection unit interrogates only a small section of the cable length. The size of this section is determined by the length of the piezoelectric sensor which is a few centimeters in length at most.

It is proposed in [10] that this system is integrated to a portion of the cable that is subject to the highest stresses throughout the system. This is typically at the location of a cable joint where the maximum electrical field might be regarded as some characteristic for the cable. Through careful analysis and record of the space charge and electric field distributions over many years the information could then be correlated to the aging state of the insulation. Furthermore, the risk of a breakdown could be accessed based on knowledge databases.

The proposed pulsed electroacoustic device is mounted inside a perfectly sealed compartment integrated into the cable as shown in figure 2.6. Furthermore, the thermal properties must be considered during the design process of such a devise so it does not interfere with the normal operation of the cable system.

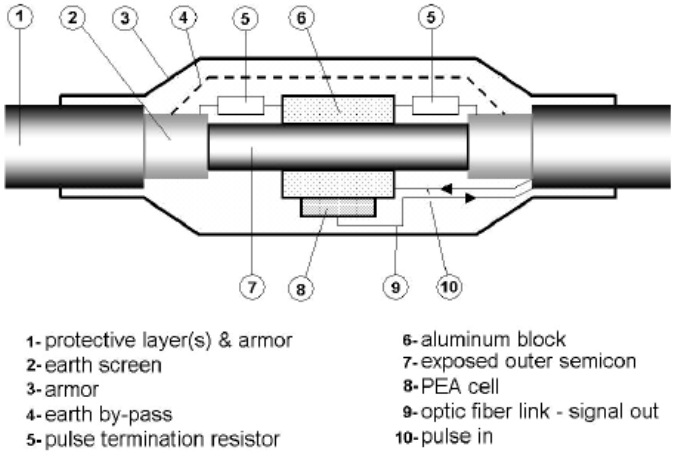


***Figure 2.6.*** *On-line on-site space charge detection in HVDC cables*

In figure 2.6 the space charge detection unit is designed to integrate seamlessly to the cable system. The device is contained within a perfectly sealed armored compartment that is sealed together with the armor of the cable. Furthermore, a bypass earth screen guarantees the integrity of the cable systems earth screen.

The device applies a pulse through an aluminum electrode to the semiconductor screen. The return pulse carrying the space charge information returns to the pulsed electroacoustic cell through the aluminum block used as the injection electrode. This also acts as a delay line for the acoustic return signal. The cell not also converts the acoustic signal into an optical signal which is then sent to the line operator via an optical fibre link.

### 2.4.1.6. Distributed Temperature Sensing (DTS)

A Distributed Temperature Sensing system is an on-site on-line technique where a detection unit receives data from a distribution of independent measurement points throughout a cable system. Optical fibers are ideal linear sensors in a cable system where temperature variations due to hotspots (at cable joints etc.) change the characteristics of the light transmission in the fibers. The resulting real time management system allows system operators to [33][34];

- confidently load and overload cable circuits
- identify high temperature points throughout the cable system
- record the thermal history to help determine the remaining life
- avoid early breakdowns.

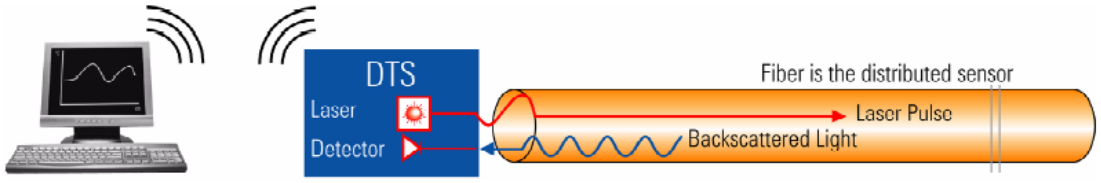


***Figure 2.7.*** *DTS System [34]*

Multi-mode step index fibers can be used for short spatial range and low spatial resolution while multi-mode graded index fibers and single-mode fibers can be chosen for long spatial range and high resolution. In general, the thermal effect at a point in a cable system induces lattice oscillations within the fiber and there is an interaction between the light photons and the molecules electrons.

The incident light in the fiber is subsequently scattered back to the source by this interaction. The returned spectrum contains a Rayleigh scattering component, a Stokes component and an Anti-Stokes component as shown in figure 2.8. Stokes line components have longer wavelengths than the Rayleigh scattering and the anti-Stokes line components have lower wavelengths. The Rayleigh light is the same wavelength as that of the laser and it can be used to identify the spatial properties of the cable. The Stokes and anti-Stokes bands are temperature dependent and temperature independent respectively and the ratio between the two returning light spectra identifies local temperature profiles.

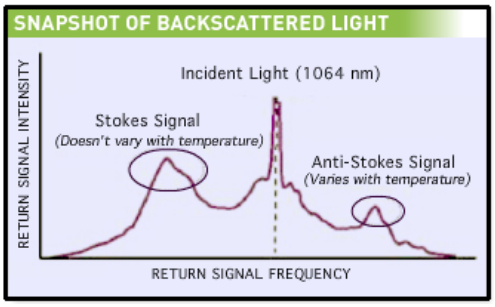


***Figure 2.8.*** *Returned Spectrum [34]*

The effects of light scattering in optical fibers are classified according to the relation between frequencies of incident and scattered photons. When incident and scattered frequencies are equal this is an instance of elastic scattering, like in Rayleigh scattering where a fraction of the optical power in one propagation mode is transferred linearly to another mode. Rayleigh scattering is a result of random inhomogeneities that occur on small scales with respect to the wavelength of light. These inhomogeneities exhibit fluctuations in the refractive index and are mainly because of the density and composition variations arising in the silica during the cooling process.

If the frequencies of incident photons and scattered photons differ then this is a case of inelastic scattering. An example of inelastic scattering is Raman scattering where the frequency shifts are equal to characteristic vibration frequencies of the molecules. A measurement of the ratio between Stokes and the anti-Stokes back-scattered light in a fiber should provide an absolute indication of the temperature of the medium, irrespective of the light intensity, the fiber geometry and even the fibers composition.

This technology presents two possible measurement techniques, Optical Time Domain Reflectometry (OTDR) and Optical Frequency Domain Reflectometry (OFDR). OTDR is the most common technique. In principle, this uses the propagation time of the back scattered light, in a direction 180 degrees from an injected laser pulse to determine the location of the temperature event. The back scattering is the combination of Rayleigh scattering caused by the density and structure of the material and Raman and Brillouin scattering occurring due to molecular and volumetric vibrations.

Temperature dependent Brillouin scattering is difficult to separate from Rayleigh scattering and for this reason the temperature dependent Raman scattering is focused on. The scattered light spectrum is dominated by Rayleigh scattering but also contains contributions of Raman scattering.

Spatial resolution is determined by the pulse width of the laser. An increased pulse width gives an increased power rating of the laser and so longer cables can be interrogated but at the expense of a decreased spatial resolution. For this reason there is a trade-off between cable length analysis and spatial resolution.

The parameters affecting the system performance are as follows:

- Fibre Length (spatial range)
- Spatial resolution and sampling interval
- Temperature resolution
- Measurement time
- Thermal response time

Alternatively, OFDR gives information on the local characteristic of the temperature event. For this technique, measurements are made in the frequency domain and it is therefore an offline process in some respects, performed when the full measurement data is retrieved.

DTS systems are typical of modern HVDC submarine cable systems where monitoring distances greater than 30 km are feasible. An example of one such system using DTS technology is the NorNed cable between Norway and The Netherlands. At the coast of The Netherlands a 28 km portion of the cable is fitted with a fiber optic DTS system embedded into the armouring. This area of the cable is monitored because this particular area of the sea bottom morphology is prone to considerable changes in temperature.

The sensitivity of such systems is interdependent on the temperature and spatial resolutions and the overall range of the system. Operational systems have typical temperature spatial resolutions of 1 meter with an accuracy of $\pm 1^{\circ}C$ at a resolution of $0.01^{\circ}C$ .

### 2.4.1.7. Idax-206 Dielectric Relaxation Analysis [ Semart ]

Pax Diagnostics have designed an on-site frequency domain dielectric spectroscopy test system (Idax-206) to investigate the integrity of medium voltage XLPE and Mass Impregnated power cables. The measurement and analysis technique for the Idax-206 system were developed extensively at The Royal Institute of Technology in Stockholm. This system records the capacitance and $\tan(\delta)$ at voltages between $0V$ and $200\hat{V}$ covering a broad range of frequencies between 10mHz and 1kHz.

An additional high voltage VAX-230 accessory is connected to the Idax-206 to increase the maximum output voltages to 30 $k\hat{V}$ where $I = |j\omega CU|$ < 30 *mA.* In operation, the Idax system generates a signal at the desired frequency using a digital signal processing unit. This signal is subsequently amplified and then applied to the sample. The voltage across the cable and the current though the cable insulation are then recorded. These measurements are then multiplied by reference harmonic voltages and integrated over a number of cycles in a process that rejects the noise and interference components. The Idax-206 instrument and the sine wave correlation technique are shown in figure 2.9.

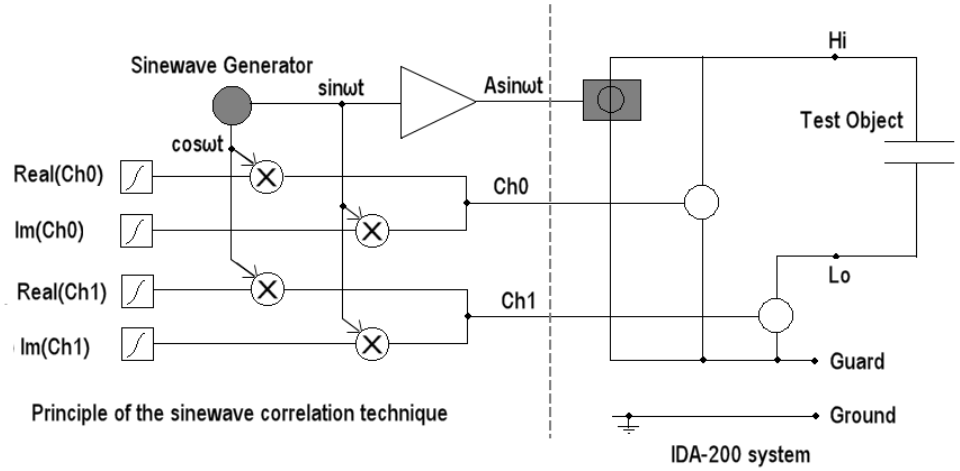


***Figure 2.9.*** *Principle of the Idax-206 instrument*

## 2.4.2. Off-Site Insulation Monitoring

### 2.4.2.1. Off-site Space Charge Detection

The archaic *field mill* and *capacitive probe* methods are today replaced by non-destructive measurement techniques to locate space charge in solid dielectric insulation.

The principle of non-destructive space charge measurements are fundamentally the same in nature whereby some physical quantity, $\alpha_1$ in figure 2.10, is applied to a test sample. When this physical quantity encounters space charge they interact, or it generates a second physical quantity $\alpha_2$ that can be measured [8].

This secondary signal is proportional to the charge distribution in the sample. The signal is detected at a sensor and the information it contains is used to locate, identify and quantify the space charge present within the dielectric insulation.

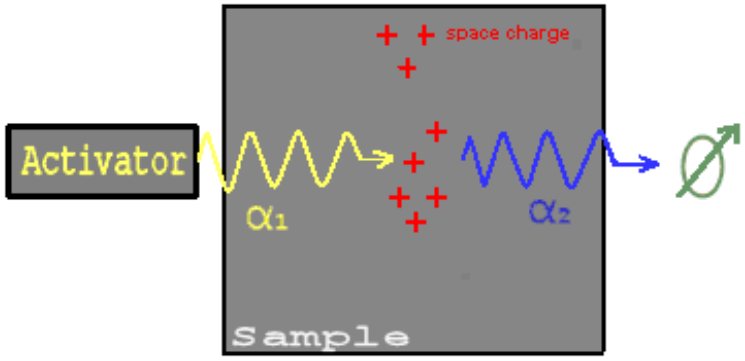


***Figure 2.10.*** *Space Charge Detection Principle*

The physical quantities produced by the activator are typically temperature, pressure, electric voltage or current [8].

As previously mentioned in chapter 1, when the space charge distribution is known the field distribution throughout the sample can be calculated by combining the following equations;

$$\nabla^2 U = -\frac{\rho}{\varepsilon_0 . \varepsilon_r} \qquad \text{and} \qquad \vec{E} = -\nabla . V$$

The non-destructive space charge measurement techniques can be summarised as follows;

- The ***Thermal Pulse / Step Methods*** [8][10] both produce a temperature wave that propagates through the insulation sample and displaces any space charge it encounters. This displacement of charge then produces a measurable electrical signal at the external electrodes

- The ***Thermal Pulse / Step Methods*** [8][10] both produce a temperature wave that propagates through the insulation sample and displaces any space charge it encounters. This displacement of charge then produces a measurable electrical signal at the external electrodes.

- The ***Laser Intensity Modulation Method*** [8][10] creates propagating temperature waves from both sides of a flat test specimen. A measurable pyroelectric current results from the interaction of the temperature waves with space charge.

- ***Optical techniques*** [10] are used where the electrical or mechanical stresses in a transparent insulation cause a measurable phase shift in a polarised light incident on the test sample. Analysis of the phase shifted light and knowledge of the optical properties of materials under stress can give details about the magnitude of the mechanical and electrical stresses present.

- The ***Piezo-electrically Induced Pressure Pulse (PIPP)*** [8][10]technique generates a pressure pulse after applying an electrical source to a piezoelectric crystal.

- The ***Laser Induced Pressure Pulse (LIPP)*** [8][10] produces a pressure pulse by focusing a laser on one of the electrodes.

- The ***Non-Structured Acoustic Pulse*** is a pressure pulse generated by a high voltage spark between a conductor and a diaphragm.

- The ***Pulsed Electro-acoustic*** method [8][10][11] applies an electrical pulse to a test specimen perturbing the space charge it encounters. A resulting acoustic wave then propagates away from the perturbation and this can be measured at a sensor.

Furthermore, it is anticipated that future development in these non-destructive space charge measurement techniques will give further insight to the conduction mechanisms, the charge carrier types and the degree of ageing in a dielectric insulation [10].

### 2.4.2.2. Off-site Partial Discharge Detection

The principle techniques in partial discharge measurements are the same for DC and AC. However, the analysis and interpretation of the measurement results differ.

At AC voltages the bipolar discharges are energised by a capacitive field and the phase and magnitude of these discharges are subsequently measured. However, at DC voltages the different field situations make the analysis more complicated. In service, HVDC equipment experience resistive, capacitive and intermediate fields with varying partial discharge behavior.

The physical behavior of these partial discharges are well represented by the a,b,c-model for a capacitive field situation. However, in intermediate and resistive field circumstances the a,b,c-model demands a slight modification where leakage resistances in parallel with capacitances a,b and c account for the polarisation effects and leakage current within the dielectric. The modified abc-circuit for a dielectric containing a discharging void is shown in figure 2.11.

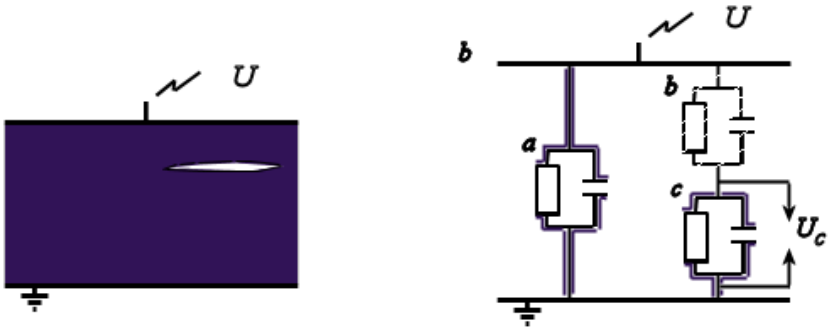


***Figure 2.11.*** *Insulation cavity and modified abc-model*

In figure 2.12 the time between successive discharges is $\Delta t = t_r + t_l$. The recovery time $t_r$ is the time to raise the voltage over the void from the residual voltage $U_r$ to the minimum breakdown voltage $U_{\min}$. The waiting time $t_l$ is time elapse until there is a starting electron and a subsequent breakdown and discharging of the void.

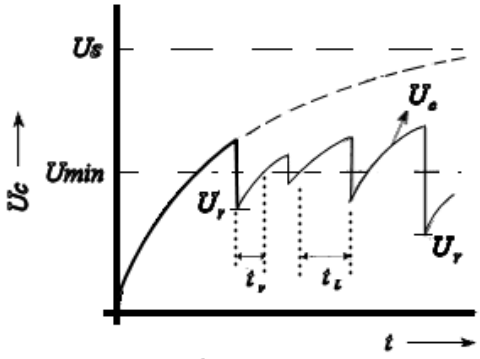


***Figure 2.12.*** *Partial Discharge Process*

The repetition rate of partial discharges $n$ is proportional to the asymptotic voltage across the void $U_s$ which itself increases linearly with the externally applied field. Therefore, $n$ is proportional to the external voltage. Also, $n$ increases when the minimum breakdown voltage $U_{\min}$ is decreasing. Furthermore, the closer the values of $U_r$ and $U_{\min}$ are the higher is the repetition rate, $n$.

The discharge frequency is often higher during the capacitive field stage than in the intermediate or resistive field stages under operational circumstances and for this reason this stage should not be ignored [9]. In the standard 270 [31] document are the standard test configurations for the measurement of partial discharges. The straight detection circuit in figure 2.13 is one such test circuit.

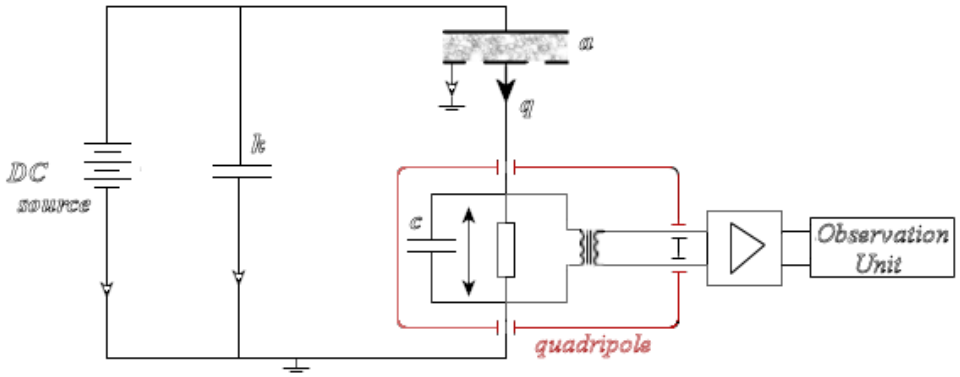


***Figure 2.13.*** *Straight Detection Circuit*

In the straight detection test circuit the discharges are detected as electrical pulses of height $\hat{v}$ in the detection impedance, otherwise known as the quadripole. In the main circuit a coupling capacitor $k$ acts as a path for the high frequency pulses. The pulses which are proportional to the partial discharge magnitude $q$ are then amplified and recorded at the observation unit.

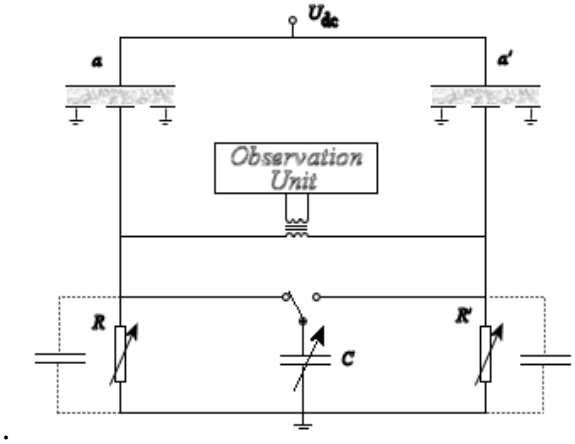


***Figure 2.14.*** *Balanced Detection Circuit*

An alternative measurement circuit for high sensitivity partial discharge measurements is the balanced (bridge) detector shown in Figure 2.14. This test circuit can localise the origins of the partial discharges and dampen external interference signals by adjusting $R$ and $C$ and balancing the bridge.

These widely used approaches often record the integral of the current displacement in a circuit external to the test object. In doing so, the time of occurrence $t$ and magnitude $q$ of partial discharges are recorded during the resistive, *pure* DC stage. However, it is frequently the case where the magnitude $q$ and the time between successive partial discharges $\Delta t$ are stored in memory (see figure 2.15).


***Figure 2.15.*** *Successive Partial Discharges*

The test circuit when upgrading the transmission capacity of the Fenno-Skan HVDC cable is shown in Figure 2.16.

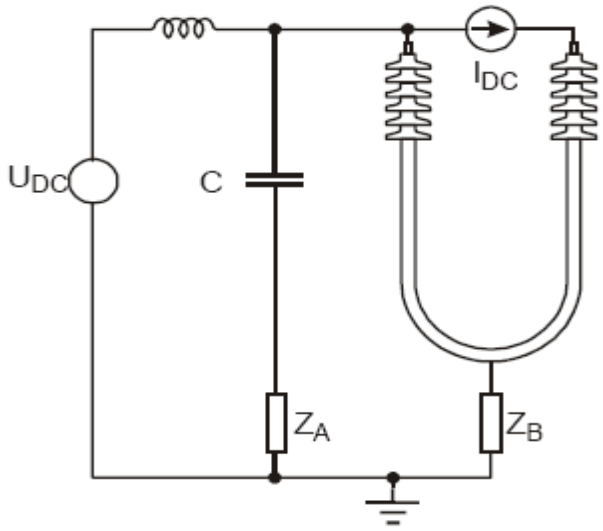


***Figure 2.16*** *Partial discharge test circuit for the uprgrading of the Fenno-Skan HVDC cable*

In this arrangement two partial discharge measurement systems measure the voltage over the impedances $Z_A$ and $Z_B$. The test system differentiates between external interference and discharges within the cable by ignoring pulses that are the same polarity and recording those of opposite polarity. For the Fenno-Skan study the registered partial discharge pulses during a time period $\Delta t$ were converted to an average partial discharge current as mentioned in chapter 1.

In general however, post measurement processing using statistical analysis or alternative methods of data representation are used to develop a system of fingerprinting. This is where different discharge characteristics can be cross-checked and used as identification markers. There are various ways to represent the recorded data offline

### 2.4.2.3. Off-site Dielectric Relaxation Analysis

In this thesis, **Broadband Dielectric Spectroscopy (BDS)** is used to investigate the frequency domain dielectric relaxations in Mass Impregnated insulation. The dielectric relaxation in cable insulation is due to the recovery of strain in the material after the removal of some external stress. The stress in this case is a harmonically varying electrical field with angular frequency $\omega$.

The response of any dielectric structure has a characteristic relaxation frequency or frequency band [11]. Here, the lower frequency band is investigated and the resulting spectral graphs depict the in-phase component $\varepsilon'(\omega)$ and the quadrature component $\varepsilon''(\omega)$ of the permittivity. Furthermore, these are effectively the capacitive and loss components of the permittivity respectively.

When analysing the dielectric relaxation in a material it is convenient to investigate $\tan(\delta)$ as a function of the frequency. This reveals the phase difference between the applied harmonic field and the resulting current through the sample. Furthermore, this has advantages when analysing subtle polarisation loss peaks which may not be so clearly evident in $\varepsilon''(\omega)$.

Traditional $\tan(\delta)$ measurements in electrical engineering measure at the power frequency, at 50Hz or 60Hz. However, at lower frequency, below the power frequencies, the behavior of $\tan(\delta)$ can reveal more about the condition of the insulation, especially through careful analysis of the dc conductivity contribution.

The dc conductivity is recognisable when the slope of $\varepsilon''(\omega)$ on a log-log scale has a value of -1. This indicates the extent of the conduction current in the insulation and can be directly related to its condition. Additionally, the aforementioned loss peaks represent dipole relaxation processes which in some cases are the result of byproducts due to material degradation.

The complex permittivity and $\tan(\delta)$ are functions of temperature. Therefore a 3D plot of $\tan(\delta)$ for instance as a function of temperature and frequency reveal the temperature dynamics of the response also. The dynamics of the dc conductivity and relaxation processes are thus also used in the dielectric analysis of the insulating material.

A typical 3D graph of $\tan(\delta)$ in figure 2.17 shows the low frequency behavior of a Mass Impregnated sample as a function of frequency and temperature. The analysis of graphs like this are explained in more detail in chapter 5.

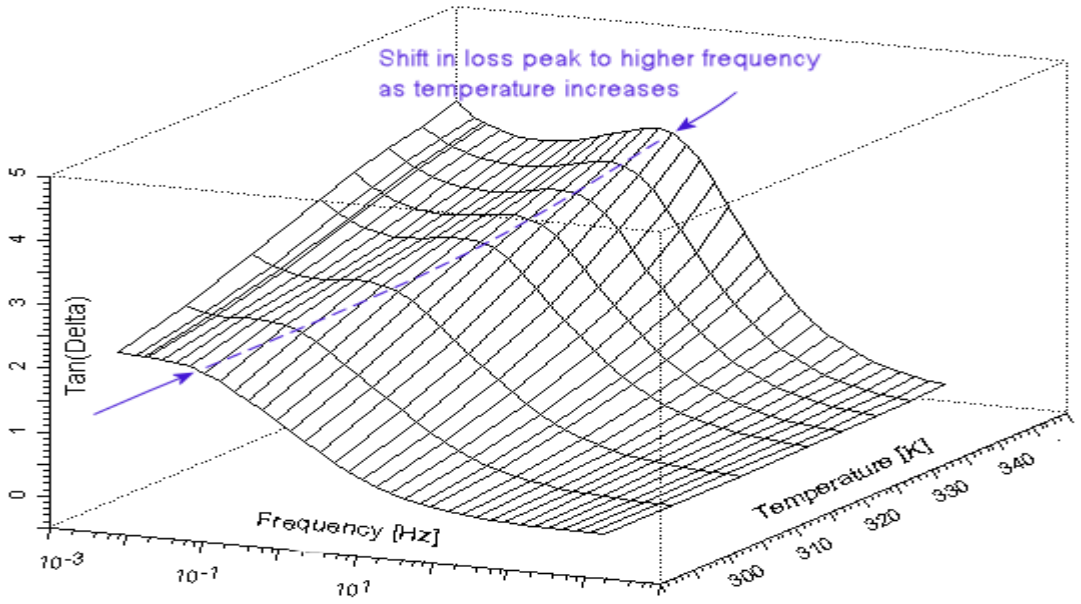


***Figure 2.17.*** *3D dielectric spectroscopy result*

The application of frequency domain dielectric spectroscopy is equally as valid in the analysis of dc insulation samples, regardless of the fact that a harmonic excitation is used. As noted already, the low frequency spectrum is often characterised by a dc conductivity term or by a low frequency dispersion effect.

The dc conductivity, identified as a slope of -1 on a log-log $\varepsilon''(\omega)$ graph gives an indication of the condition of the insulation sample. Intuitively, samples with higher losses should then exhibit a shift in the dc conductivity term at low frequency to higher values. Furthermore, relaxation loss peaks can indicate the presence of ageing by products. This is investigated further in chapter 5.

Therefore, relaxation characteristics such as dc conductivity and relaxation loss peak contributions can be used as identification markers in assessing the integrity of dc insulation. A knowledge base can be developed to compare measurements with a database containing previous results. In essence, the database entries are identification markers which can give an indication of the test samples condition. The outcome is an assessment of the integrity of the dc insulation based on previous findings.

The principle of operation of the Novocontrol frequency response analyser is depicted in figure 2.18.

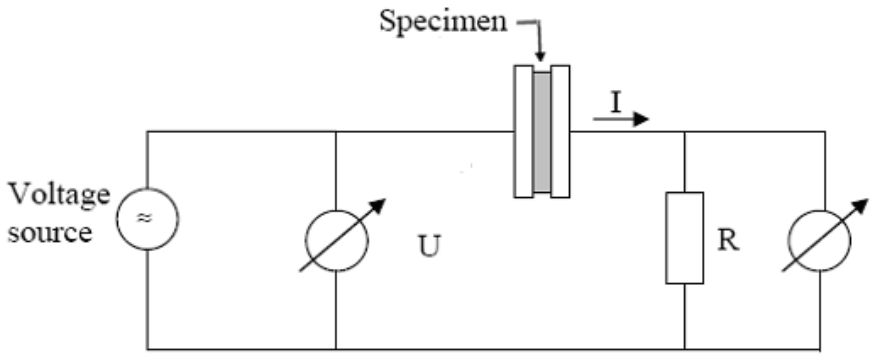


***Figure 2.18.*** *Frequency Response Analyser Circuit Model*

The dielectric specimen under analysis is placed between two metallic electrodes in a parallel plate capacitor arrangement. An excitation voltage $U$ with angular frequency $\omega$ is then applied to the test specimen. The excitation has an operational test voltage of $1V$ or $3V$ with a range of measurement frequencies between $3\mu Hz$ and $20MHz$.

Phase sensitive voltmeters measure the amplitude and the phase of the voltage and the current through the test sample where the resistance $R$ converts the sample current to a representative voltage signal for the second voltmeter. The complex impedance $Z$ of the specimen is then recorded by the analyser,

$$\text{Complex Impedance: } Z = \frac{U}{I}$$

When $Z$ is recorded and the geometry of the sample is known the complex permittivity can then be found as follows

$$\text{Complex Permittivity: } \varepsilon = \varepsilon' - i\varepsilon'' = C\frac{d}{\varepsilon_0 A}$$

.

by substituting the complex impedance $Z$ with the sample capacitance $C$.

The test circuit is held in a cryostat with an adjustable temperature range between $-160\,^{\circ}C$ and $400\,^{\circ}C$ controlled by gas heaters and a liquid supply of nitrogen.

In **Time Domain Dielectric Relaxation Analysis**, the polarisation current, $I_{pol}(t)$ the de-polarisation current $I_{dpol}(t)$ and the return voltage measurement (RVM) are used to characterise a dielectric insulation, shown in figure 2.19.

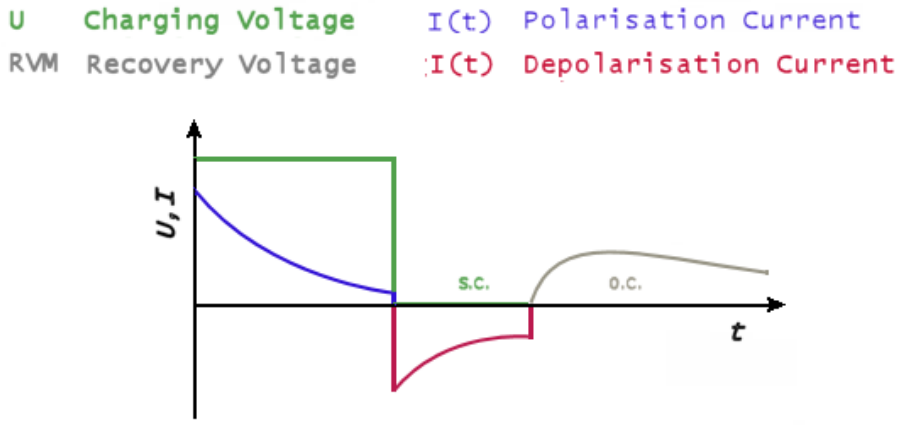


***Figure 2.19*** *Time domain dielectric relaxation measurement*

When a step voltage is applied to a fully discharged test object a polarisation current ensues, exhibiting a decreasing characteristic and eventually settling to a steady state value known as the conduction current.

The polarisation current consists of two parts, one representing the many polarisation processes in the material and the other a conductivity term. When the voltage source is removed and the terminals of the sample are short circuited a depolarisation current flows which fully characterise the relaxations within the medium.

$$I_{pol}(t) = C_0 U_0 \left[ \frac{\sigma_{dc}}{\varepsilon_0} + \varepsilon_\infty \delta(t) + f(t) \right]$$

$$I_{dpol}(t) = -C_0 U_0 \left[ \varepsilon_\infty \delta(t - t_1) + f(t - t_1) - f(t) \right]$$

The dielectric response function *f(t)* can be ascertained from $I_{pol}(t)$ or $I_{dpol}(t)$ as is clear from the above equations. The influence of the conductivity is shown in figure 2.20 where $I_{pol}(t)$ and $-I_{dpol}(t)$ deviate somewhat as time develops.

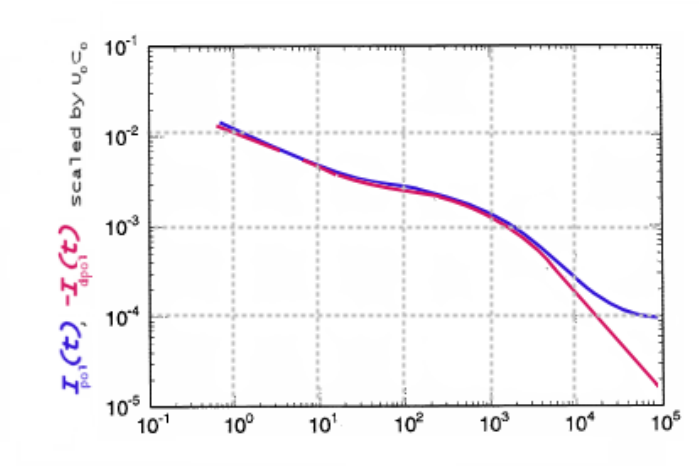


***Figure 2.20.*** *Polarisation and depolarisation currents*

The Return (recovery) Voltage Measurement investigates the slow polarisation processes which are not fully relaxed during the depolarisation current measurement stage and are therefore not identified. Subsequently, the test specimen is open-circuit and induced charges on the electrodes resulting from persisting relaxations contribute to a return voltage. The RVM method is a popular technique for the on-site diagnostics of bulk dielectric properties. Furthermore, it is claimed that the RVM spectrum can be used to quantify the moisture contents in a transformer pressboard composite insulation.

#### 2.4.2.4. Off-site Schering Bridge Loss Measurement

The Schering Bridge is a very sensitive loss measurement test with potentially very high accuracy in the results. In principle, a high voltage is applied to one diagonal of a bridge circuit and a null detector is applied to the opposite diagonal. This is shown in figure 2.21.

The impedances $Z_{2-4}$ are adjusted until the null detector indicates zero. The impedance of the test object $Z_1$ and the subsequent loss measurement $\tan(\delta)$ are then found through the relation $Z_1 : Z_3 = Z_2 : Z_4$ when the bridge is balanced. This loss measurement is typically at the 50Hz power frequency.

Furthermore, the sensitivity of this measurement is high when the ratio between the applied voltage $U$ and the smallest detectable voltage at the null detector $\Delta U_0$ is large. This sensitivity can be as low as $1 \cdot 10^{-8}$ [14].

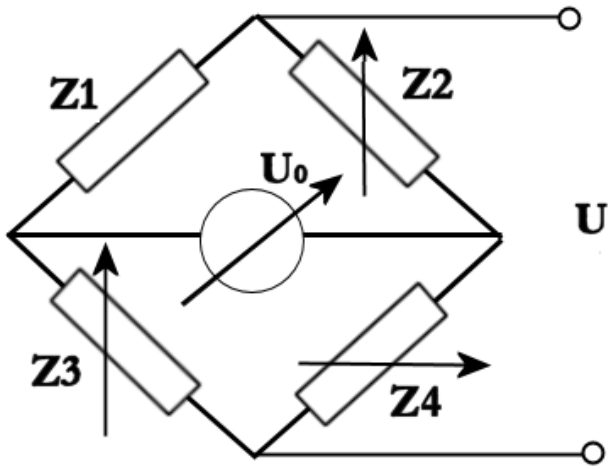


***Figure 2.21*** *Schering Bridge*

# 2.5. Fault Location Techniques

## 2.5.1. Traveling Wave Based Fault Location [36]

This traveling wave based fault locating system for HVDC transmission lines integrates a traveling wave acquisition and processing unit, a communications channel and a control station together into one functional system that has proven reliable and accurate in operation. The system records the traveling waves indirectly as induced signals in the grounding leads of the transmission lines over voltage suppression capacitors. This is made possible using specially designed traveling wave couplers as shown in figure 2.22.

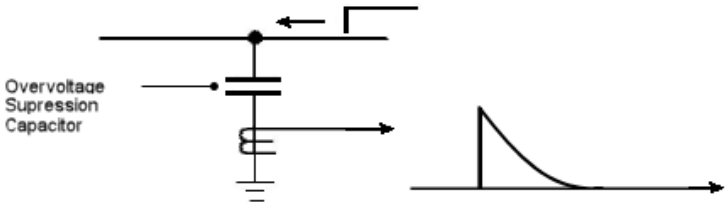


***Figure 2.22*** *Measuring Impulse Flowing Through Overvoltage Suppression Capacitor*

The traveling wave based system supports modern double ended and single ended traveling wave measurement techniques simultaneously. Transient current and voltage waves propagate in two directions away from faults when they arise.

The type D double ended principle measures the transients at both ends of the HVDC transmission line and determines the fault location depending on the absolute arrival times of the waves. This principle uses Global Positioning to synchronise the clocks at the two ends of the transmission line.

The Type A principle uses single ended measurements, recording reflected waves from the fault and those reflected from the opposite end of the transmission line. Type A is used in validating the results from type D recordings in this case.

The system is in use on the 2175MW 500kV Gezhouba – Shanghai HVDC system in China where a maximum error of 3 km was found when locating faults over the 1046 km line. The structure of the fault locating system is presented in figure 2.22, a slight variation and more generic representation of the system in use on the Gezhouba – Shanghai HVDC system.

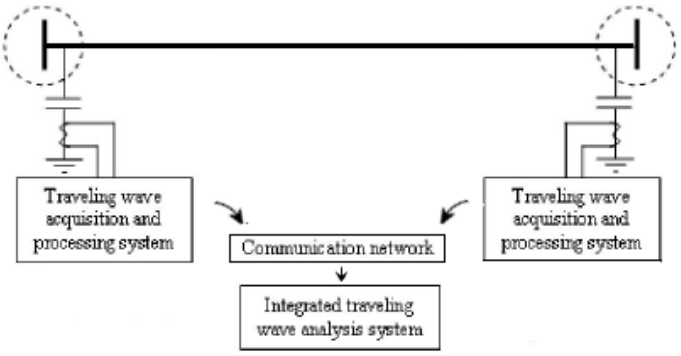


***Figure 2.22.*** *Structure of the Fault Locating System*

## 2.5.2. Alternative Fault Location Techniques

Faults can be located with precision using a combination of high voltage pulse generators (thumpers) with Time Domain Reflectometry (TDR) measuring the traveling time of the reflected voltage waves. This TDR measurement principle is similar to that used in the Gezhouba – Shanghai HVDC transmission system.

Furthermore, for more accuracy in the fault location technique power pulse generators create a flashover at the location of the fault which is subsequently recorded by microphones.

# 3. Mass Impregnated Insulation

In any field of study the interpretation of test results is crucial, especially for concluding remarks based on experimental observation. The validity of a relaxation analysis is often related to some knowledge of the physical structure of the material and its behavior as a function of temperature, pressure etc.

For this reason it is worthwhile to include a chapter in this thesis work relating to the physics of Mass Impregnated paper and how this knowledge is applied when interpreting the results of dielectric spectroscopy measurements.

In section 3.1 the structure of cellulose paper and the process of oil impregnation are explained. The steps involved in the production of an existing submarine HVDC Mass Impregnated cable are then discussed.

In Section 3.2 the processes of degradation in Mass Impregnated insulation are given. Furthermore, the lifetime models in paper composite insulation systems and their relation to the kinetics of degradation in cellulose are explained.

The concluding section to this chapter introduces the principle of the *universal* dielectric response which is judged to simplify the presentation and treatment of dielectric spectroscopy results. The physical structure of impregnated paper is then related to the measurement, discussing the effects of degradation and contaminants on the resulting dielectric relaxation.

## 3.1. Mass Impregnated (Kraft) Paper Insulation

As noted by G. T. Kohman at Bell Laboratories in an AIEE transaction in 1939, the applications of cellulose paper insulation are nearly as old as the electrical industry itself [37]. The colourful history of paper use in insulation has evolved over the last century in a range of electrical applications spanning different technologies such as transformers, capacitors, power cables and telephone cables amongst others. For centuries cellulose has been the material of choice in electrical insulation simply because there is a plentiful supply of this natural resource and not because of any superior insulating properties [38].

Cellulose is a polymer of glucose units and it is the predominant constituent of paper. A polymer is a compound with a typically high molecular weight consisting of up to millions of repeated linked units where each unit is a relatively light and simple molecule. The repeated glucose units that constitute a cellulose polymer is shown in figure 3.1.

The glucose units are linked in the polymer chain via oxygen atoms. This is referred to as glucosodic linkage. Each glucose unit has many side groups, including 3 hydrohyl (-OH) groups. In figure 3.1 the symbol *R* represents a hydrogen atom in a cellulose structure. Furthermore, two (-OR) groups exist and one ($-CH_2OR$) methylol group. The methylol is attached to the glucose ring [40]

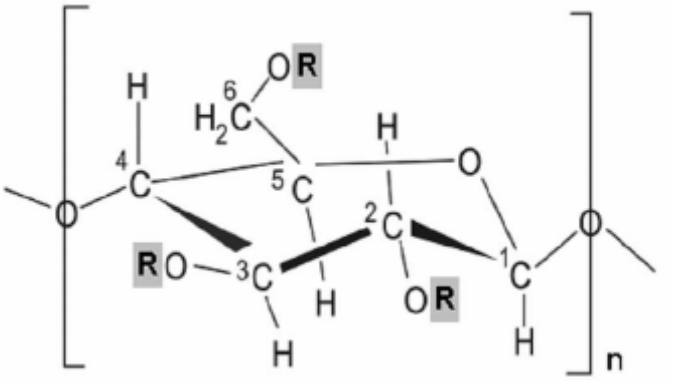


***Figure 3.1.*** *Glucose unit [40]*

In practice, cellulose paper is combined with oil as insulation in electrical equipment. Individually, paper and oil have poor electrical insulating properties. However, when combined the resulting material is a high grade electrical composite. In industrial applications the majority of cellulose paper is produced by pressing together moist cellulose fibers derived from cotton or wood.

The late 1920's and early 1930's witnessed important developments in experimental works on paper-oil insulation systems and in the 1940's this became the technology of choice in high voltage applications. This observation is further strengthened by the research trends in paper chemistry that ensued during the 1950's [38].

Paper-oil insulation has had a dominant foothold in markets for HVDC submarine cable systems since the commissioning of the first submarine *Gotland 1* cable in 1954. The most extensively used cables are those of the Mass Impregnated (MI) kind. An alternative to the MI submarine cable is the *Self Contained Oil Filled (SCOF)* cable, capable of higher power transmission capacities. However, the downside to *SCOF* cable systems is a requirement for oil feeding units every 10 to 20 km.

A seldom used cable system for submarine applications is the *Gas-Pressure Cable* developed from cellulose paper impregnated with high pressure gas. A somewhat rare case of the *Gas-Pressure Cable* is in operation along the Cooke Strait connecting the Northern and Southern islands of New Zealand [8].

Advancements in power electronics have resulted in polymeric insulation technology becoming viable alternatives in submarine HVDC applications. However, before the real benefits of *Extruded Polymeric Cables* can be realised the persistent problems arising from space charge accumulation must be overcome or further circumvented.

Mass Impregnated paper insulation as used in HVDC power cables consists of Kraft paper impregnated with high viscosity oil. The oil is of a paraffinic or naphtenic type, having less affinity for moisture than aromatic oils. The sulphate or Kraft chemical process produces high strength paper which has excellent impregnation properties. This process involves a combination of soft wood fibers for mechanical strength and hard wood fibers, providing a smoothened finish to the Kraft paper.

The unprocessed wood pulp at the beginning of this process consists of 40-55% cellulose, 15-35% lignin and 25-40% hemi-celluloses. The lignin, a brownish aromatic polymer and the hemi-cellulose, a polysaccharide similar to cellulose are almost fully removed during this chemical process and the resulting Kraft paper has an increased cellulose content of approximately 78-80%. This is consistent with a reduction in lignin to 2-6% and the hemi-cellulose content to 10-20% [41].

A general approach to produce Mass Impregnated HVDC submarine power cables is the following; The Kraft paper is meticulously wrapped around a conductor core ensuring a consistent position, angle and tension in the paper. The cable is then placed in an oil impregnation tank where it is dried under vacuum and subsequently impregnated by oil under pressure. The temperature is an important parameter during the drying process when removing gases and moisture from the paper.

The cable is then returned to the ambient temperature at which point sheathing, armoring and other layers are added. Precision equipment ensures the layers are continuous and that the minute tolerance levels are not breached [39].

.

## 3.2. Degradation of MI Paper Insulation

The ageing of Mass Impregnated paper is a degradative process that causes irreversible deleterious changes to the serviceability of the insulation. Frequently discovered ageing byproducts in paper-oil insulation are moisture and organic carboxylic acids that tend to further accelerate the ageing process [42-44][47].

Cellulose paper is susceptible to ageing in many forms including pyrolysis, oxidation and hydrolysis. The hydrolytic action is a catalytically governed process where the rate of degradation depends on the number of carboxylic acids dissociated by the moisture. Since both moisture and carboxylic acids cause ageing this process is auto-accelerating. It is believed that oxidation is catalysed by the hydroxyl radicals produced by the decomposition of the hydrogen peroxide and organic hydroperoxides. Furthermore, pyrolysis can occur without access to moisture or oxygen but has little relevance below $140^{\circ}C$ [41]. A significant consequence of the aforementioned degradation is a loss in mechanical strength due to breakdowns in chain lengths and hydrogen bonds. This results in weakened and brittle fibers.

It is apparent from various studies that hydrolysis is the most detrimental of these factors whereby the dissociation of the carboxylic acids in paper creates free $H^{+}$ ions [2],[4],[8]. The low molecular weight carboxylic acids (formic, acetic, levulinic) that concentrate in the cellulose paper are hygroscopic and are decidedly more harmful to the insulation than the high molecular weight carboxylic acids (stearic, naphtenic) that persist in the oil [41], [46],[50].

Hence, the implicit disadvantage of cellulose paper is that it is hygroscopic and needs to be processed and maintained free from moisture. This is evident during the impregnation process of paper as described in the previous section [48],[3.2].

Degradative ageing of paper insulation is described by the *Degree of Polymerisation (DP)* of the cellulose macrostructure. The *DP* refers to the number of anhydroglucose (AHG) units in the cellulose chain, held together by glycosidic linkages that make cellulose a long, rigid molecule. Thus, the *DP* gives a direct indication of the decomposition of the cellulose macromolecule. The scission of the glycosidic bonds between the glucose monomers leads to decreasing values of *DP* and results in degradation byproducts and a decreased tensile strength of the cellulose paper [47]. In transformers a reduction in tensile strength of 50% is considered the end of life [41].

The *DP* is determined by viscometric measurements of cellulose in solution and the result indicates the degree of degradative ageing. In literature, representations of the *DP* such as the *Chain Scission Number* and the *Scission Fraction of Cellulose Unit* are common [42] The *DP* of natural cellulose is typically greater than 20,000 and is approximately 1200 in the case of insulation grade Kraft paper [41],[51],[52].

The IEC's loading guides, in accordance with Montsinger [65] state that the ageing of transformer pressboard is doubled for every 6 $^{\circ}C$ in the temperature range from 80$^{\circ}C$ to 140$^{\circ}C$. This simple relation is regarded as a more basic realisation of the Arrhenius law as used in IEEE loading guides [41].

### 3.2.1. Kinetics of degradation

*DP* measurements have historically been used to assess the level of degradation of cellulose paper and they are included as bases in the IEEE loading guide references on the ageing of cellulose in transformers and for other electrical equipment [42].[53].

From a historical perspective studies on the degradation of cellulose are based on a statistical approach by Kuhn et al. in 1930 [66] and a kinetic model on degradation was later developed by Ekamstam in 1936 [67] The basis of these studies treats every polymer bond to be identical to the next and therefore equal probabilities exist in breaking individual bonds.

The kinetics of degradation assumes a random first order chain scission reaction which demonstrates a direct relationship between the time elapse and the reciprocal of the *DP* by approximating to a zero order solution;

$$\frac{1}{DP_t} - \frac{1}{DP_0} = k * t$$

, where *k* is the reaction rate, $DP_0$ is the initial degree of polymerisation and $DP_t$ is the degree of polymerisation after time *t*. In many publications this Ekamstam formula is used to describe the kinetics of degradation (of Kraft paper) under varying conditions.

However, this first/zero order relationship is found to be inconsistent at a point when low values of *DP* are reached and when high reaction rates are evident [52]. Under these circumstances the cellulose is somewhat degraded and it is important to estimate the remaining lifetime as accurately as possible. In 1997 Emsley et al. [55] developed a model more consistent with the observed low DP behavior. In this model the kinetics of degradation are formulated as follows;

$$\frac{dDP}{dt} = k_1 DP^2 \qquad \frac{dk_1}{dt} = k_1 k_2$$

Combining and integrating it follows that,

$$\frac{1}{DP_t} - \frac{1}{DP_0} = \frac{k_1}{k_2}\left[1 - e^{-k_2 t}\right],$$

, where $k_1$ is the rate of change in DP and $k_2$ the rate of change in $k_1$. This model accounts for the variation in probabilities of covalent bonds breaking in the cellulose. From this point of view the importance of the Emsley/Heywood kinetic degradation model is apparent and its significance is further strengthened in the findings of experimental work on aged cotton paper showing the centre of polymer chains to be more susceptible to the breakage of bonds than the chain ends of the polymer.

However, cellulose contains high-crystalline and amorphous regions. Two-stage kinetics describe rapid reaction rates sometimes observed at the onset of degradation followed by a linear stage. The rapid initial stage is thought to arise from the weak covalent bonds in the amorphous regions of cellulose [50]. These weak links are thought to arise every 500 monomer units and the reaction rates are some 10,000 times faster than those in the highly ordered crystalline region

# 3.3. Relaxation Analysis in MI Paper

The kinetic models on the degradation of cellulose are somewhat limited in how well they predict oil-paper insulation lifetimes [55]. A detailed knowledge of the temperature distribution and moisture-oxygen-dynamics is important for a more conclusive understanding of the ageing process

The Ekamstam equation models the kinetics of the degradation in a polymer. If the degradation rate *k* and the end of life DP value are known then the lifetime of the insulation can be reasonably well estimated by using the Ekamstam equation from section 3.2.1 as follows,

$$\frac{1}{DP_{final}} - \frac{1}{DP_0} = k * lifetime$$

Here, *k* is the degradation rate which has the following form;

$$k = Ae^{-\frac{\Delta E}{RT}}$$

The pre-exponential factor *A* is dependent on the material and its environment. *T* is the temperature, *R* the gas constant and $\Delta E$ the activation energy.

The rate equation has an Arrhenius type form where the activation energy $\Delta E$ is the minimum energy that must be overcome in order for some chemical reaction to occur. In this case the reaction is the degradation process in the cellulose due to chain scissions.

Furthermore, relaxation processes in the frequency domain often exhibit this behavior. The frequencies at which individual loss peak maximums $\omega_p$ occur show an Arrhenius type temperature dependence such that,

$$\omega_p \propto \exp\left(\frac{-\Delta E}{RT}\right)$$

If the process observed demonstrates a true Arrhenius form then the logarithm of $\omega_p$ varies linearly with the reciprocal of the temperature *T*. The activation energy $\Delta E$ is subsequently the slope of a straight line intersecting the data points in the log ($\omega_p$) versus 1/*T* graph. A typical Arrhenius plot is illustrated in figure 3.1.

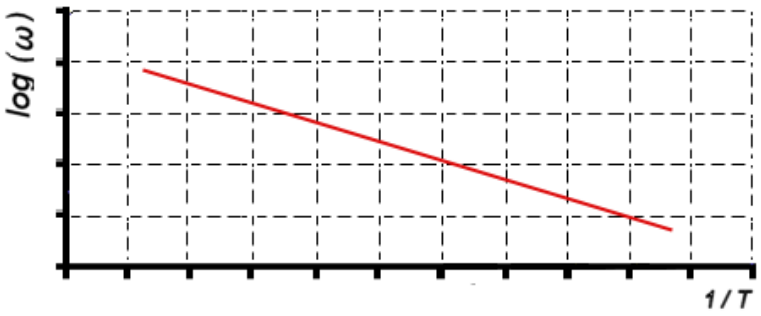


***Figure 3.1.*** *Typical Arrhenius graph*

Frequency domain spectra contain a wealth of information concerning relaxation processes in materials. This is evident in the large number of measurements recorded over a broad frequency range for a fixed parameter under investigation such as the temperature or pressure.

In attempts to interpret frequency domain responses the principle of the *universal* dielectric response helps simplify the presentation and theoretical treatment of measurement results [54]. The complex dielectric susceptibility $\tilde{\chi}(\omega)$ and permittivity $\tilde{\varepsilon}(\omega)$ are two informative ways to represent dielectric measurements where a physical emphasis is on parallel processes contributing to the real and imaginary components.

Furthermore, a log-log form is an informative way to represent the dielectric susceptibility $\tilde{\chi}(\omega)$ which is often a power-law function of frequency $\omega$ such that,

$$\tilde{\chi}(\omega) \propto (i\omega)^{n-1} \qquad 0 < n < 1$$

in the frequency region above any loss peaks. The nature of this response is governed by the *universal* law.

It is theorised that dielectric responses take either a *dipolar* or a *charge carrier* type generic form [54]. *Dipolar* responses leave no residual effect after the voltage strain across the insulation is removed whereas a charge carrier response is identified by a partial recovery when discharged and a finite polarisation component. The leakage current is an example of a charge carrier response.

Many functions try to accurately model the relaxation behavior in dielectrics. The classical Debye response is based on the concept of dipoles giving rise to a polarisation and is formulated as follows;

$$\tilde{\chi}(\omega) = \frac{B}{1 + i\omega/\omega_p}$$

, where $\omega_p$ is the loss peak frequency. This response, shown in figure 3.2 is found in simple dielectric liquids but it is rarely found in solid dielectrics. The response applies to an assembly of non-interacting ideal dipoles having the same waiting time before a transition or for an assembly of identical dipoles having a loss of energy proportional to their frequency.

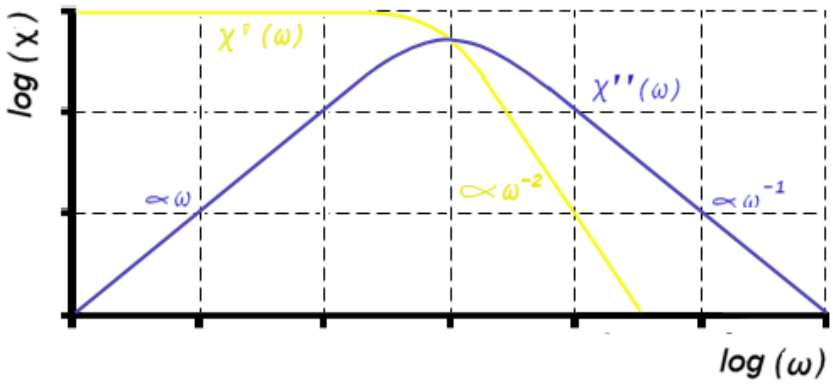


***Figure 3.2.*** *Debye frequency response*

However, instances of slight and very pronounced deviations from the Debye response exist. In figure 3.3 a response close to Debye behavior is shown on the left. On the right hand side in figure 3.3 a more pronounced, almost flat deviation in the response characteristic is evident.

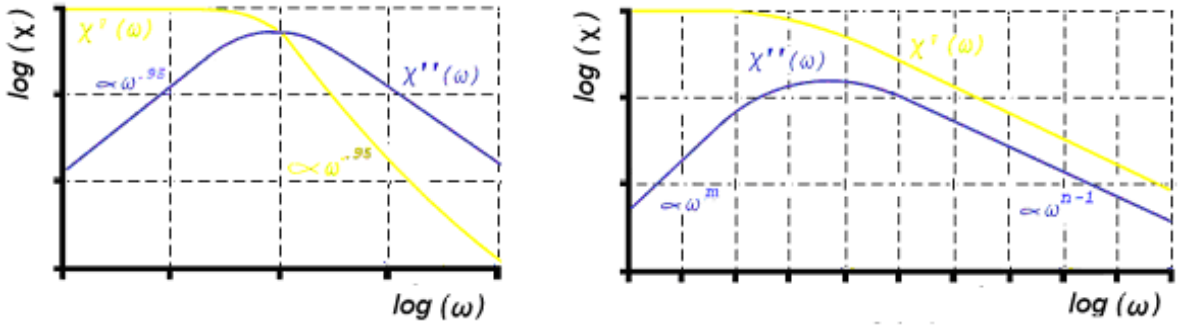


***Figure 3.3.*** *Close to Debye response (left) and an almost flat response (right)*

A general rule that best describes all frequency responses has the form of a fractional power law such that;

$$\chi''(\omega) \propto \omega^{m} \qquad \text{for the rising values of } \chi''(\omega) \text{ where } \omega << \omega_p$$

and

$$\chi''(\omega) \propto \omega^{n-1} \qquad \text{for the falling values of } \chi''(\omega) \text{ where } \omega >> \omega_p$$

$$\text{where} \quad 0 < m,\ n < 1$$

Experiments show this *universal* power-law is very applicable to dipolar systems [C]. Also, a variation on the Debye model, the Havriliak-Negami model, represents well the asymptotic nature of the response [54]. The Havriliak-Negami model has the following analytical form;

$$\tilde{\chi}(\omega) \propto [1 + (i\omega / \omega_p)^m]^{(n-1)/m}$$

In the low frequency range the dielectric response is characterised by a dc conduction term or in some cases a Low Frequency Dispersion (LFD) behavior which in a superficial analysis can be considered to represent dc also [54]. This LFD response is illustrated in figure 3.4.

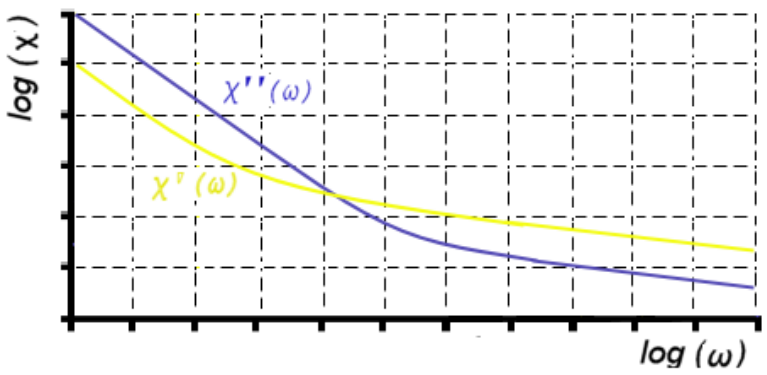


***Figure 3.4.*** *Low Frequency Dispersion LFD*

In the case of LFD, slowly moving charge carriers such as ions or hopping electrons dominate the response. No loss peaks occur since no dipolar processes are involved. The low frequency part still obeys the fractional power law with a much smaller exponent for *n*.

The physical significance of LFD is that the prominent rise in $\chi'(\omega)$ at low frequencies implies a finite and reversible storage of charge at interfaces or in the bulk of the material. This distinguishes it from true dc conduction where there is no charge storage and $\chi'(\omega)$ is independent of frequency, characterized by a horizontal line [54].

Frequency domain analysis is broadly categorised by a number of spectral ranges. The low frequency range is characterised by LFD or a dc conduction contribution. The intermediate range which is characterised by a universal frequency dependence which sometimes comprises of superimposed dipolar processes. This range can extend from below $10^0$ Hz up to $10^9$ Hz. Above this is the optical frequency range.

Originally, responses were thought to arise from the concept of Distributrion of Relaxation Times DRTs, a modified notion of the Debye response through integration over a distribution function of loss peak frequencies. The superficial argument behind this was the analogous inhomogeneities of a material. However, this fails to interpret the existence of the *universal* power law behavior which represents well the high frequency spectra.

Furthermore, research by Weron and Jurlewicz [68] use a probabilistic approach to model dielectric relaxation in solids. This is based on a mathematical founding related to the classical form of Kolrausch's stretched exponential law;

$$f(t) \propto -\frac{d}{dt}\exp[-(\omega_p t)^{\beta}] \qquad \beta < 1$$

Here, *f(t)* is the dielectric response function. It is understood that relaxation processes, especially chemical reaction kinetics follow this law well. In saying this, only certain solutions of the relaxation function are permissible which points to the stochastic nature of the relaxations, irrespective of any particular boundary conditions.

This approach highlights the mathematical properties of probabilistic relaxations without the need for a detailed knowledge of the processes themselves as a microscopic justification. Hence, the outcome is a theoretical model for the *universal* law that is based on a mathematical theory for relaxation in disordered systems as proposed by Weron and Jurlewicz [68]

### 3.3.1. Moisture Effects

In literature a broad range of research is dedicated to the effects of moisture in paper-oil insulation systems. A quantitative analysis of the moisture content is informative about the ageing of paper-oil insulation [57],[59],[60],[63-65]. Furthermore, water in insulation has a notable effect on relaxation processes and related properties.

Impregnating cellulose paper with oil reduces the rate of moisture saturation, but this does not reduce the moisture content itself [56]. In transformers the moisture content of paper-oil insulation is estimated using the Fabre-Pichon curve. This curve describes the migration of moisture between oil and paper as temperature varies. The blue lines in the Fabre-Pichon curves in figure 3.5 represent the migration of moisture between oil and paper as a function of the oil temperature.

For the case of an air-paper-oil complex, the green lines in the Fabre-Pichon curve in figure 3.5 show the migration of the moisture as a function of oil temperature and air humidity. Transformer pressboard is usually inaccessible and for this reason an indirect measurement is taken whereby the moisture in an oil sample is measured and the Fabre-Pichon curve is then used to estimate the moisture content of the paper.

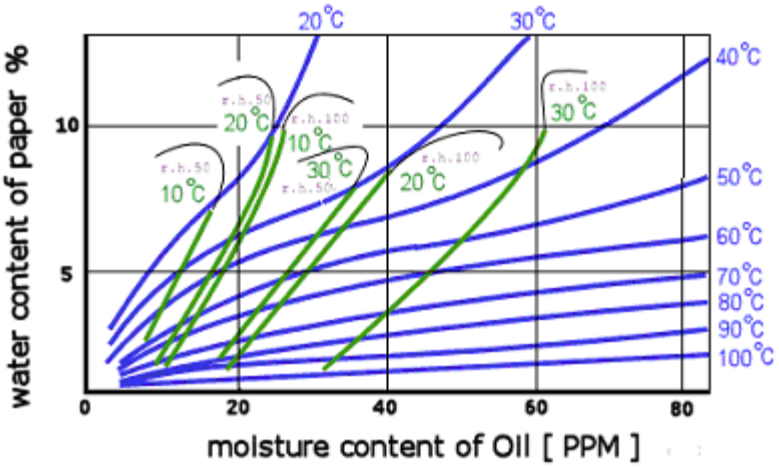


***Figure 3.5*** *Fabre-Pichon curve [58]*

It is understood that paper-oil insulation with a low moisture content has few ionic pathways through the paper and hence a low conductivity term. The presence of moisture causes a considerable increase in the number of ionic paths from electrode to electrode leading to a large conductivity term and hence increased losses [C][63].

Conversely, mineral oil has a very low affinity to moisture because of the size difference between the hydrocarbon and water molecules [56]. Furthermore, the absorption properties of oil are a function of its chemical structure, the temperature and its contamination by fibers and ageing byproducts [C].

.

In this research study the analysis focuses on the low frequency range. This was mentioned in the previous section as those frequencies characterised by a dc conductivity term or by Low Frequency Dispersion. If the conductivity term alone dominates at the lower frequencies then $\varepsilon''(\omega)$ has a slope of -1 in a log-log plot [63]. Moreover, the contribution due to moisture at these frequencies is identified in various publications to be a relaxation peak superimposed on the dc conductivity term in the $\varepsilon''(\omega)$ graph or/and the $\tan(\delta)$ graphs [58][63].

In many dielectric materials, increases in temperature cause a logarithmic shift in $\varepsilon''$ and $\tan(\delta)$ as functions of amplitude and frequency without a change in shape [63-65]. Therefore, the effect of temperature incurs the following displacement;

$$\varepsilon''(\omega,T) = A_{\varepsilon''}(t)F\left(\frac{\omega}{A_{\omega}(t)}\right)$$

where $A_{\varepsilon''}(t)$ and $A_{\omega}(t)$ can be expressed by Arrhenius-type activation energies such that;

$$A = \exp(-\frac{\Delta E}{RT})$$

In practice this theory has important significance. The dielectric response spectra for various temperature measurements can be shifted to a reference frequency and an extended-frequency-range *mastercurve* is subsequently created. The activation energies are then calculated by the shifts [65].

Furthermore, an analogous technique in calculating the activation energy is as follows. The angular frequency where a peak maximum occurs is subsequently used to determine the relaxation time for a fixed temperature point as follows;

$$\tau = \frac{1}{\omega_p}$$

This relaxation time, $\tau$, represents the ease at which the dipoles involved in a relaxation can oscillate.

For a range of temperature points the log $(1/\tau)$ plot is a linear function of the reciprocal of the absolute temperature *T*. The activation energy of the relaxation process is then determined from the slope of the straight line that intersects the data points in the graph.

In general, primary $\alpha$ - relaxation processes are associated with temperatures above the glass transition temperature $T_g$. At these temperatures, the system is liquid-like while below this temperature the system has a solid, rigid nature.

$\alpha$ - relaxation processes are understood to arise from the cooperative motion of a number of polar segments of the main molecular chain [11]. The response is generally narrow and more Debye-like in nature showing a typically non-Arrhenius form [11],[54],[62]. This response is in sharp contrast to the behavior of a $\beta$-relaxation, showing a typically Arrhenius type temperature dependency. Therefore, careful analysis can identify the nature of observed relaxations.

A $\beta$-relaxation is characterised by a broader peak to such an extent that the response can become almost flat in nature. This relaxation is typically associated with temperatures below the glass transition temperature $T_g$ [54]. The broad relaxation peak can extend over several decades in the frequency spectrum and are thought to arise due to the segmental (local chain) motion in the polymer via the glucosidic linkages [71] .

It is reported in literature that moisture or other swelling solvents in a sample modify the relaxation processes, increasing the activation energy and the cooperativity of the local chain motion [71]. Furthermore, when the cellulose crystallininty decreases the intensity of the observed $\beta$-relaxation increases. The main problem in interpreting dielectric spectroscopy results is when relaxation processes overlap. In this case it is difficult to pinpoint the relaxations involved. The overlapping effect is illustrated in figure 3.6

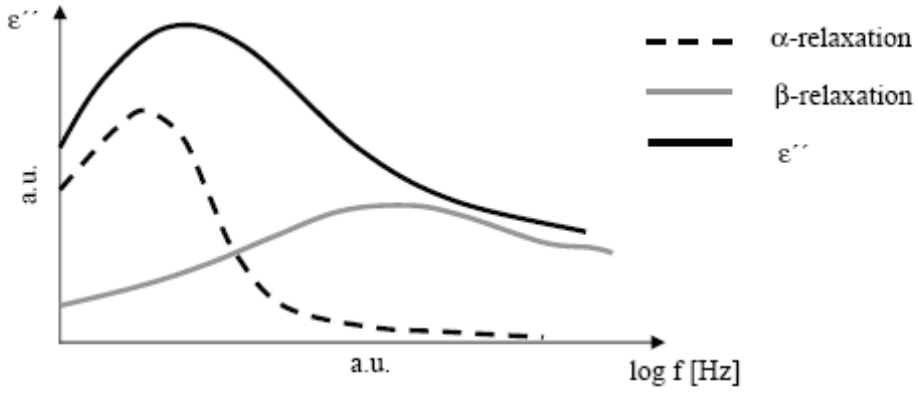


***Figure 3.6.*** *An exaple of* $\varepsilon''(\omega)$ *and the contribution of two relaxation processes*

In onr study dielectric spectroscopy tests were made on Mass Impregnated cable insulation samples removed from two different cables [69]. The samples were all oven treated to reach a base moisture level of 0.2%, considered dry, before varying levels of moisture were added to samples using saturated salt solutions.

In the dielectric spectroscopy tests it was noted that the loss tangent $\tan(\delta)$ has a minimum for samples with moderate moisture contents and that this minimum was observed to increase for samples containing higher moisture contents. Subsequently, the authors developed an expression to fit the moisture content to the measured minima of the loss tangent $\tan(\delta)$. This was formulated as follows,

$$\text{moisture content} = A + B \cdot \ln\left[\tan(\delta_{\min})\right]$$

Figure 3.7 shows the minima of $\tan(\delta)$ in samples from both cables correlate well with the above formula. Furthermore, the resulting formula coefficients for the case of both cables were found to correspond closely.

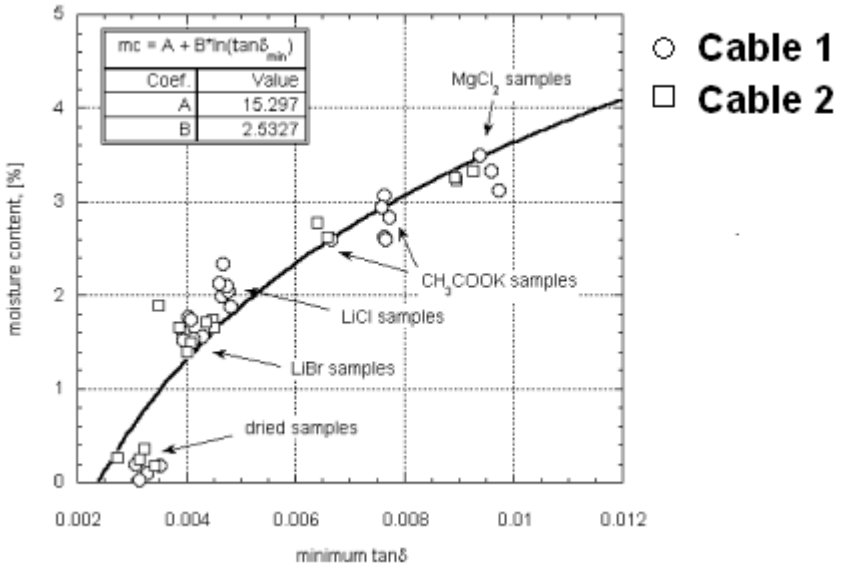


***Figure 3.7.*** *Moisture content as a function of minimum loss Tangent for cables 1 and 2*

Similar experiments were made by the same authors in [70] and it was again found that the relation between the moisture content and the minima of the loss tangent held. However, an investigation by a different research group disputes this finding [61]. Based on their experimental results they conclude that this relationship does not hold. Therefore, in dielectric spectroscopy, the idea that the loss tangent minima correspond to particular moisture levels remains a matter of contention.

# 4. Experimental Methods

## 4.1. Introduction

This chapter outlines the experimental test methods as used in this thesis. Section 4.2 introduces the Novocontrol Broadband Dielectric Spectroscopy test equipment and explains in detail the test routines used to investigate the relaxation processes in dielectric samples.

Furthermore, two experimental methods to investigate the moisture content of test samples feature in sections 4.3 and 4.4. Section 4.3 explains the principle of Karl Fischer Titration and the coulometric test equipment used to determine the moisture content. Section 4.4 explores an alternative method to calculate the moisture content of test samples. This involves a process of drying the samples in a vacuum oven and then measuring the subsequent reduction in weight on a precision scales.

## 4.2. Dielectric Spectroscopy in the Frequency Domain

In this work, frequency domain spectroscopy is used to investigate the dielectric relaxation processes in mass impregnated paper insulation.

Dielectric measurements are made over a broad frequency range at fixed temperature points, under isothermal conditions. A typical sequence of fixed measurement points used in this thesis starts at $20^{\circ}C$ and increases in increments of $10^{\circ}C$ to $50^{\circ}C$. At $50^{\circ}C$ the incremental step is adjusted to $5^{\circ}C$ until $70^{\circ}C$ is reached. This sequence is then repeated in reverse order back down to $20^{\circ}C$. This up-down cycle is repeated twice.

This elaborate scheme removes pre-existing tension, nullifies the preferential directions of polarisable parts and delivers a more consistent relaxation response within the material. Furthermore, the small temperature step helps identify the temperatures where subtle changes arise in the material response.

The temperature in the sample cell in figure 4.1 is controlled by a special heating element in the nitrogen vessel. The heating element creates a controlled pressure in the dewar vessel which subsequently delivers a constant flow of nitrogen gas to the sample cell inside the cryostat. The cryostat is thermally isolated by a rotary vane low vacuum (< 10 μbar) pump.

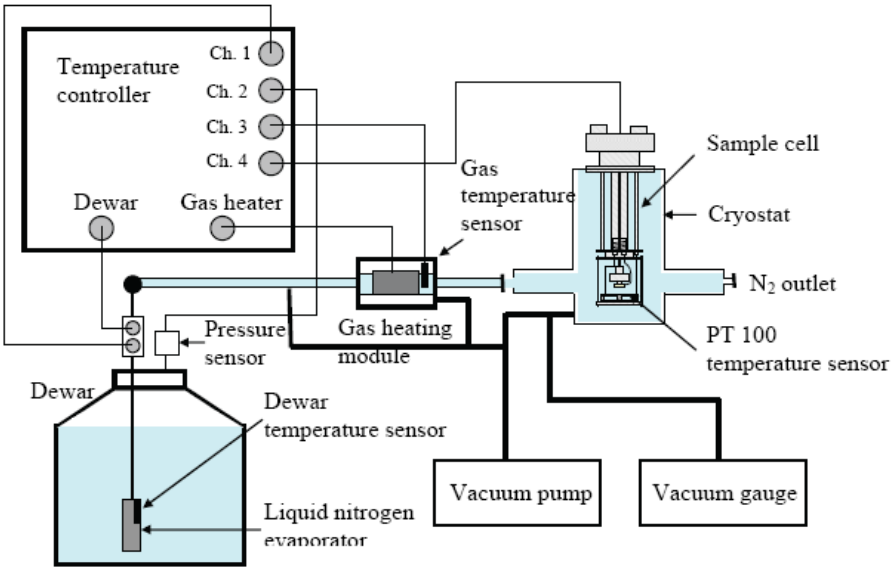


**Figure 4.1: Sample Cell and Temperature Control System**

A Novocontrol software package is used to configure the test program, providing isothermal control and temperature stepping. Additionally, the frequencies of the harmonic test signal and the frequency range can be specified. Furthermore, a data point averaging setting is adjustable so that the average value of more than one result is recorded for each measurement frequency.

# 4.3. Karl Fischer Titration

In 1935, the German chemist Karl Fischer devised the classic titration technique to investigate trace amounts of moisture in materials. Today, coulometric and volumetric Karl Fischer titration techniques are used to determine the weight percentage of moisture in new and aged, oil impregnated electrical insulation.

The principle of Karl Fischer titration is based on solvent extraction of water from a sample. During titration, a *titrant* (reagent/titrator) of known concentration (a standard solution) and volume reacts with a solution of the *titrand* which has unknown concentration.

For the case of volumetric Karl Fischer titration, the *titrant*, usually iodine is added mechanically to a solvent containing the sample using a burette. Water is quantified by the volume of *titrant* consumed where iodine and moisture are consumed in a 1:1 ratio. However, this classical volumetric titration suffers from the disadvantage that *titrants* are not completely stable during the titration and they must be analysed at various time intervals [73].

The advantages of coulometric Karl Fischer titration as used in this thesis are the simple handling procedures, rapid titration reactions and most importantly the accuracy of the results [72]. Furthermore, the iodine *titrant* is generated electrochemically and *in situ* during the titration.

Coulometric titration is a variation on the classical water determination method devised by Karl Fischer. The technique uses a methanolic solution of iodine, sulphur dioxide and a base as a buffer. The titration reaction has the following form [74];

$$H_2O + I_2 + [RNH]SO_3CH_3 + 2RN \Leftrightarrow [RNH]SO_4CH_3 + 2[RNH]$$

The moisture and iodine reaction is quantative and this forms the basis in determining the moisture content. Throughout the reaction process the iodine required is generated at generator electrodes by electrolytic oxidation, resulting in an immediate Karl Fischer reaction. The quantative relationship between the electric charge and the amount of iodine generated is used for high precision dispensing of the iodine..

According to Faraday's law of electrolysis the water content can be determined direct from the charge required for the electrolytic oxidation. The moisture content is therefore quantified on the basis of the total charge Q passed. This is recorded as current and time measurements according to the following relationship [73]:

Q = 1 Coulomb = 1 Amp x 1 second, where 1 mg $H_2O$ = 10.72 C

The electrolysis cell is shown in figure 4.2

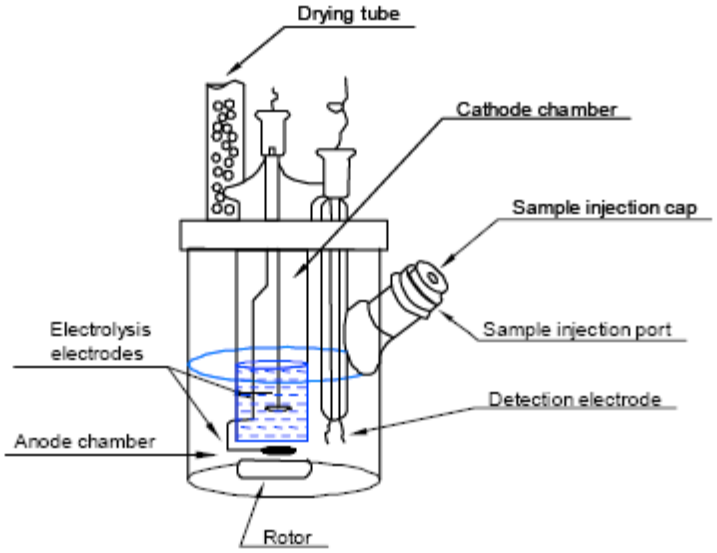


***Figure 4.2.*** *Electrolysis cell and heating chamber for coulometric Karl Fischer titration*

Thus, this titration method is an absolute determination and it is not necessary to determine the *titrant* concentration. It is only necessary to insure that the reaction which generates the iodine runs with 100% current efficiency. With the *titrants* available today this is always the case [74].

The end point of the titration is indicated by a change in the voltage between electrodes in the electrolysis cell. A voltage difference between indicator electrodes is drastically lowered in the presence of minimal quantities of free iodine. This event is used to determine the end point of the titration. The test apparatus is shown in figure 4.3.


**Figure 4.3: 756 KF Coulometer**

The titration vessel (electrolysis cell) in figure 4,3 consists of the anode and cathode electrodes. The *titrants* for coulometric moisture calculation with generator electrodes consist of an anode solution (anolyte), which is filled into the titration vessel and a cathode solution (catholyte) which is filled into the generator electrode.

The display screen of the coulometer in figure 4.3 not only provides a clear presentation of the parameters, but also shows graphically the course of the Karl Fischer determination as µg of moisture versus time. This facilitates the assessment of the determination and is a great help in method development and validation.

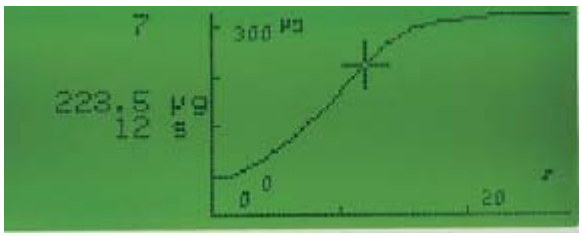


**Figure 4.3: Coulometer Screen**

The low detection limit of water using coulometric Karl Fischer titration is some µg of water [75]. However, the method is reliable but it is very susceptible to the following;

- Pre-test moisture ingress from exposure to the atmosphere.
- Differences in water bond strengths. In the cellulose the bonds are hydrogen and Van Der Waals types. In the oil the water may be bound in different ways. Therefore, not necessarily all water will be released during the titration.

# 4.4 Vacuum Oven – Precision Balance

An alternative test procedure is investigated to determine the moisture content in paper-oil insulation. Samples under investigation are placed in glass vials which are then weighed using a high precision scale as in figure 4.4. The initial weights are then recorded.

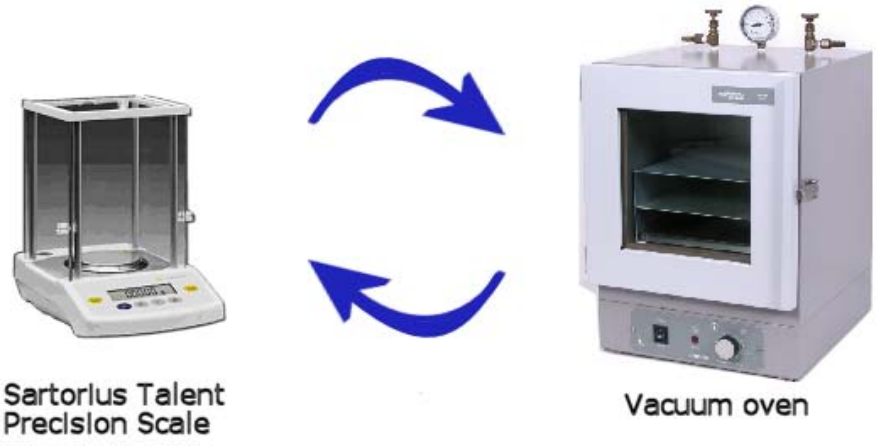


***Figure 4.4.*** *Precision scale and vacuum oven*

The vials are then placed in a vacuum oven at $50^{\circ}C$. After 24 hours the samples are removed from the oven and are re-weighed. The weights are recorded and the samples are returned to the oven for a further 72 hours at $50^{\circ}C$ in vacuum. When removed after the 72 hours has elapsed the vials are again weighed and the final measurements recorded.

While in the oven it is anticipated that only moisture is removed from the samples. Therefore it is proposed that the level of moisture is determined from the reduction in weight of the samples.

# 5. Results

## 5.1. Introduction

This chapter presents the experimental results from this thesis. In principle, a dielectric relaxation consists in the recovery of strain upon the removal of some stress. In this work broadband dielectric spectroscopy uses a harmonically varying test signal (stress) to investigate insulation of the Mass Impregnated type.

In electrical engineering, this technique is traditionally used to investigate ac insulation samples but its applications are equally as valid as an analysis tool for dc insulation. Aging processes affect polarisation phenomena in the insulation, whether the application is ac or dc. To investigate the dielectric polarisation spectra an ac test signal is used. However, this test signal is unrelated to how the insulation is stressed, whether ac or dc.

In chapter 3, chain scission in the cellulose polymer is identified as one such degradation process, referred to as depolymerisation. Furthermore, degradation byproducts such as moisture and organic carboxylic acids can sometimes manifest, thereby auto-accelerating the ageing process.

The low frequency spectra investigated in this work are typically charaterised by a dc conductivity term, a Low Frequency Dispersion effect or by some combination of the two. When superimposed relaxation loss peaks arise this makes interpretation of the results quite challenging.

In saying this, the dc conductivity term is identified in a log-log $\varepsilon''(\omega)$ graph as the low frequency response having a slope value of -1. This indicates how well the insulation conducts current and can be used to interpret the condition of the material. Intuitively, samples with higher losses should then exhibit a shift in the low frequency dc conductivity term to higher values. Furthermore, relaxation loss peaks can be used to identify the presence of some ageing byproducts as will be shown in some of the test results here.

In section 5.2 the dielectric spectroscopy results on insulation samples of the Mass Impregnated type are investigated. The relaxation spectra for samples subject to accelerated thermal ageing are compared to those of an un-aged reference sample and the effects of the thermal ageing are discussed. Furthermore, the dielectric spectroscopy results are compared to the Schering Bridge tests performed on identical samples by A.G. Ejigu at the TU Delft high voltage laboratory.

In following, section 5.3 investigates insulation samples of the Mass Impregnated kind which exhibit a pronounced loss peak in their relaxation spectra. The characteristic spectra observed are subsequently compared with results from literature in an attempt to resolve the underlying cause of the loss peaks.

Furthermore, the experimental methods discussed in chapter 4 to determine the moisture content in samples is used here to draw more definitive conclusions as to the origins of the loss peaks. To conclude, section 5.4 investigates the relaxation spectra of Non-Impregnated, Kraft paper insulation acquired from Prysmian Cables and Systems in Delft, The Netherlands

# 5.2. Results for Thermally Aged MI Paper Insulation

## 5.2.1. Introduction

In this section the dielectric relaxation spectra of thermally aged Mass Impregnated paper insulation samples are analysed and compared to those of an un-aged reference sample. The different samples investigated are first subject to a process of accelerated thermal ageing for durations of 53, 1128 and 1385 hours respectively, in an oven at $100^{\circ}C$. This temperature is thought to be sufficient to induce accelerated thermal ageing in accordance with various papers in literature [69-70].[76]. These papers typically record the degree of polymerization DP as a function of temperature and time. In figure 5.1 a result from literature shows the change in DP as a function of time for samples that are heated to different temperature levels. It is noted that even at the relatively low temperature of $65^{\circ}C$ there is a noticeable change in the DP value with time.

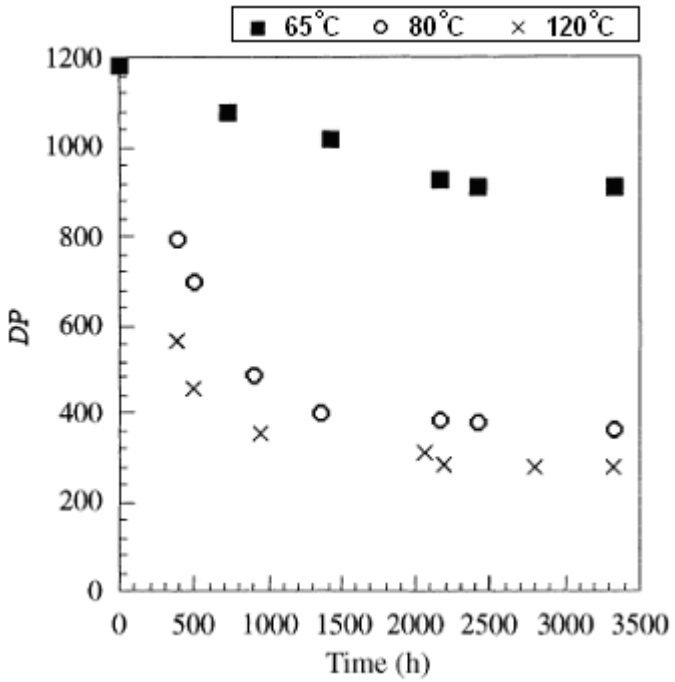


***Figure 5.1.*** *DP versus time for the degradation of Kraft paper in transformer oil [77]*

In the tests on the thermally aged samples the dielectric spectroscopy measurements are recorded over a broad frequency range at fixed temperature points. The programmed temperature sequence used during testing starts at $20^{\circ}C$ and increases in increments of $10^{\circ}C$ to $50^{\circ}C$. At $50^{\circ}C$ the incremental step is adjusted to $5^{\circ}C$ until $70^{\circ}C$ is reached. The step sequence is then repeated in reverse order back down to $20^{\circ}C$.This up-down temperature cycle is repeated twice as is shown in figure 5.2.

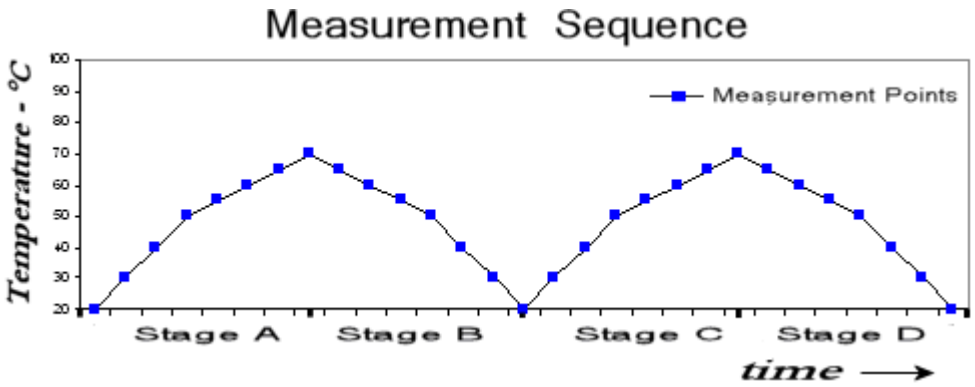


***Figure 5.2.*** *Measurement sequence used in dielectric spectroscopy measurement*

## 5.2.2. Reference Sample

Figures 5.3 show the dielectric relaxation spectra for the unaged reference sample during the final stage (D) of the temperature measurement cycle. For a more clear presentation of results only the measurements at $20^{\circ}C$, $50^{\circ}C$ and $70^{\circ}C$ are shown. The complete set of results can be found in appendix A.

In figure 5.3 it is found that the real (capacitive) component $\varepsilon'(\omega)$ of the permittivity has a generally flat response throughout the frequency spectrum. The loss tangent $\tan(\delta)$ and the loss component of the permittivity $\varepsilon''(\omega)$ show an increase in losses at low frequency. This is more pronounced for higher temperature measurements. However, the losses are in general considered to be low.

At higher temperatures the slope in $\varepsilon''(\omega)$ is observed to increase and at $70^{\circ}C$ this slope approaches a value of -1. This could be due to a dc conductivity term perhaps combined with some other relaxation effect at low frequency.

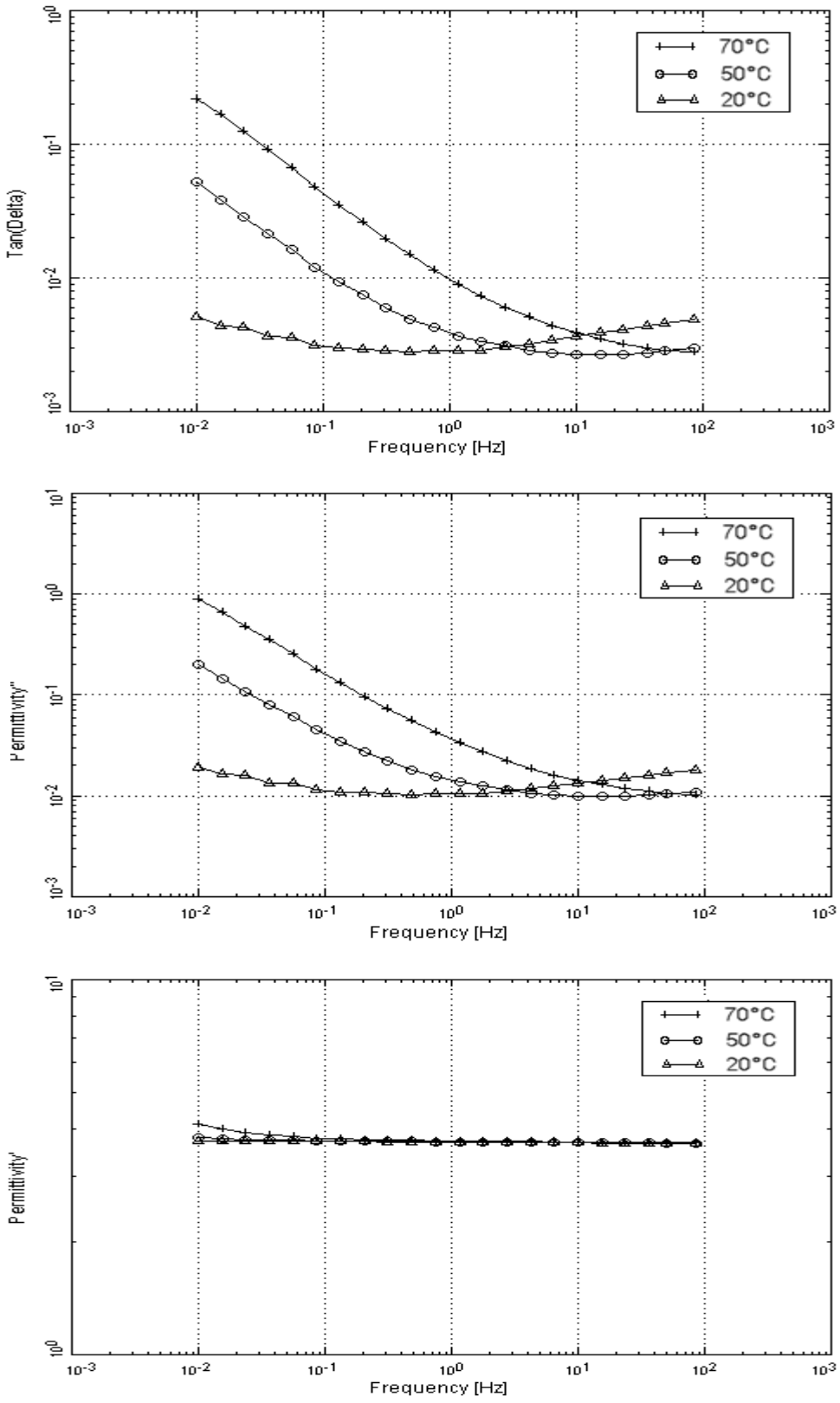


***Figure 5.3.*** *Dielectric spectroscopy results for reference unaged Mass Impregnated sample*

## 5.2.3. Thermally Aged Samples

In figure 5.4 the $\tan(\delta)$ spectrum for a sample thermally aged for 53 hours is compared to the reference sample. The loss measurement is observed to have increased considerably at the lower frequencies.

Furthermore, there is the first sign of a subtle loss peak appearing at the $50^{\circ}C$ measurement in the thermally aged sample. The frequency where the maximum of this relaxation loss peak occurs is unclear. However, at the increased temperature of $70^{\circ}C$ this relaxation appears to have shifted to a higher frequency.

This would suggest that the loss peak could have an Arrhenius type temperature dependency. However, the superposition of other low frequency effects makes it difficult to interpret the low frequency behavior.

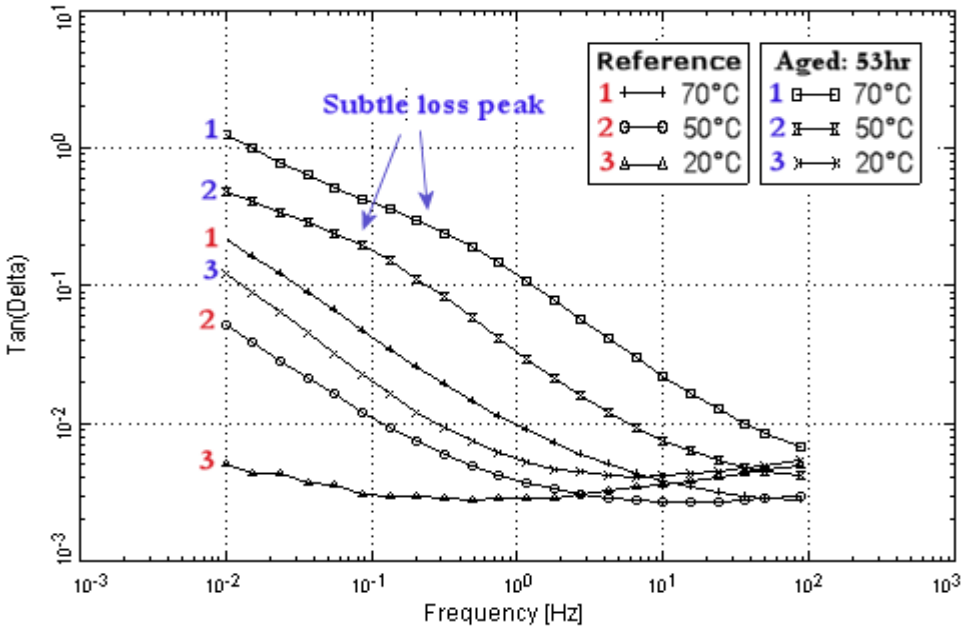


***Figure 5.4.*** *tan(δ) for the sample thermally aged for 53 hours compared to the reference sample*

This behavior is also evident in the $\varepsilon''(\omega)$ spectrum in figure 5.5. Again, a subtle loss peak is observed, shifting to a higher frequency as the temperature is increased.

Furthermore, in figure 5.5 the low frequency measurements for the real component of the permittivity $\varepsilon'(\omega)$ now diverge from the flat response observed for the reference sample.

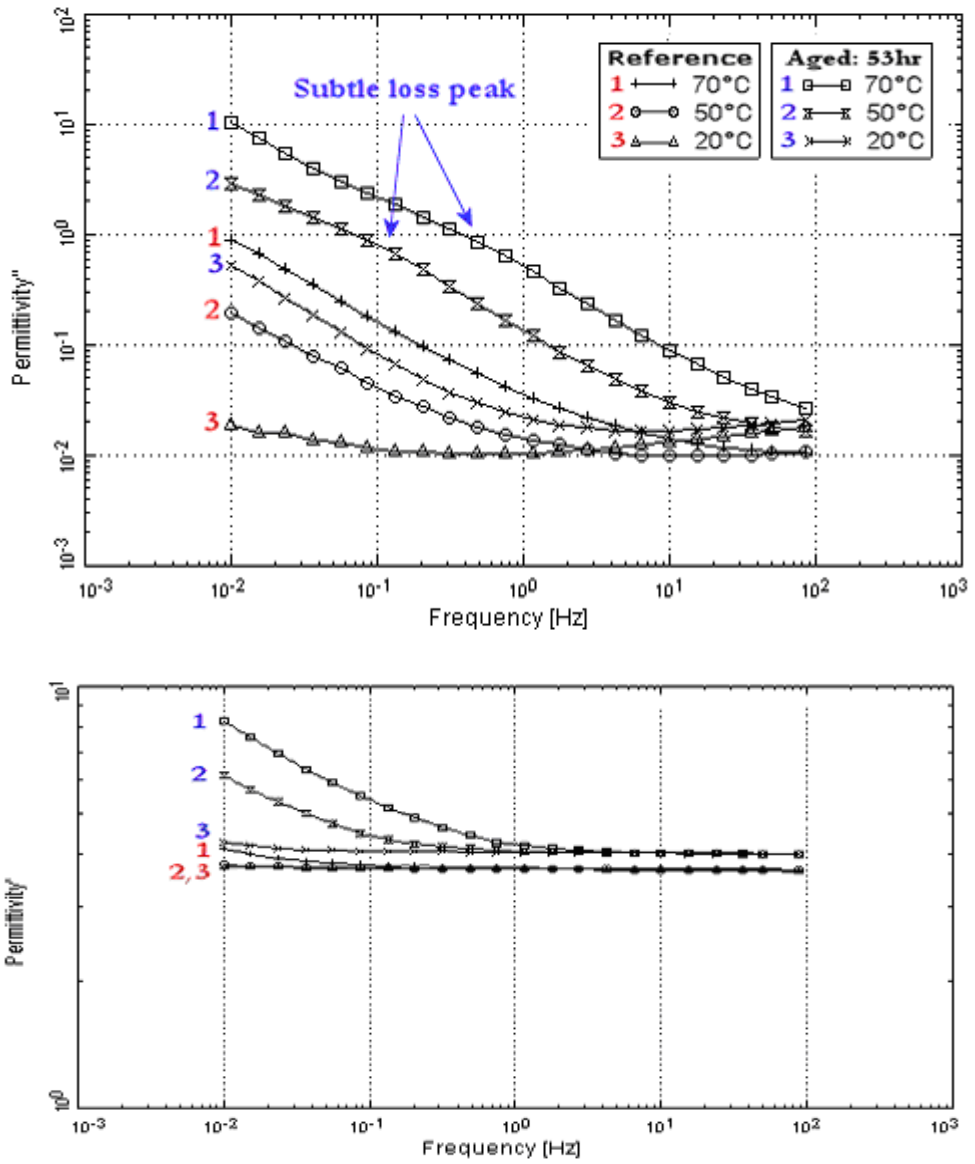


***Figure 5.5.*** *Comparison of* $\varepsilon''(\omega)$ and $\varepsilon'(\omega)$ *results for unaged reference sample to thermally aged sample (53 hours)*

For the remaining tests it was observed that the samples aged for 53, 1128 and 1320 hours showed only minute differences. In figure 5.6 the $\tan(\delta)$ measurements at $20^{\circ}C$ and $70^{\circ}C$ for each thermally aged sample are shown.

This demonstrates that there is very little difference between the results of the aged samples. In $\varepsilon'(\omega)$ and $\varepsilon''(\omega)$ only small changes are again observed. All results are shown in Appendix A.

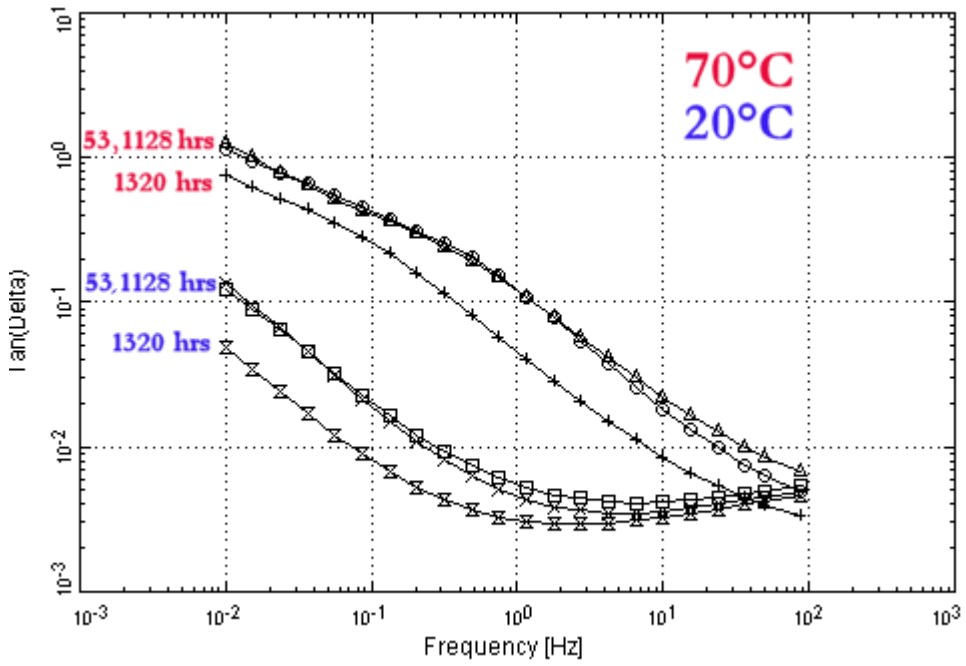


***Figure 5.6.*** *Comparison of* $\tan(\delta)$ *results for samples thermally aged for 53, 1128 and 1320 hours*

Various studies in literature have used frequency domain dielectric spectroscopy to investigate the effects of moisture on the relaxation spectra of insulation samples removed from ac Mass Impregnated cables. These studies typically treat the samples after they are removed by first drying them in an oven until they are considered dry. The samples are then placed in dessicators with saturated salt solutions. The samples absorb different levels of moisture depending on the saturated salt solution used [69][70][76]

When the results from literature are compared to the dielectric spectroscopy results for thermally aged samples in this work the similarities are striking. In figure 5.7 the $\tan(\delta)$ result for the sample thermally aged for 1320 hours is compared to a result from literature where moisture was added to the samples using the technique just described [69].

On the left hand side in figure 5.7 the $\tan(\delta)$ measurements at $20\,^{\circ}C$ (red) and $30\,^{\circ}C$ (blue) for the sample thermally aged for 1320 hours at $100\,^{\circ}C$ are shown. On the right hand side the results from literature for samples with varying moisture levels between 0.18% and 8.69% are shown. Highlighted on the right hand side are those results for samples with 1.76% (red) and 2.05% moisture respectively. It is understood that the measurements on the samples containing moisture were recorded at an ambient temperature, between $16\,^{\circ}C$ and $18\,^{\circ}C$.

In comparison, the similarities between the $20\,^{\circ}C$ and $30\,^{\circ}C$ measurements from this work and the 1.76% and 2.05% moisture level samples from literature can be summarised as follows;

- At $1\cdot10^{-2}$ Hz the magnitude of $\tan(\delta)$ for all highlighted measurements falls between the values of $1\cdot10^{-1}$ and $1\cdot10^{0}$.
- The frequencies where all minima in $\tan(\delta)$ occur for all highlighted measurements are between $5\cdot10^{0}$ Hz and $6\cdot10^{1}$ Hz.

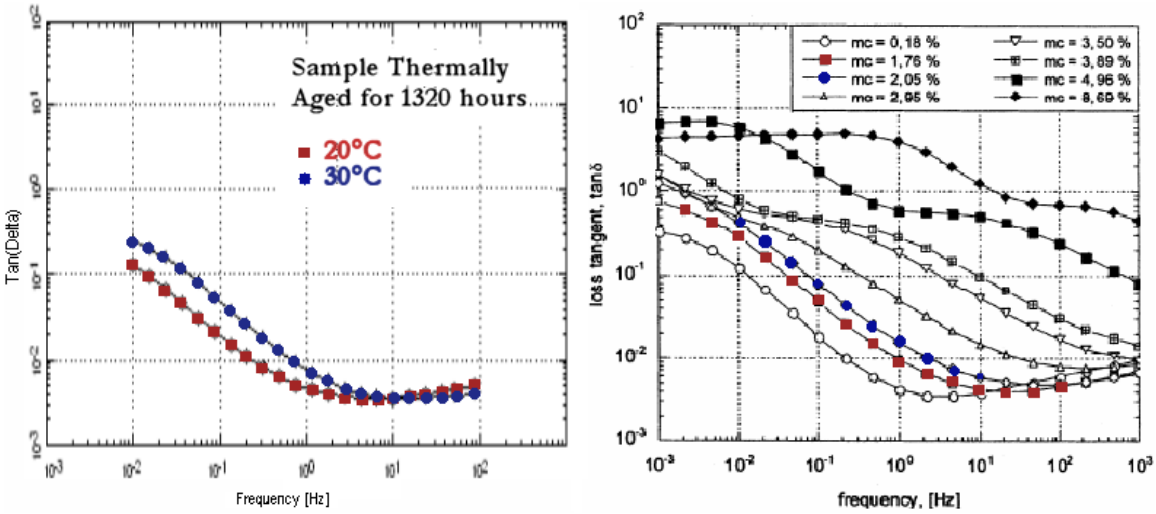


***Figure 5.7.*** *Comparison of tan( $\delta$ ) for the thermally aged sample (1320 hours) to results from literature*

In figure 5.8 a similar comparison is made for the loss component of the permittivity $\varepsilon''(\omega)$.

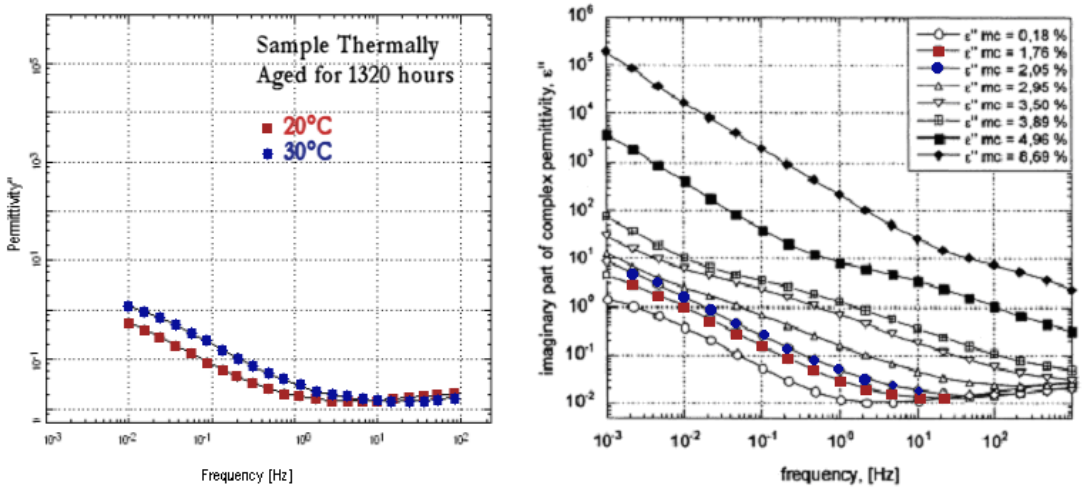


***Figure 5.8*** *Comparison of $\varepsilon''(\omega)$ for the thermally aged sample (1320 hours) to results from literature*

Compairing the two results again in figure 5.7 the following can be said;

- At $1 \cdot 10^{-2}$ Hz the magnitudes of $\varepsilon''(\omega)$ for all highlighted measurements are very close to $1 \cdot 10^{0}$.
- The frequency where each minima for $\varepsilon''(\omega)$ occurs in all highlighted measurements are in the vicinity of $1 \cdot 10^{1}$ Hz.

In figure 5.8 the final comparison is made for the capacitive component of the permittivity $\varepsilon'(\omega)$.

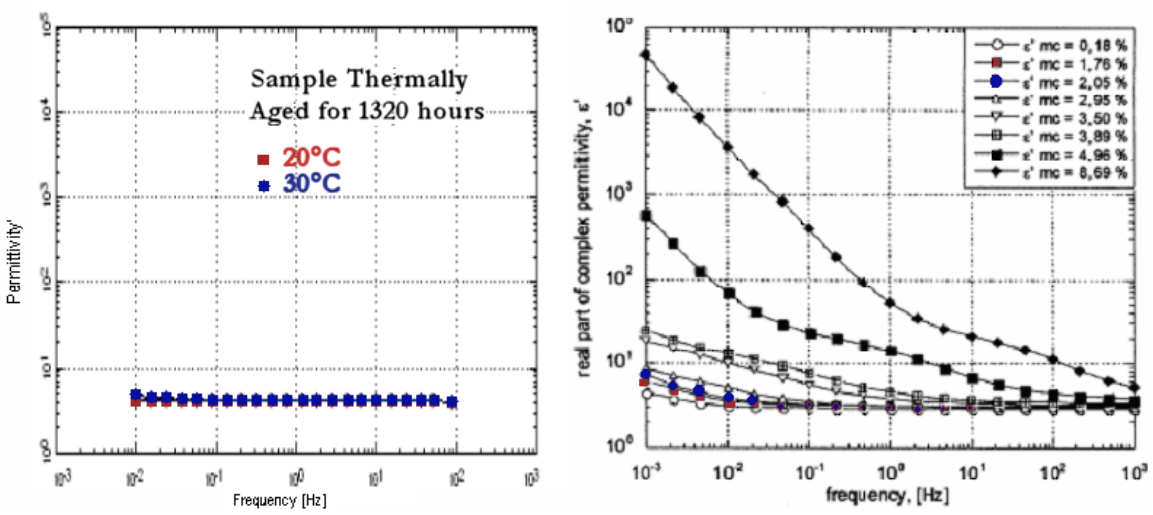


***Figure 5.8.*** *Comparison of $\varepsilon'(\omega)$ for the thermally aged sample (1320 hours) to results from literature*

Comparison of the results for $\varepsilon'(\omega)$ in figure 5.8 yields the following observations;

- At $1 \cdot 10^{-2}$ Hz the magnitude of $\varepsilon'(\omega)$ for all highlighted measurements falls between the values of $1 \cdot 10^{1}$ and $1 \cdot 10^{0}$.
- The responses for all highlighted measurements are generally flat above $1 \cdot 10^{-1}$ Hz. Furthermore, the value of $\varepsilon'(\omega)$ from $1 \cdot 10^{-1}$ Hz up to the higher frequencies is between 4 and 6.

From this analysis it is plausible that the differences in results between the reference sample and the thermally aged samples in this work are due to increased moisture content in the thermally aged samples. This could possibly be attributed to degradation by chain scission during thermal ageing with moisture as the subsequent byproduct.

To further check the validity of this argument the moisture content in the samples were determined using two experimental techniques. The first method investigated the moisture content in the samples using Karl Fischer Titration as explained in section 4.2. The results from these tests are presented in figure 5.9.

| | KFT Test A | KFT Test B |
|---|---|---|
| Reference Sample | 0.32% mc | 0.38% mc |
| Sample Aged for 53 Hours | 2.5% mc | 2.1% mc |

***Figure 5.9.*** *Results of moisture content (mc) determination by Karl Fischer Titration*

The second method for investigating the moisture content in samples is explained in section 4.3. This involved placing the samples in a vacuum oven for 24 hours at 50ºC and then measuring their subsequent weight loss percentage. The samples were then returned to the oven for a further 72 hours and the weighing process was repeated. The resulting moisture contents determined from the percentage weight loss for each sample are presented in figure 5.10.

| | In Vacuum Oven at 50°C | |
|---|---|---|
| | 24hrs | 96hrs |
| Reference Sample | 0.08% mc | 0.33% mc |
| Sample Aged for 53 Hours | 1.6% mc | 2.2% mc |

***Figure 5.10.*** *Results of moisture content (mc) determination by vacuum oven method*

These tests confirm that there is additional moisture in the aged samples. The Karl Fischer Titration shows the two aged samples tested to have moisture contents of 2.5% and 2.1% respectively. Furthermore, the moisture in the two reference samples tested was found to be 0.32% and 0.38% respectively.

Alternatively, the determination method using the vacuum oven calculated a moisture content of 2.2% for the thermally aged sample and 0.33% for the reference sample.

## 5.2.4. Comparisons with Schering Bridge Results

In parallel with the dielectric spectroscopy measurements in this thesis work, Schering Bridge loss measurements were made on the same thermally aged Mass Impregnated test samples. These measurements were made by a fellow MSc. student, A.E.Ejigu, at the High Voltage Laboratory at TU Delft. The Schering Bridge tests record $\tan(\delta)$ as a function of the test voltage at a frequency of 50Hz, the power frequency.

The spectroscopy measurements in this thesis typically cover a broad range of frequencies between $10^{-2}$ Hz and $10^{5}$ Hz. However, the Novocontrol software package allows the user to specify what frequencies the measurements are recorded at. It is therefore possible to select 50Hz and compare the results with the Schering Bridge test.

In the tests made by A.G. Ejigu the Schering Bridge result for the reference sample are shown in figure 5.11. The loss measurements are made at an ambient temperature between $20^{\circ}C$ and $30^{\circ}C$. During the test the $\tan(\delta)$ measurement ranges from a minimum value of 19.2 $\cdot 10^{-4}$ at a test voltage of 50V to a maximum of value of 29.82 $\cdot 10^{-4}$ at a test voltage of 650V.

With reference to the dielectric spectroscopy measurement on the reference sample, the value of $\tan(\delta)$ at 50Hz is $45.5 \cdot 10^{-4}$ and $38 \cdot 10^{-4}$ at $20^{\circ}C$ and $30^{\circ}C$ respectively. The results don't agree very closely with those results from the Schering Bridge test.

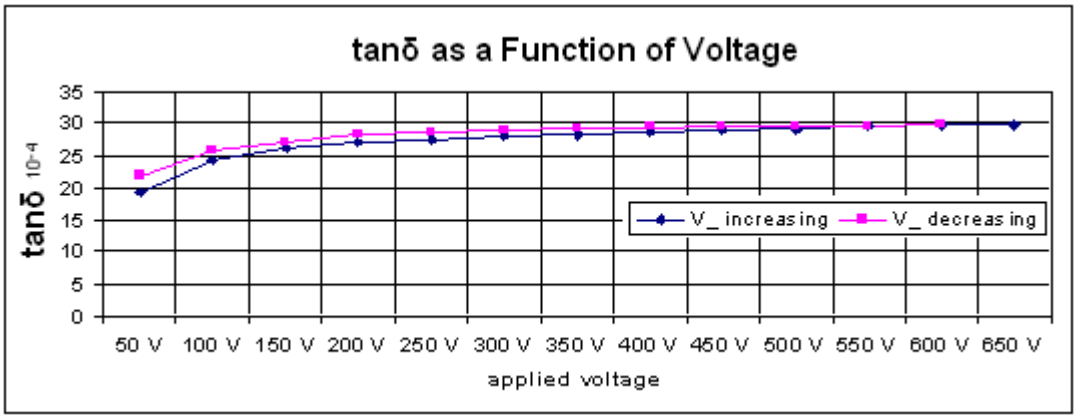


.

***Figure 5.11.*** *Schering Bridge result for tan(δ) versus applied voltage for reference sample.*

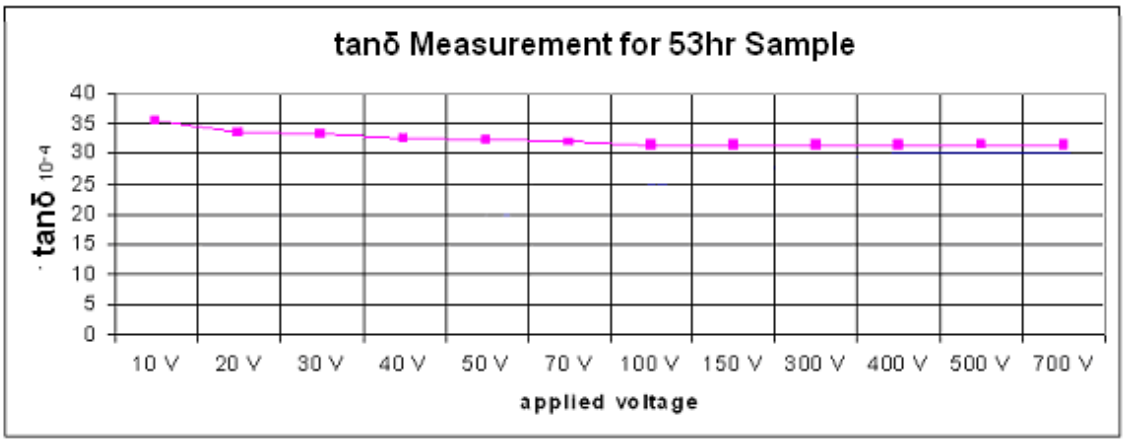


***Figure 5.12.*** *Schering Bridge result for tan(δ) versus applied voltage for the sample Aged for 53 hours.*

The Schering Bridge test result for the sample aged for 53 hours is shown in figure 5.12. Again, the loss measurements are made at an ambient temperature between $20^{\circ}C$ and $30^{\circ}C$. During the test the $\tan(\delta)$ measurement ranges from a minimum value of $35.58 \cdot 10^{-4}$ at a test voltage of 900V to a maximum of $43.03 \cdot 10^{-4}$ at a test voltage of 10V.

In reference to the dielectric spectroscopy result for the sample thermally aged for 53 hours, the values for $\tan(\delta)$ are $44.5 \cdot 10^{-4}$ and $41 \cdot 10^{-4}$ at $20^{\circ}C$ and $30^{\circ}C$ respectively. The results are somewhat closer to those results from the Schering Bridge test.

The remaining dielectric spectroscopy results are shown in figure 5.13. The value for $\tan(\delta)$ at 50Hz is $43.5 \cdot 10^{-4}$ and $34 \cdot 10^{-4}$ at $20^{\circ}C$ and $30^{\circ}C$ respectively for the sample thermally aged for 1128 hours. Furthermore, the values for $\tan(\delta)$ at 50Hz are $45 \cdot 10^{-4}$ and $37 \cdot 10^{-4}$ at $20^{\circ}C$ and $30^{\circ}C$ respectively for the sample thermally aged for 1320 hours.

| | Thermally Aged Samples | | | |
|---|---|---|---|---|
| Sample: | Reference | 53 Hours | 1128 Hours | 1320 Hours |
| $\tan(\delta)_{20^{\circ}C}$ | $47 \cdot 10^{-4}$ | $44 \cdot 10^{-4}$ | $43 \cdot 10^{-4}$ | $45 \cdot 10^{-4}$ |
| $\tan(\delta)_{30^{\circ}C}$ | $38 \cdot 10^{-4}$ | $41 \cdot 10^{-4}$ | $34 \cdot 10^{-4}$ | $37 \cdot 10^{-4}$ |

***Table 5.13.*** *Summary of tan(δ) results at 50Hz from dielectric spectroscopy measurement*

## 5.2.5. Discussion

The dielectric spectroscopy measurements for all thermally aged samples were compared to one another and the differences in the relaxation spectra were deemed minute. However, all samples showed a clear divergence from the dielectric response of the reference sample. Thermally aged samples were typically characterised by increased losses at low frequencies and by the appearance of a subtle loss peak at low frequency, arising in $\varepsilon''(\omega)$ and $\tan(\delta)$ at increased temperatures. Furthermore, at low frequency the capacitive component of the permittivity $\varepsilon'(\omega)$ was judged to have increased from the generally flat response observed in the reference sample. However, one point of note is that there is no noticeable change in the response at the 50Hz power frequency due to the thermal ageing effect.

Firstly, to investigate the origins of the observed changes the results were compared to similar works in literature. Various research endeavors investigating samples with different levels of moisture content showed results which matched closely those results in this thesis work. Following this, two experimental methods were used to investigate the moisture content in the reference sample and in thermally aged samples. The results confirmed the aged samples had an increase in moisture to somewhere around 2% or above. This is in contrast to the moisture found in the reference sample by the same investigation which was determined to be between 0.3% and 0.4%. It is proposed that the increase in moisture is the byproduct of the thermal ageing of the insulation.

Furthermore, it is difficult to interpret the exact behavior of the responses at low frequency due to the different overlapping relaxation processes. However, it is here proposed that the subtle loss peaks, observed in $\varepsilon''(\omega)$ and $\tan(\delta)$ at increased temperatures are $\beta$-relaxation processes. This interpretation is supported by the following arguments;

- The observed loss peaks are not very distinct but it appears that what is visible is only a small portion of a much broader relaxation. It is known that $\beta$-relaxation processes can span a broad a broad range of frequencies [11].
- The loss peaks display what could be an Arrhenius type temperature dependency shifting somewhat towards higher frequencies at increased temperatures. The exact shift is somewhat difficult to determine since the maximum of the crest is hard to distinguish considering it is hidden by other low frequency processes. If the process is in fact Arrhenius then the possibility of $\alpha$-relaxation can be ruled out.
- The increased moisture levels measured behave as a swelling solvent with tendencies to increase the activation energy and the cooperativity of the local chain motion [3.3.111]. Therefore, if the DP value has reduced due to thermal ageing, the cooperativity of the segmental chain motion will increase due to the additional moisture. $\beta$-relaxation is attributed to the segmental (local) chain motion of the polymer backbone.

When comparing the dielectric spectroscopy results to those results from the Schering Bridge test the measurements do not agree precisely. This could be because the test environments for the two techniques are very different. The dielectric spectroscopy measurement uses a test cell supplied by a flow of nitrogen gas for temperature control. On the other hand the Schering Bridge test is exposed to the ambient air. Therefore, the results from these tests may be influenced by any number of factors such as air the humidity etc.

The last point is related to the consistency of the measurements at the 50 Hz power frequency in the dielectric spectroscopy tests. The measurements recorded have values between $34 \cdot 10^{-4}$ and $47 \cdot 10^{-4}$ for all samples tested. Therefore, there is no very obvious difference between the response of the reference sample and the response of aged samples at the 50Hz power frequency. The differences are all observed at low frequencies.

The reason why the effect of this thermal ageing is observed at low frequency and not at 50Hz might be related to the DP. If the DP has not decreased too far then the polymer chains remain large. At the power frequency the segmented chains can not keep up with the alternating electrical field. However, at low frequencies they are able to alternate their direction to some extent with the changing field. Furthermore, the effect of moisture could have a similar effect. It might have a synergistic effect with the segmented chains at low frequency and have little effect at 50Hz.

# 5.3. Samples Showing Prominent Loss Peaks

## 5.3.1. Introduction

The dielectric spectroscopy measurements in section 5.2 were recorded in parallel with the Schering Bridge tests made by A.G. Ejigu at the TU Delft High Voltage laboratory. The general test procedure was the removal of Mass Impregnated insulation samples from the oven after a fixed duration of time, and the simultaneous measurement of the losses using the two test systems. The loss measurements from both tests were then compared to one another.

However, some samples were first tested using the Schering Bridge test equipment and were subsequently tested using the dielectric spectroscopy measurement. In effect, the sample used in the dielectric spectroscopy measurement was first subject to a Schering Bridge test. The resulting graphs from the spectroscopy tests showed some very interesting features. In the $\tan(\delta)$ graphs a very prominent loss peak was observed which shifted to higher frequencies, becoming more pronounced as the temperature increased.

Furthermore, the magnitude of $\tan(\delta)$, the loss component of the permittivity $\varepsilon''(\omega)$ and the capacitive component of the permittivity $\varepsilon'(\omega)$ showed an overall shift in magnitude to high values with respect to those measurements made in section 5.2. Two tests where this behavior was evident are now discussed.

## 5.3.2. Sample A

The first of the two Mass Impregnated insulation samples to show a prominent loss peak was sample A. This sample was first thermally aged for 168 hours at $100^{\circ}C$ before the Schering Bridge measurement was made. During the Schering Bridge test, the sample was exposed to temperatures ranging from $21.4^{\circ}C$ to $75^{\circ}C$ and the loss measurement was recorded as a function of temperature. Furthermore, the maximum electric field strength applied to each sample during testing was 4.5 kV/mm.

Following the Schering Bridge test a dielectric spectroscopy measurement was recorded over a broad frequency range, at fixed temperature points. The same test procedure was used as in section 5.2.1. The test sequence starts at $20^{\circ}C$ and increases in increments of $10^{\circ}C$ to $50^{\circ}C$. At $50^{\circ}C$ the incremental step is adjusted to $5^{\circ}C$ until $70^{\circ}C$ is reached. The step sequence is then repeated in reverse order back down to $20^{\circ}C$.The up-down temperature cycle is repeated twice. This measurement sequence is shown again in figure 5.14 for clarity.

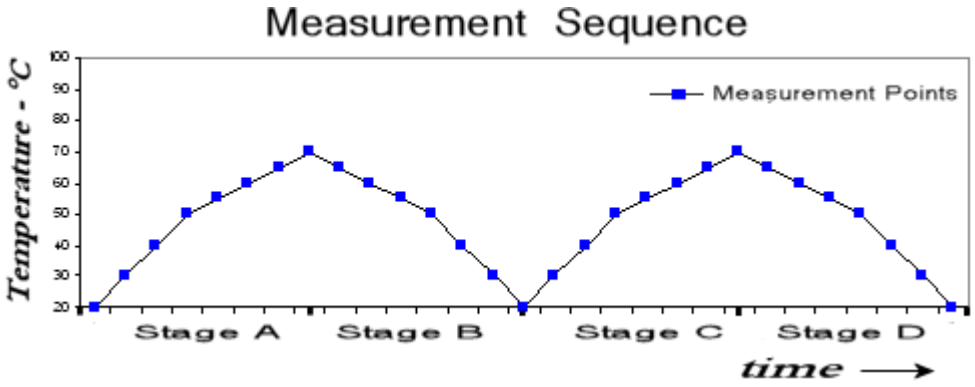


***Figure 5.14.*** *Measurement sequence used in dielectric spectroscopy measurement*

Figures 5.15 show the dielectric relaxation spectra for sample A during the final stage (D) of the temperature measurement cycle. Again, for a more clear presentation of the results only measurements at $20^{\circ}C$, $50^{\circ}C$ and $70^{\circ}C$ are shown.

The $\tan(\delta)$ result in figure 5.15 is characterised by very high losses across the whole frequency spectrum. It is noted that the losses are particularly high at the lower frequencies and the prominent loss peak mentioned earlier is also visible at all temperatures, increasing in severity as the temperature rises.

Furthermore, the magnitude of $\varepsilon'(\omega)$ and $\varepsilon''(\omega)$ in figure 5.15 are also high across all frequencies. To investigate if the process causing the observed loss peaks exhibits an Arrhenius type temperature dependency, the frequencies $\omega_p$ where the maximum of a loss peak occurs in $\tan(\delta)$ must be recorded accurately.

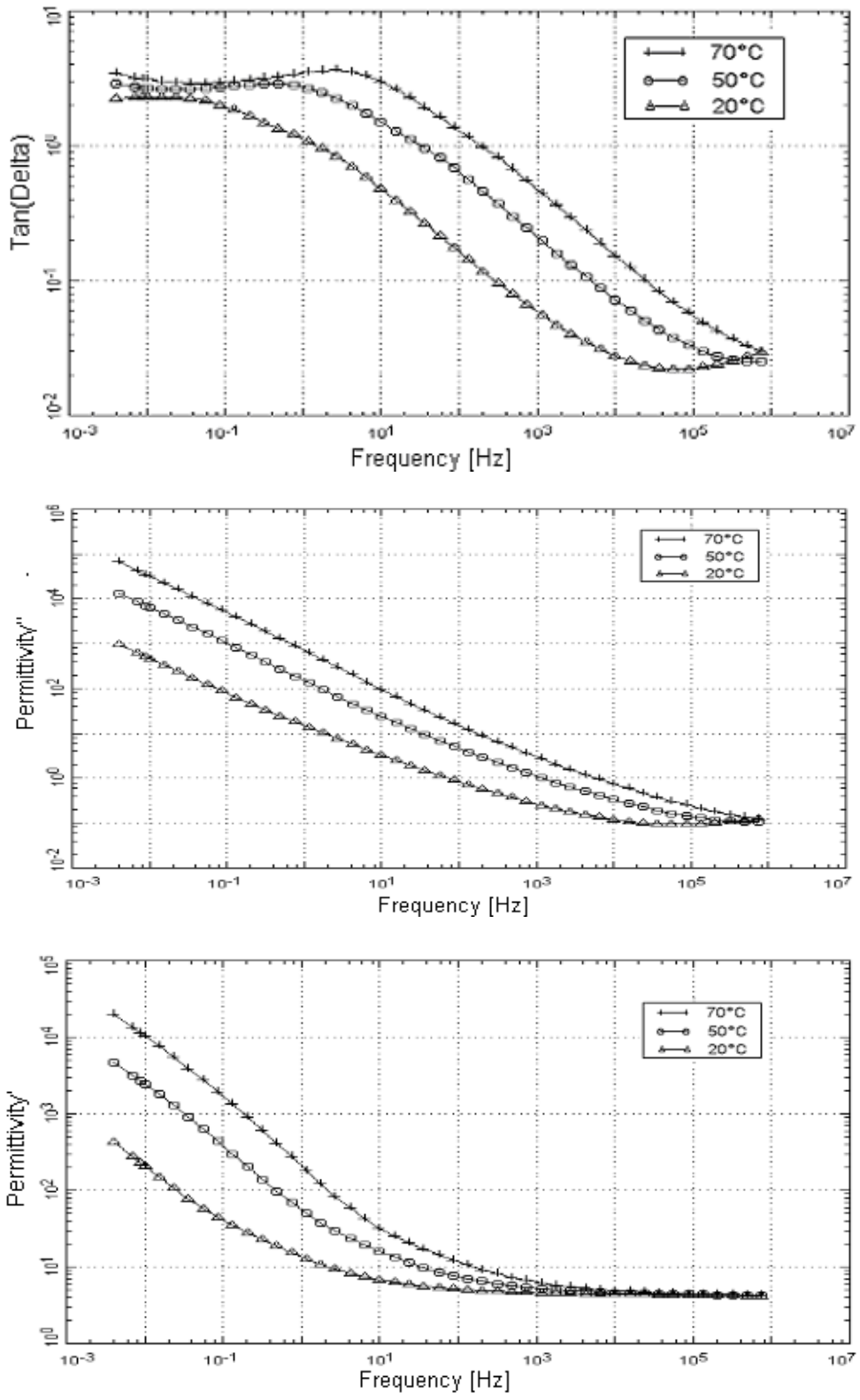


***Figure 5.15*** $\tan(\delta)$, $\varepsilon''(\omega)$ and $\varepsilon'(\omega)$ *results for sample A*

To check if the relaxation loss peaks have an Arrhenius type temperature dependency it is convenient to view the $\tan(\delta)$ spectrum with a linear scale on the y-axis as in figure 5.16. This allows easier location of the exact $\omega_p$ frequencies.

Furthermore, the 3D graph of $\tan(\delta)$ as a function of temperature and frequency can reveal some clues about the nature of relaxation processes. In figure 5.16 the 3D shows (marked in blue) a relaxation peak increasing in amplitude and moving to higher frequencies with increasing temperature

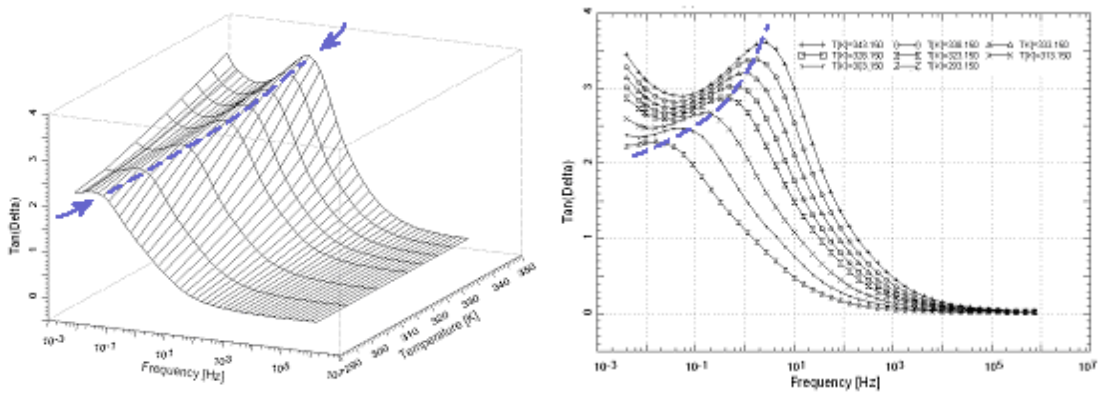


***Figure 5.16..*** *3D and 2D graphs of tan (δ) as a function of frequency and temperature for sample A*

Furthermore, if the observed process has a true Arrhenius form then the logarithm of $\omega_p$ varies linearly with the reciprocal of the temperature *T*. In figure 5.17 the logarithm of the $\omega_p$ values are graphed against *1000/T* which results in a straight line, showing the process to be Arrhenius.

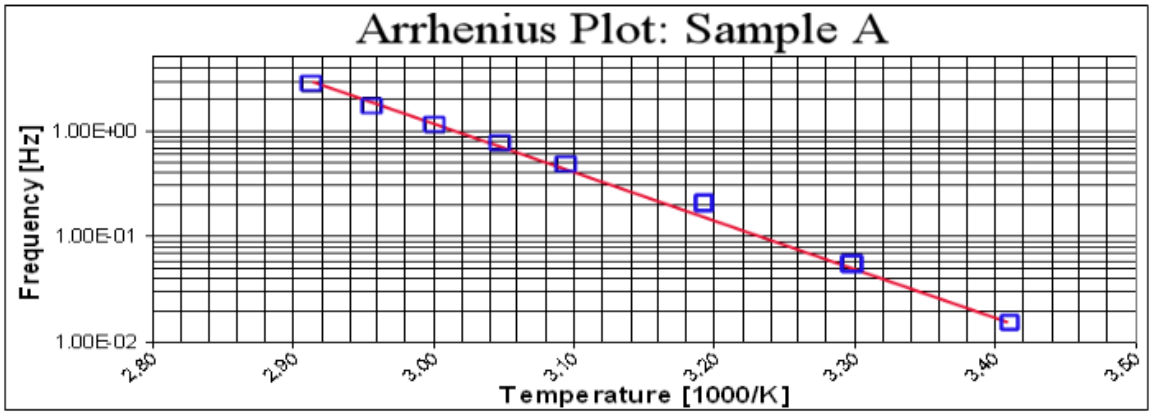


***Figure 5.17.*** *Arrhenius plot for sample A*

In figure 5.17 the activation energy $\Delta E$ for this process was determined from the slope of the straight line and was calculated to be 0.89 eV.

### 5.3.3. Sample B

The second insulation sample where a prominent loss peak is evident is in sample B. This sample was first thermally aged for 360 hours at $100^{\circ}C$ before the Schering Bridge measurement was made.

During the Schering Bridge test, the sample was exposed to temperatures ranging from $21.4^{\circ}C$ to $40^{\circ}C$. The loss measurement was subsequently recorded as a function of temperature. Similarly, the maximum electric field strength applied to each sample during testing was 4.5 kV/mm.

Following the Schering Bridge test a dielectric spectroscopy measurement was made where the test procedures were the same as those for sample A. The results for sample B which are almost identical to those for sample A are shown in appendix A at the end of this work.

In figure 5.18, 2D and 3D graphs of $\tan(\delta)$ are shown. Again, the linear y-axis makes it easier to locate precisely the $\omega_p$ frequencies. From this an Arrhenius plot is constructed as in figure 5.19 and the activation energy behind the relaxation loss peaks in sample B can be determined. This activation energy was calculated from the slop of the Arrhenius graph to be 0.92 eV.

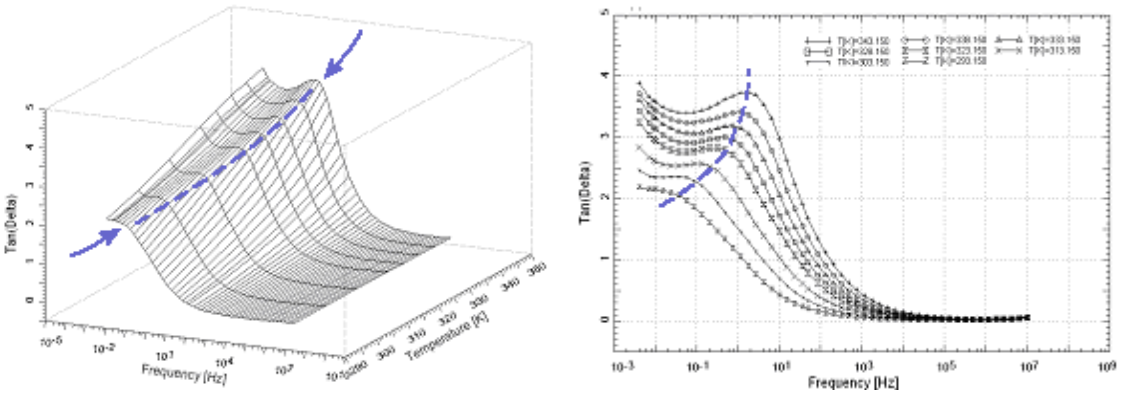


***Figure 5.18.*** *3D and 2D graphs of tan ($\delta$) as a function of frequency and temperature for sample B*

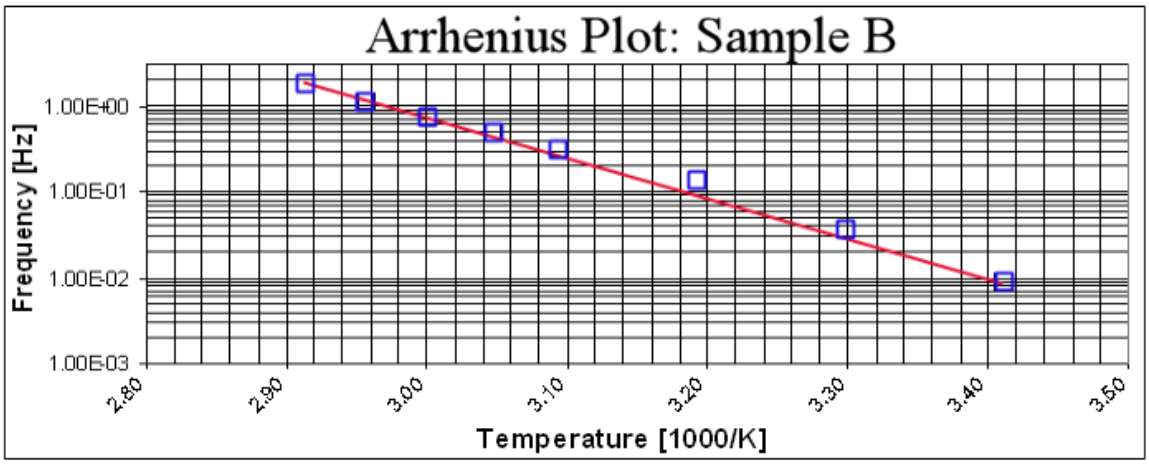


***Figure 5.19.*** *Arrhenius plot for Sample B*

In an attempt to determine the origins of the observed loss peaks the results from sample B in this work were compared to similar dielectric spectroscopy results found in literature for Mass Impregnated insulation [69-70].[76-78].

In figures 5.20, 5.21 and 5.22 the dielectric spectra for sample B are compared with experiments in literature on samples containing different levels of moisture [69]. These samples were removed from a 10kV Mass Impregnated cable that was produced in 1979 by KWO and was in service between 1981 and 1998.

Furthermore, the samples were treated before testing; first placed in a vacuum oven, dried at $110\,^{\circ}C$ for 24 hours and then at $140\,^{\circ}C$ for 1 hour to reach an estimated moisture content of less than 0.5%. Saturated salt solutions were then used to create moisture levels between 0.18% and 8.69% within the samples. The spectroscopy tests were made at ambient temperature, *circa* 16-18 $^{\circ}C$ .

Comparing the $20\,^{\circ}C$ measurement from sample B in this work (left) to the result for the sample containing 4.96% moisture (right) in figure 5.20 the following similarities were observed;

- At $1\cdot10^{-2}$ Hz the magnitude of $\tan(\delta)$ for the highlighted results fall between the values of $1\cdot10^{1}$ and $1\cdot10^{0}$ .
- The loss peaks for the highlighted results occur at frequencies close to $1\cdot10^{-2}$ Hz.
- At $1\cdot10^{2}$ Hz the value for both $\tan(\delta)$ highlighted results are close to $2\cdot10^{-1}$ .

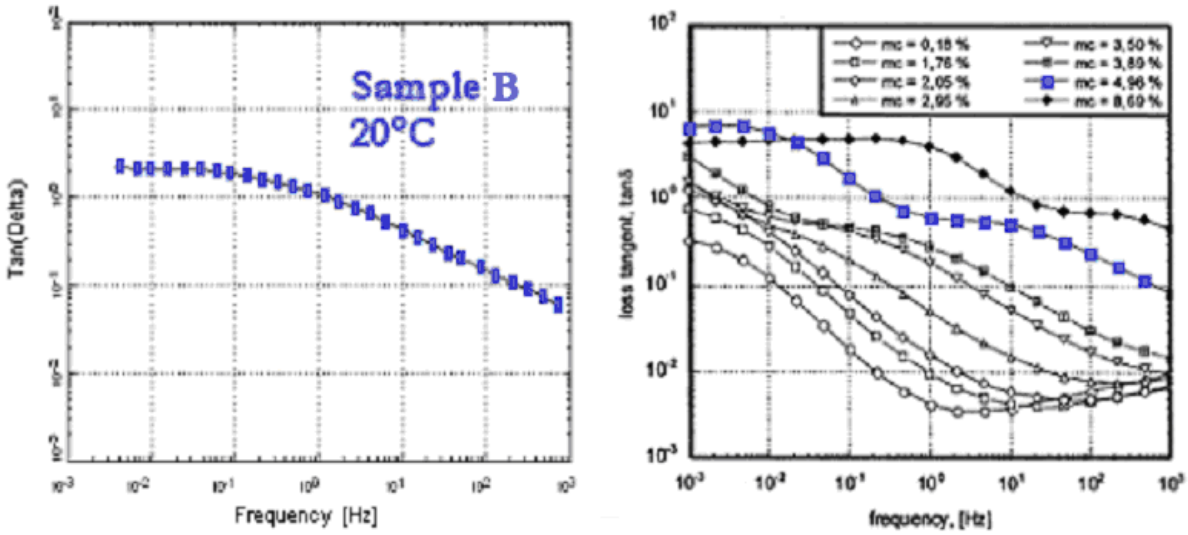


***Figure 5.20.*** *Comparison of tan( $\delta$ ) for sampleB to results from literature*

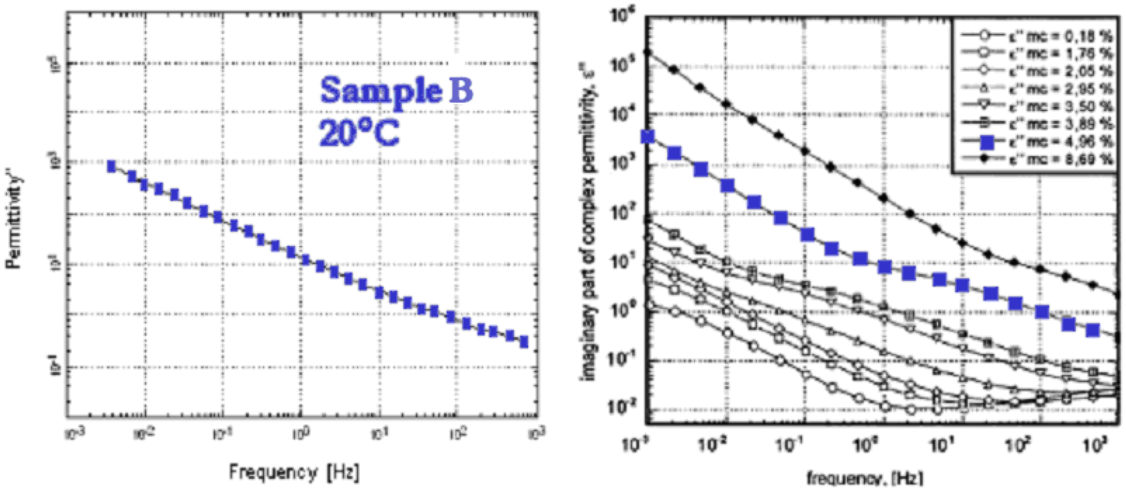


***Figure 5.21.*** *Comparison of* $\varepsilon''(\omega)$ *for sample B to results from literature*

In figure 5.21 a similar comparison is made for the loss component of the permittivity $\varepsilon''(\omega)$. The following similarities were observed;

- The highlighted curves have a similar shape.
- At $1 \cdot 10^{-2}$ Hz the magnitude of $\varepsilon''(\omega)$ for the highlighted measurements are both close to $1 \cdot 10^{2}$.

- At $1 \cdot 10^{2}$ Hz the magnitude of $\varepsilon''(\omega)$ for the highlighted measurements are both close to $1 \cdot 10^{0}$.

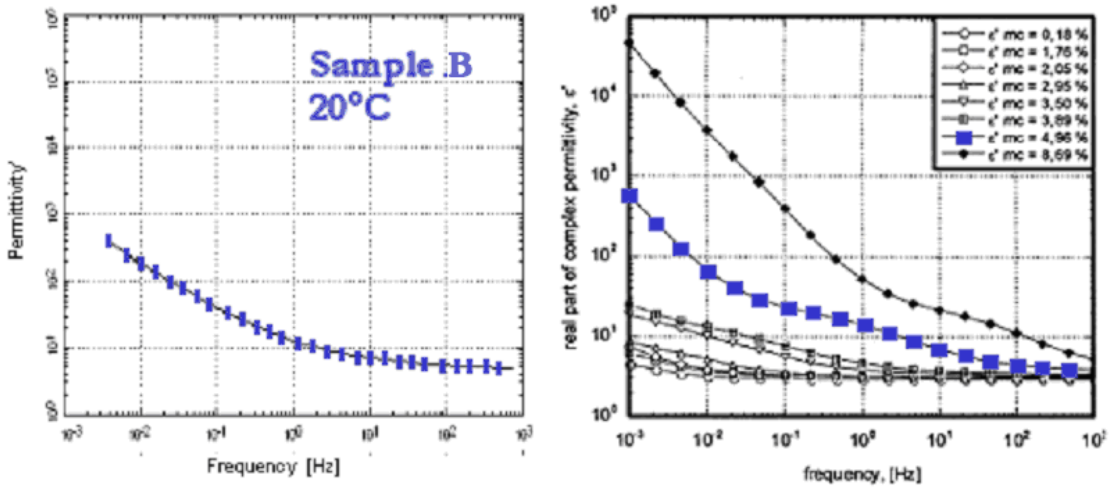


***Figure 5.22.*** *Comparison of* $\varepsilon'(\omega)$ *for sample B to results from literature*

In figure 5.22 the final comparison is made for the capacitive component of the permittivity $\varepsilon'(\omega)$. From this the following conclusions were drawn;

- The highlighted curves have a similar shape.
- At $1 \cdot 10^{-2}$ Hz the magnitude of $\varepsilon''(\omega)$ for the highlighted measurements are very close to $1 \cdot 10^{2}$.
- As the measurement approached higher frequencies the magnitude of $\varepsilon''(\omega)$ for both highlighted results have values between 1 and 10

In figure 5.23 the dielectric spectroscopy results from samples containing various moisture levels are presented in a paper by R.Neimanis, R.Ericksson and T.K.Saha [70]. The samples in this case are from a 12kV Mass Impregnated cable.

However, the preparation work to achieve the desired moisture levels was the same involving saturated salt solutions. In [70] the dielectric spectroscopy tests were made under the following conditions; Test cell temperature: 20-22 Degrees. Test cell humidity 8-13%. Test Voltage: 5V.

In figure 5.23 the result for the sample with 5.19% (red) moisture content shows similarities with the dielectric response observed in sample B at $20\,^{\circ}C$ in figure 5.20, 5.21 and 5.22. Similar to the previous comparison, at a frequency of 10mHz the values for $\varepsilon''(\omega)$ are close to $1 \cdot 10^{3}$; and the values of $\varepsilon'(\omega)$ are both close to $1 \cdot 10^{2}$. Furthermore, in both $\tan(\delta)$ graphs a peak maximum is observed at a frequency close to 10mHz.

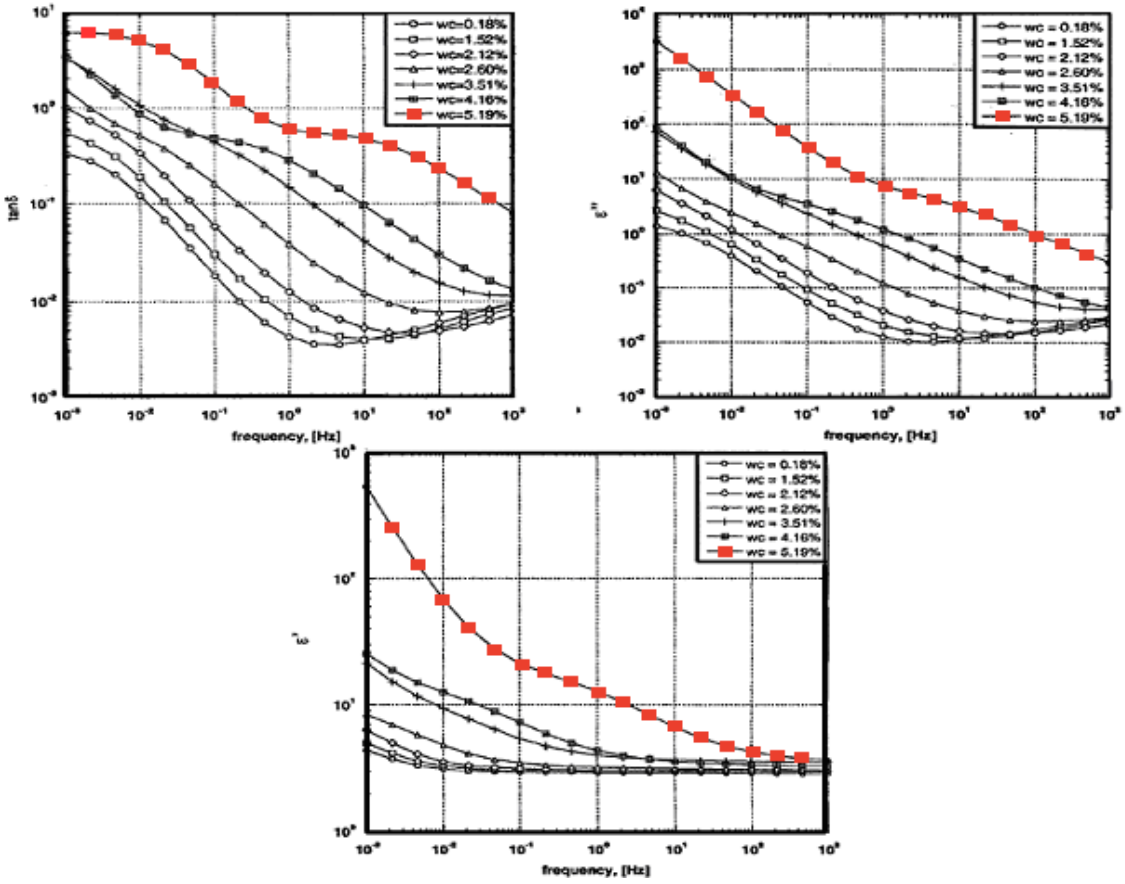


***Figure 5.23.*** *Dielectric results from samples with varying moisture contents [70]*

In figure 5.24 the dielectric spectroscopy results investigating water ingress into a Mass Impregnated cable are examined in a paper published by R.Neimanis, R.Eriksson and R.Papazyan [76]. The 10kV Mass Impregnated cable used during the test had previously been in service for 17 years.

An artificial incision was made in the cable and frequency domain spectroscopy measurements were recorded at different times as shown in figure 5.17. The $\tan(\delta)$ graph on the left is for the test made on a cable length of 0.4m and the $\tan(\delta)$ graph on the right hand side is for a cable length of 2.8m.

In figure 5.24 there is further evidence that the observed results in sample B can be attributed to the moisture content within the sample. In the $\tan(\delta)$ graph to the right in figure 5.14 the results above 248 hours of water ingress compare well with the $20^{\circ}C$ result for sample B in figure 5.20.

This is also the case in the $\tan(\delta)$ graph to the left in figure 5.24. For water ingress durations at 258 hours and exceeding that time the result is similar to the $20^{\circ}C$ result for sample B in figure 5.20.

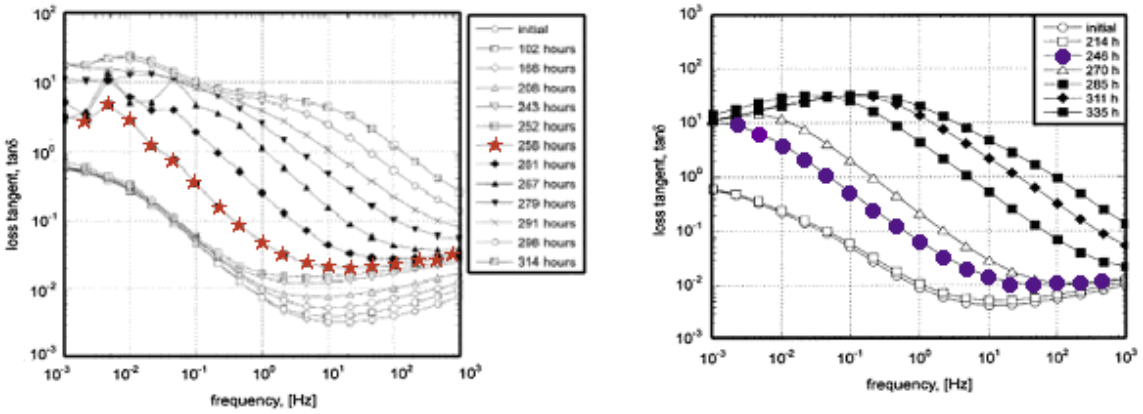


***Figure 5.24.*** *Dielectric results from samples with varying moisture ingress times [4]*

In figure 5.25 dielectric spectroscopy results are shown from a paper by P. Werelius [77] investigating new and a field aged cables.

The losses in the field aged cable at 10mHz are again very similar to those observed in the results from sample B.

According to this paper the field aged cable has a moisture level between 4.1 and 4.9%.

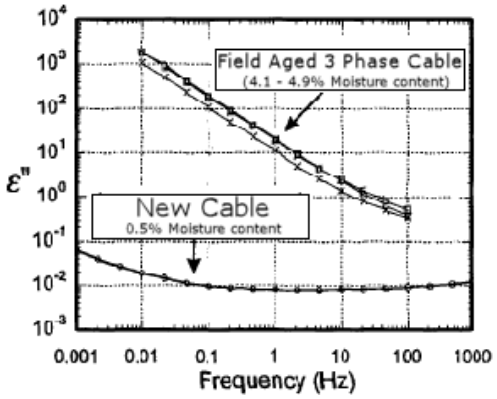


***Figure 5.25.*** *DS Result from New and Field Aged Cables [77]*

To determine the actual moisture content of the samples used in this work the two experimental methods described in chapter 4, section 4.2 and 4.3 are used. The first technique uses Karl Fischer Titration to determine the moisture levels in samples. The results from this test are shown in figure 5.26.

| | KFT Test A | KFT Test B |
|---|---|---|
| Reference Sample | 0.32% | 0.38% |
| Sample Aged for 53 Hours | 2.5% | 2.1% |
| Sample B | 4.1% | 3.8% |

***Figure 5.26.*** *Moisture content in samples determined by Karl Fischer Titration*

The second test method to determine the moisture content in samples using a vacuum oven is explained in section 4.3. The results of this test are shown in figure 5.27.

| | Sample 1 **Reference** | Sample 2 **Aged Sample (53 hours)** | sample 3 **Sample B** |
|---|---|---|---|
| **Moisture Content %** (after 24 hours in vacuum oven at 50 ºC ) | 0.08% | 1.61% | 3.77% |
| **Moisture Content %** (after 96 hours in vacuum oven at 50 ºC ) | 0.33% | 2.20% | 4.53% |

***Figure 5.27.*** *Moisture Content in Samples Determined by Vacuum Oven Drying*

These tests confirm that the moisture levels in sample B are somewhat high as originally suspected. The Karl Fischer Titration result shows the two type B samples tested have moisture contents of 4.1% and 3.8% respectively. The two reference samples tested are found to have 0.32% and 0.38% moisture. The increase in moisture level in samples is therefore quite considerable compared to the low values in the reference samples.

Furthermore, the second determination method calculated a moisture content of 4.53% for sample B after 96 hours in the vacuum oven at 50 ºC.

## 5.3.4. Discussion

From the experimental work described in section 5.3 the origins of the prominent relaxation loss peaks observed in the $\tan(\delta)$ graphs for samples A and B can be explained. Firstly, it is proposed that these loss peaks are $\beta$-relaxation processes. This interpretation is supported by the following arguments;

- The observed loss peaks are distinct and have a broad frequency span which is a characteristic feature of a $\beta$-relaxation process [11].
- The process has an Arrhenius type temperature dependency. The possibility of an $\alpha$-relaxation can therefore be ruled out.
- The increased moisture levels measured behave as a swelling solvent with tendencies to increase the activation energy and the cooperativity of the local chain motion [71]. Therefore, if the DP value has reduced due to thermal ageing, the cooperativity of the segmental chain motion will increase due to the additional moisture. $\beta$-relaxation is attributed to the segmental (local) chain motion of the polymer backbone.

The activation energies for the underlying processes were calculated from the Arrhenius graphs in figures 5.17 and 5.19 and were subsequently found to be 0.89eV and 0.92eV respectively. In literature, the following research studies investigate the activation energy for degradation processes in cellulose and paper composite insulation;

Experimental work by L.E.Lundgaard investigated the activation energy for a thermally activated kinetic process in oil-impregnated paper insulation. In this case the activation energy was found to be 1.181eV [79].

A thorough review by A.M.Emsley investigating the kinetics and mechanisms of the low-temperature degradation of cellulose calculate the activation energy to be $1.15 \pm 0.06$eV [80].

In work by H. Ding and Z. Wang [81] the activation energies for degradative processes in many different materials were determined using the Arrhenius equation. The following values were calculated;

- Kraft paper in air: 0.118eV
- Kraft paper in mineral oil: 0.34eV.
- Kraft paper in mineral oil (low moisture and oxygen levels): 0.753eV.
- Kraft paper in dried and degassed transformer oil: 0.946eV
- Thermally upgraded paper in mineral oil: 1.24eV
- Bleached bisulfite pulp in sealed glass jars, 75% RH: 0.85eV

In the same paper by H. Ding and Z. Wang [5.3.3] the activation energies for degradative processes in different materials were determined using the time temperature superposition principle (TTSP). The basis of this technique is analogous to shifting data curves in the frequency domain to form a master curve.

However, in the case of TTSP the raw data representing the degree of degradation are shifted to the lowest temperature yielding a master curve. The resulting shifts are used to determine the activation energy of the degradation process. The following activation energies for the same samples as before were determined using this principle.

- Kraft paper in air: 0.44eV
- Kraft paper in mineral oil: 0.366eV
- Kraft paper in mineral oil (low moisture and oxygen levels):1.19eV
- Kraft paper in dried and degassed transformer oil: 1.01eV
- Thermally upgraded paper in mineral oil: 1.15eV
- Bleached bisulfite pulp in sealed glass jars, 75% RH: 1.07eV

The final work investigated was a paper by Emsley and Heywood [82] investigating the degradation of cellulose insulation in transformers and the effects of moisture and oxygen. The paper states that the activation energies for cellulose in oil are between 0.88eV and 1.24eV in various research findings.

Therefore, when compared to literature the activation energies of 0.89eV and 0.92eV for samples A and B are considered plausible. Moreover, the dielectric spectroscopy measurements recorded for samples A and B were subsequently compared to similar measurements in literature [69-70].[76-78] Various works investigating insulation samples with increased moisture levels showed results matching closely the observations in this thesis. The measurements in literature were typically characterised by very high values in all dielectric relaxation spectra for samples having increased moisture levels. Furthermore, the contribution of distinct relaxation loss peaks was also evident in these works.

The conclusions from these literary findings were that the dielectric relaxation behavior at low frequency was certainly due to additional moisture content. Furthermore, samples from literature with moisture levels close to 5% showed very similar test results to the $\tan(\delta)$, $\varepsilon''(\omega)$ and $\varepsilon'(\omega)$ measurements found in the experimental work in this thesis.

To investigate this further, two experimental methods were then used to determine the moisture content in sample B in this work. The results were fairly conclusive showing sample B contained levels of moisture between 3.8% and 4.53%. This is in contrast to the moisture levels typically between 0.3% and 0.4% found in the reference sample by the same determination technique.

The origin of this increased moisture content is still a matter of contention. It is plausible that moisture manifested due to the thermal ageing of the sample in the oven at $100^{\circ}C$ for 360 hours. However, samples thermally aged for 1320 hours in section 5.2 showed moisture levels in the vicinity of 2%. This 2% moisture is likely a byproduct of chain scission degradation in the cellulose.

However, this doesn't account for the additional moisture that was discovered in the sample. It is likely that the excess moisture was absorbed from the air after the Schering Bridge test was complete. When the sample was removed from the Schering Bridge after the final $40^{\circ}C$ measurement it was still hot and the hot oil subsequently absorbed moisture rapidly from the air.

The reasoning behind this high absorption of moisture is as follows. With reference to the Fabre-Pichon curve in figure 5.28 the dynamic behavior of moisture is shown by the green lines for an air-paper-oil complex. At increased air humidity the moisture in the oil increases considerably. This is observed as a general shift in the green curve to the right of the graph for the higher air humidity. Furthermore, when the oil is at high temperature and the humidity is high also the horizontal shift of the green line is even more pronounced.

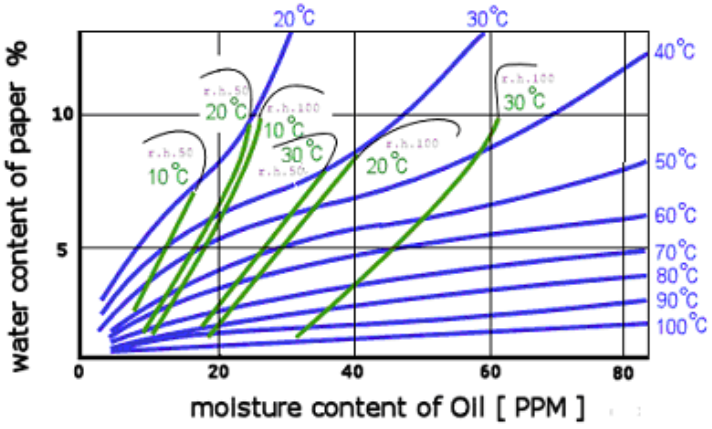


***Figure 5.28*** *Fabre-Pichon curve [58]*

This could account for the additional moisture found in the samples. From this point of view the importance of proper sample handling is essential. Gloves should be used at all times and the samples should be exposed to the air as little as possible. This is good practice to ensure samples don't become contaminated.

# 5.4. Non-Impregnated Kraft Paper

## 5.4.1. Introduction

In this section dielectric spectroscopy tests are used to investigate the dielectric response of Non-Impregnated Kraft Insulation paper. The samples tested are from electrical grade Kraft insulation paper acquired from Prysmian Cables and Systems in Delft, The Netherlands. The dielectric spectroscopy test sequence used for the samples measures at the fixed temperature measurement points shown in figure 5.29.

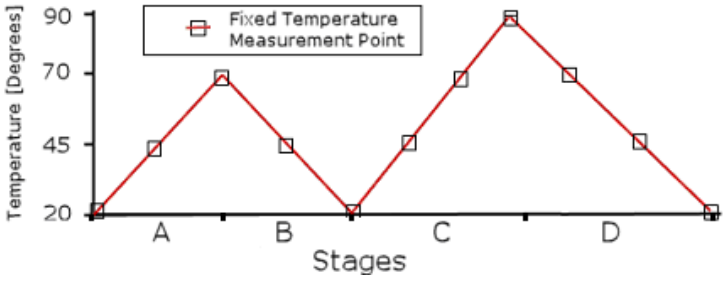


***Figure 5.29.*** *Dielectric spectroscopy fixed temperature measurement point sequence*

## 5.4.2. Results

In figure 4.30 the $20^{\circ}C$ $\varepsilon''(\omega)$ measurement is shown for stages A, B and D. The losses decrease considerably as the test proceeds through the stages. This could be due to the removal of moisture from the paper within the test cell by the combinations of temperature cycling and the effect of the constant flow of nitrogen gas in the test cell.

In figure 5.31 $\varepsilon''(\omega)$ and $\varepsilon'(\omega)$ are plotted on the same graphs at temperature measurement points during stages A and B. In these graphs there is an initial low frequency dispersion LFD effect evident at $20^{\circ}C$ and at $45^{\circ}C$ in stage A. In the measurement at $70^{\circ}C$ in stage A the response is beginning to diverge from this LFD behavior. Finally at $45^{\circ}C$ in stage B the LFD has fully disappeared and the capacitive component of $\varepsilon'(\omega)$ becomes flat in nature.

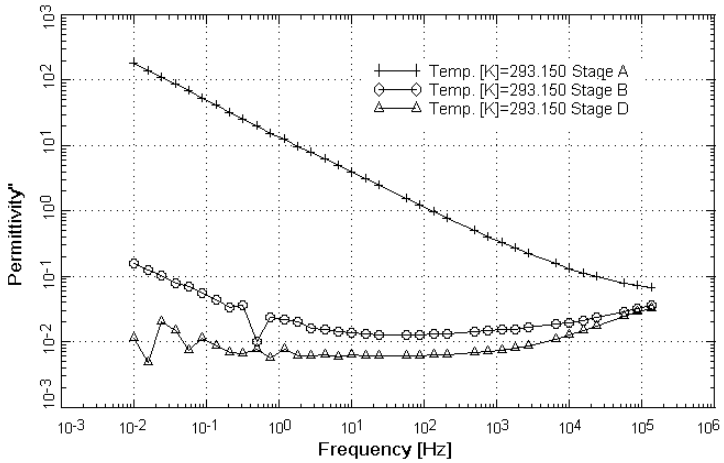


***Figure 5.30.*** *The loss component of the permittivity for the measurements At 20 degrees Celsius for all stages.*

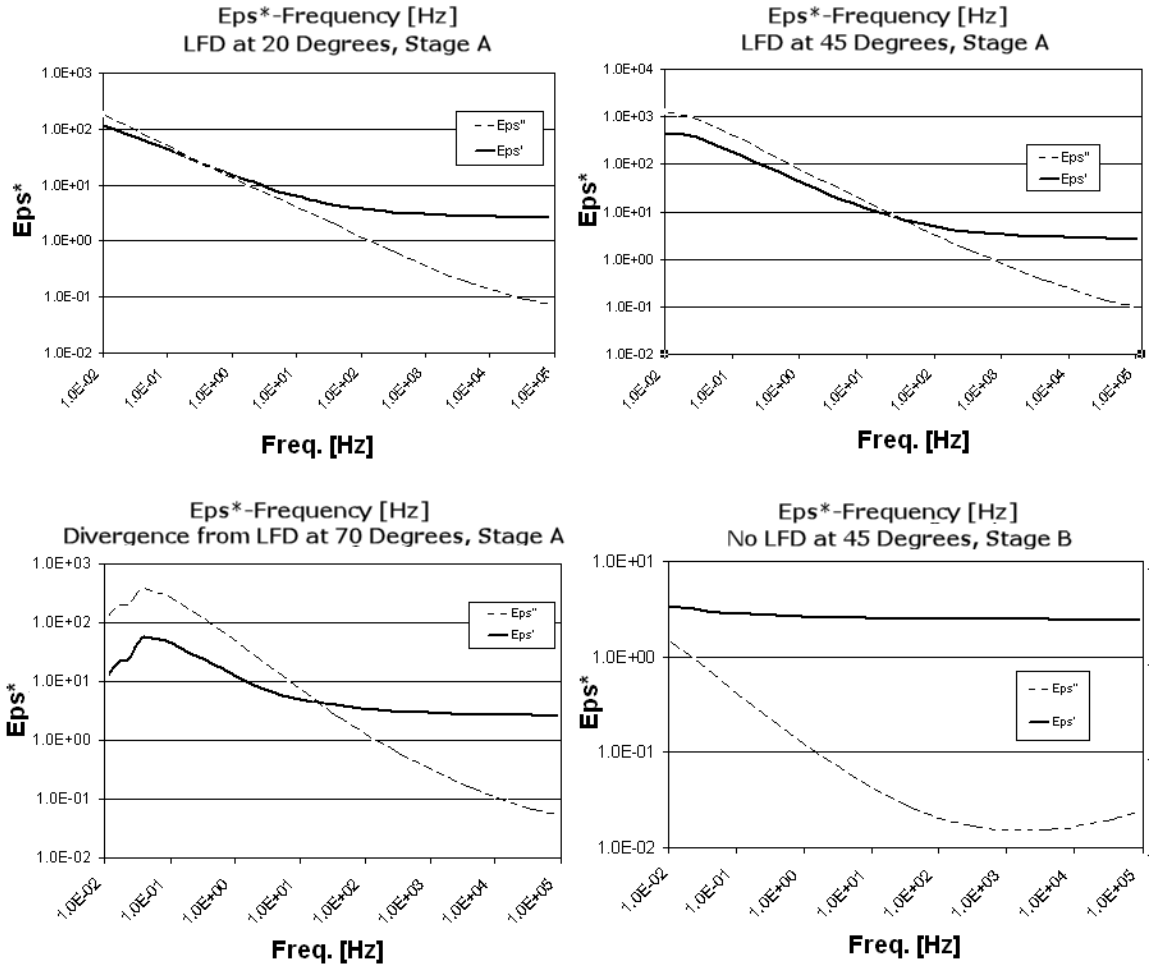


***Figure 5.31.*** *Dielectric spectroscopyresult showing LFD in Kraft insulation*

### 5.4.3. Discussion

In stage A the low frequency value of $\varepsilon'(\omega)$ and $\varepsilon''(\omega)$ are considerably high with respect to those measurements in stage D. There is a LFD phenomenon evident in stage A that arises due to slowly moving charge carriers such as ions or hopping electrons at the electrode interface or in the bulk or the insulating material. In stage A this LFD dominates the response at low frequency.

Furthermore, it is difficult to identify any other polarisation processes such as loss peaks which may be contributing at low frequency. This is possibly due to the predominance of this LFD effect where other processes may be overshadowed.

In [8] ionic conduction is proposed as the most probable mechanism of charge injection into the Mass Impregnated paper. It is understood that Schottky injection occurs at the dielectric interface due to the dissociation of impurities etc from the insulation itself.

Perhaps this LFD is in fact due to the dissociation of surface moisture in the paper insulation sample. This is plausible since the paper is hygroscopic by nature. Furthermore, in this case there is no oil impregnation making the paper particularly susceptible to absorbing moisture from the air. This may therefore be the cause of the low frequency dispersion effect observed initially during stage A.

The losses decrease considerably during stage D of the measurement cycle. This might be due to a reduced injection of ionic carriers at the electrode interface or by some effect that arose due to the temperature cycling or by the effects of the constant stream of nitrogen gas through the test cell.

A final point to note is that the losses are lower in the 20 measurement in stage D for the paper than in the same measurement for the reference Mass Impregnated sample in figure 5.3. This is as expected since the oil is more conductive and because the measurement is made in a controlled environment with nitrogen gas. If the test were performed in the ambient air then the hygroscopic action of the paper could lead to higher losses than those observed in the impregnated paper.

# 6. Conclusions

This thesis is as an in dept resource for information concerning *high voltage direct current* power transmission. Developments in this technology since the '*battle of the currents' circa 1880*, are highlighted and some existing operational systems are discussed.

The implications of faults arising in such cable systems are far reaching and from this perspective a repository for insulation monitoring systems was developed. This repository is subcategorised into *on-site* and *off-site* solutions in this work and some existing operational systems were discussed.

It was noted that many *on-site* techniques exist to monitor insulation systems, identifying localised and integral processes of degradation. Furthermore, it is envisaged that many of such techniques, traditionally used on ac cable systems are just as applicable to dc cable systems.

It was proposed that techniques such as the *Oscillating Wave Test System* can be used to interrogate a limited length of a HVDC cable system and monitor the localised partial discharge activity present.

Furthermore, already operational *on-site on-line* techniques such as *Distributed Temperature Sensing* are discussed. The *DTS* solution helps identify hotspots in lengths of cable systems using optical fibres. Yet again this technology has limited spatial reach and generally speaking there appears to be no system that can monitor a full HVDC cable system.

In the context of the experimental work in this thesis, *off-site broadband dielectric spectroscopy* is proposed as a tool to assess the condition of insulation of the Mass Impregnated type. This type of insulation is investigated since predominantly classical HVDC systems throughout the world typically employ Mass Impregnated cables.

*Broadband dielectric spectroscopy* is a sophisticated tool which can be used in the quality assessment of the cable insulation. Analysis of the dielectric relaxation behavior of the insulation can reveal a lot about the extent of degradation in the insulation samples.

Furthermore, different byproducts of insulation degradation are sometimes identifiable by telltale characteristics in the resulting relaxation spectra. It was therefore proposed in this work that dielectric spectroscopy measurements on insulation samples can be compared to a database of pre-existing relaxation spectra. The condition of the insulation under test can therefore be assessed based on this pre-existing knowledge base.

.

In summation, the experimental work in this thesis uses frequency domain, dielectric relaxation analysis to investigate the integrity of Mass Impregnated paper insulation. The spectroscopy tests focus on the low frequency relaxation processes in insulation samples, usually characterised by a dc conductivity term or by some Low Frequency Disperion (LFD) effect. Furthermore, these effects lend to challenges in the interpretation of results at low frequencies, more often so when loss peaks arise and appear superimposed on a dc conductivity term.

The following samples were investigated in this work using frequency domain dielectric spectroscopy;

- The low frequency dielectric response of Mass Impregnated paper insulation subject to artificial thermal ageing,
- The underlying source of prominent loss peaks discovered in two Mass Impregnated paper insulation samples and,
- The low frequency dielectric response of Non-Impregnated Kraft insulation paper.

In light of this work it was found that samples containing increased moisture levels were identifiable by characteristic relaxation spectra. Some moisture was found to have manifested as a result of the thermal ageing of samples as in section 5.2.

However, in section 5.3 there was evidence of some increased moisture levels due to the same thermal ageing but also due to sample contamination. The readiness of Mass Impregnated insulation to absorb moisture from the ambient air shows that proper handling procedures for this material is essential at all times.

Samples should be stored in air tight dessicators and gloves should be used when handling. When tests are made, the exposure times of the samples to the ambient surroundings should be as short as possible.

To recapitulate, this work proposes that the frequency domain relaxation characteristics of Mass Impregnated insulation are used as identification markers for the integrity of operational HVDC cable systems. Furthermore, this analysis technique should involve knowledge base of existing results coupled with processes of fingerprinting and statistical analysis. In saying this, some concluding remarks concerning the experimental test results in section 5.2, 5.3 and 5.4 are now discussed.

# 6.1. Mass Impregnated Insulation Subject to Artificial Thermal Ageing

The dielectric spectroscopy results for thermally aged Mass Impregnated insulation show small divergences from the low frequency response observed in the reference, un-aged samples. However, the small increase in losses and the appearance of subtle loss peaks at low frequency are consistent for all thermally aged insulation samples tested in section 5.2 of this thesis.

It was therefore concluded that thermal ageing at $100^{\circ}C$ had an apparent effect on the insulation. However, the cause of this effect required further investigation. In attempts to interpret the observed low frequency behavior the relaxation spectra were compared to similar research endeavors in literature. From this literary investigation it was noted that the relaxation behavior observed in the thermally aged samples showed strong similarities with the dielectric response for samples containing approximately 2% moisture.

Subsequent to these findings the moisture levels in the samples were determined using Karl Fischer Titration and a second experimental technique involving a process of vacuum oven drying the samples and calculating their percentage weight loss.

The results from these experimental determination methods indicate the moisture level of the thermally aged samples to be between 2.1% and 2.5%. This showed a strong divergence from the moisture levels between 0.32% and 0.38% determined for the un-aged reference sample.

It was therefore concluded with reasonable certainty that moisture levels slightly above 2% were consistent with the observed relaxation effects at low frequency. Furthermore, in this analysis the relaxation loss peaks in question were identified as $\beta$-relaxation processes caused by the segmental chain motion in the cellulose polymer. This chain motion is understood to be further enhanced by the presence of additional moisture in the samples.

Further justification for this interpretation is given in section 5.2 which cites degradative chain scission of the cellulose paper due to thermal ageing as the underlying cause. The additional moisture was adjudged to be the byproduct of these chain scissions.

From this analysis there is conclusive evidence that thermal ageing has occurred in the Mass Impregnated samples which were placed in the oven at $100^{\circ}C$. Furthermore, characteristic relaxation spectra exhibiting increased losses and the appearance of subtle relaxation loss peaks at low frequency are the proposed identification markers of this degradation. The observations also correlate to the increased moisture levels which have manifested as a byproduct of this degradation process.

## 6.2. The Source of Prominent Loss Peaks in Mass Impregnated Insulation

The source of the pronounced loss peaks in $\tan(\delta)$ and the high values in all dielectric spectroscopy spectra for two Mass Impregnated insulation samples was investigated in section 5.3 of this thesis. The loss peaks in $\tan(\delta)$ were found to exhibit an Arrhenius type temperature dependency. From the resulting Arrhenius graphs the activation energies for the underlying processes were found to equal 0.89 eV and 0.92 eV for the samples investigated.

To check the validity of these results various papers in literature investigating the degradation kinetics of paper-composite insulation were referred to. In these papers a wide range of activation energies were reported making it difficult to draw definitive conclusions as to the validity of the results for the activation energies in this work.

Furthermore, in the majority of these papers there appears to be no general consensus on what the activation energy should be. However, one paper investigating the thermal ageing of cellulose in transformers states a range of activation energies between 0.88eV and 1.24eV as reported in literature.

To identify the source of the observed dielectric relaxation behavior, the results were compared to various publications in literature. It was thus concluded with some certainty that the observed behavior was consistent with samples having moisture levels of about 5%. In light of these findings the moisture levels in the samples from this work were investigated using the two experimental tests mentioned earlier.

The results of these determination methods confirmed that moisture levels between 3.8% and 4.53% were present in one sample. This was noted to be substantially high compared to the 0.32% to 0.38% levels determined in the reference sample. Moreover, the thermal ageing of these samples only accounts for some of the moisture. The additional moisture present still needed to be accounted for.

It was therefore proposed that the moisture content in the two samples was the result of two processes. The initial moisture levels in the two samples were understood to be due to the thermal ageing of the samples at $100^{\circ}C$. This would imply that a moisture level between 2.1% and 2.5% had already manifested before the Schering Bridge test.

It is proposed that the additional moisture found in the samples is absorbed from the surrounding air immediately after the Schering Bridge tests were complete. At this point in time the samples were still hot.

In support of this argument the Fabre-Pichon curves for an air-paper-oil complex suggest that oil absorbs higher levels of moisture at increased air humidity. Furthermore, it is also observed that when the oil temperature is increased this effect is more pronounced. It is thus reasoned that even during short exposure times the samples absorbed moisture from the air as they cooled down from the Schering Bridge test temperature.

Therefore, it is thought that the addition of moisture to the samples by this process is dependent on the sample temperature immediately after the test, the humidity of the surrounding environment and the exposure time of the samples to the surrounding air.

In summation, the moisture levels in the samples were found to be around 5% resulting from a process of thermal degradation and exposure to the air. The prominent relaxation loss peaks in the samples were identified as $\beta$-relaxation processes and were attributed to the segmental chain motion in the cellulose polymer. The thermal ageing was deemed to have caused the chain scissions in the cellulose. This effect is otherwise known as depolymerisation. This chain motion is understood to be enhanced by the presence of the level of moisture in the samples.

## 6.3. Dielectric Relaxation Response of Non-Impregnated Kraft Insulation Paper

In section 5.4, the dielectric spectroscopy measurements investigate the low frequency dielectric relaxations in Non-Impregnated Kraft insulation paper. The relaxation spectra are characterised by high losses and a dominant Low Frequency Dispersion (LFD) effect at the beginning of the test (during the first temperature cycle).

This LFD is understood to be the result of slow moving ions at the dielectric interface, possibly due to Schottky injection. Furthermore, it is believed that these ions arise due to the dissociation of surface moisture on the paper insulation sample. This is plausible since the paper is hygroscopic by nature and may contain a lot of surface moisture at the beginning of the test.

The LFD effect disappears as the measurement nears the end of the first temperature cycle. This is possibly due to the decrease in moisture at the papers surface as the test progresses. Furthermore, the losses are found to decrease to very low values as the test proceeds to the end of the last temperature cycle. This might be due to a further reduction in any remaining moisture within the sample.

In general, when compared to Mass Impregnated paper the losses were found to be lower at the $20^{\circ}C$ measurement at the end of both tests. This is as expected since the oil is more conductive and the losses are expected to be higher. Furthermore, the measurement is made in a controlled environment with nitrogen gas. If the test were performed in the ambient air then the hygroscopic action of the Non-Impregnated paper could lead to higher losses than those observed in the impregnated paper.

# Appendix A

## Thermally Aged Samples:

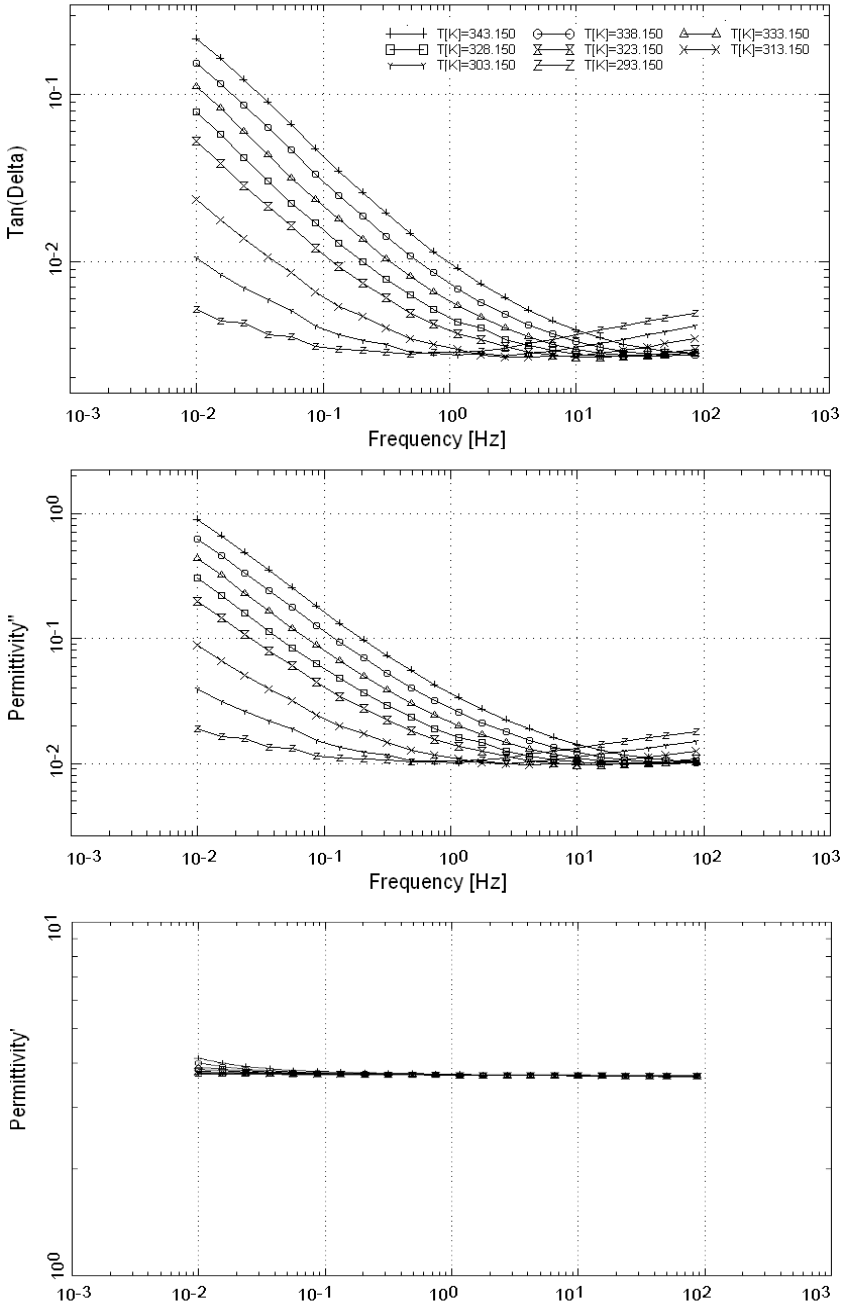


***Figure A.1.*** *Dielectric spectroscopy result for unaged reference sample, Stage D*

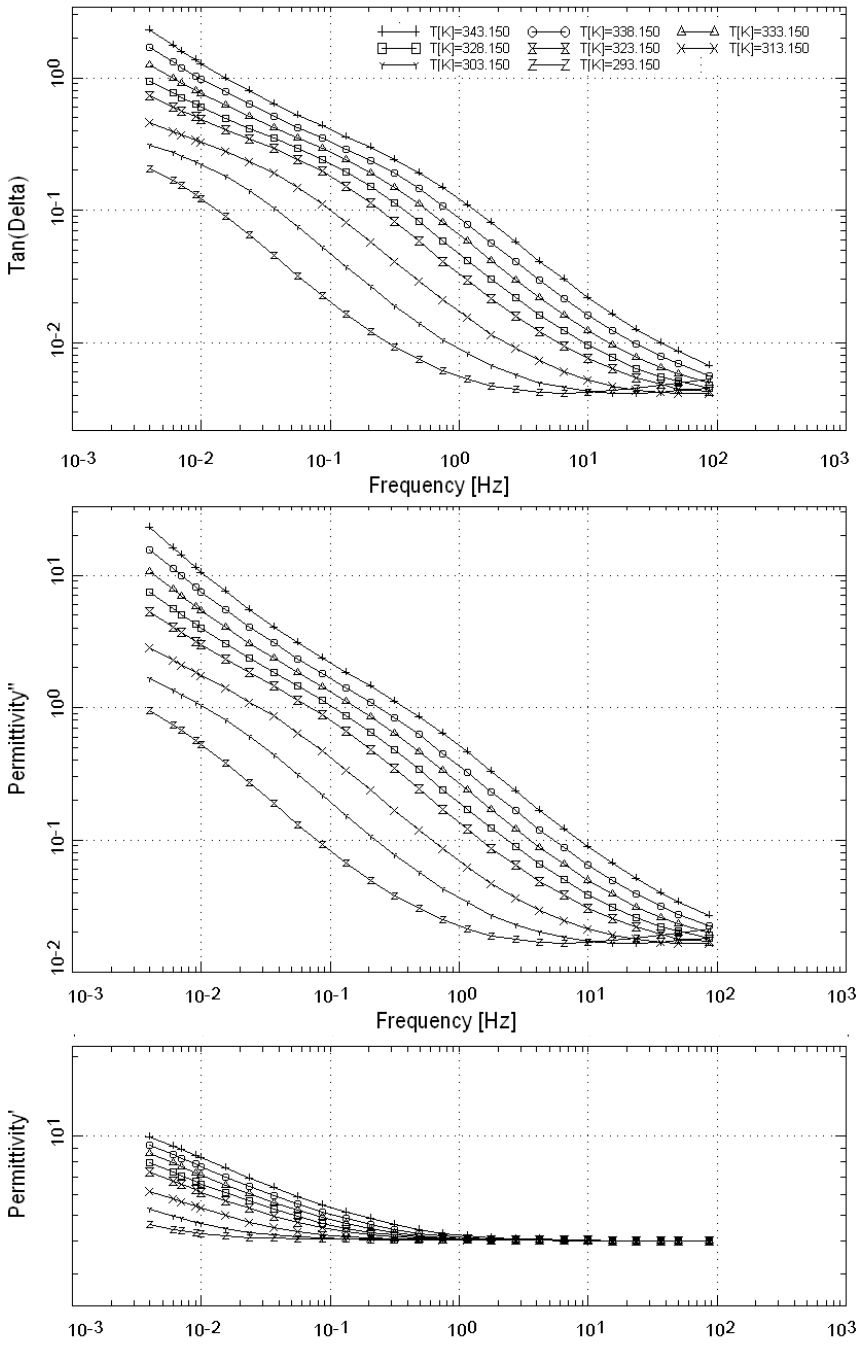


***Figure A.2.*** *Dielectric spectroscopy result for sample thermally aged for 53 hours, Stage D*

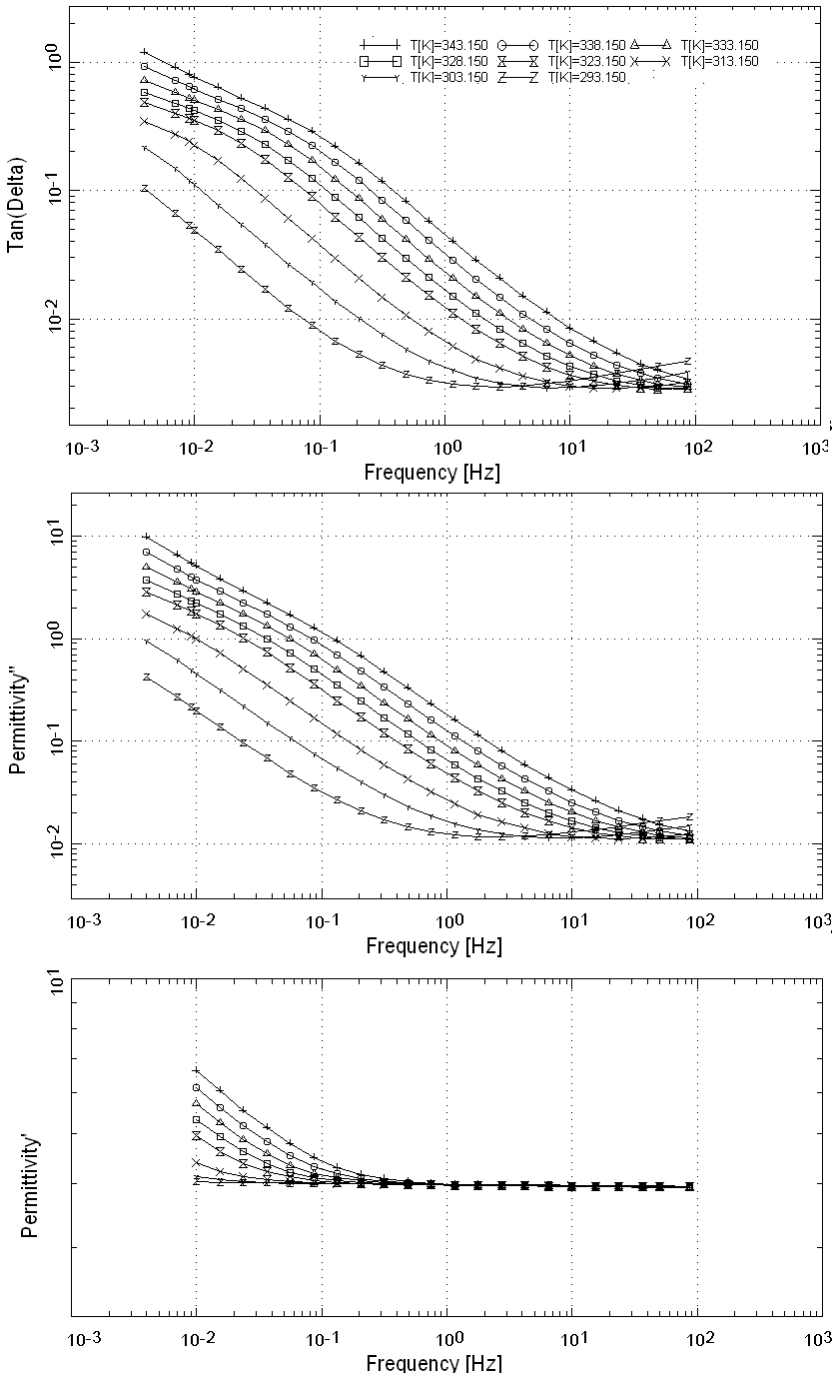


***Figure A.3.*** *Dielectric spectroscopy result for sample thermally aged for 1128 hours, Stage D*

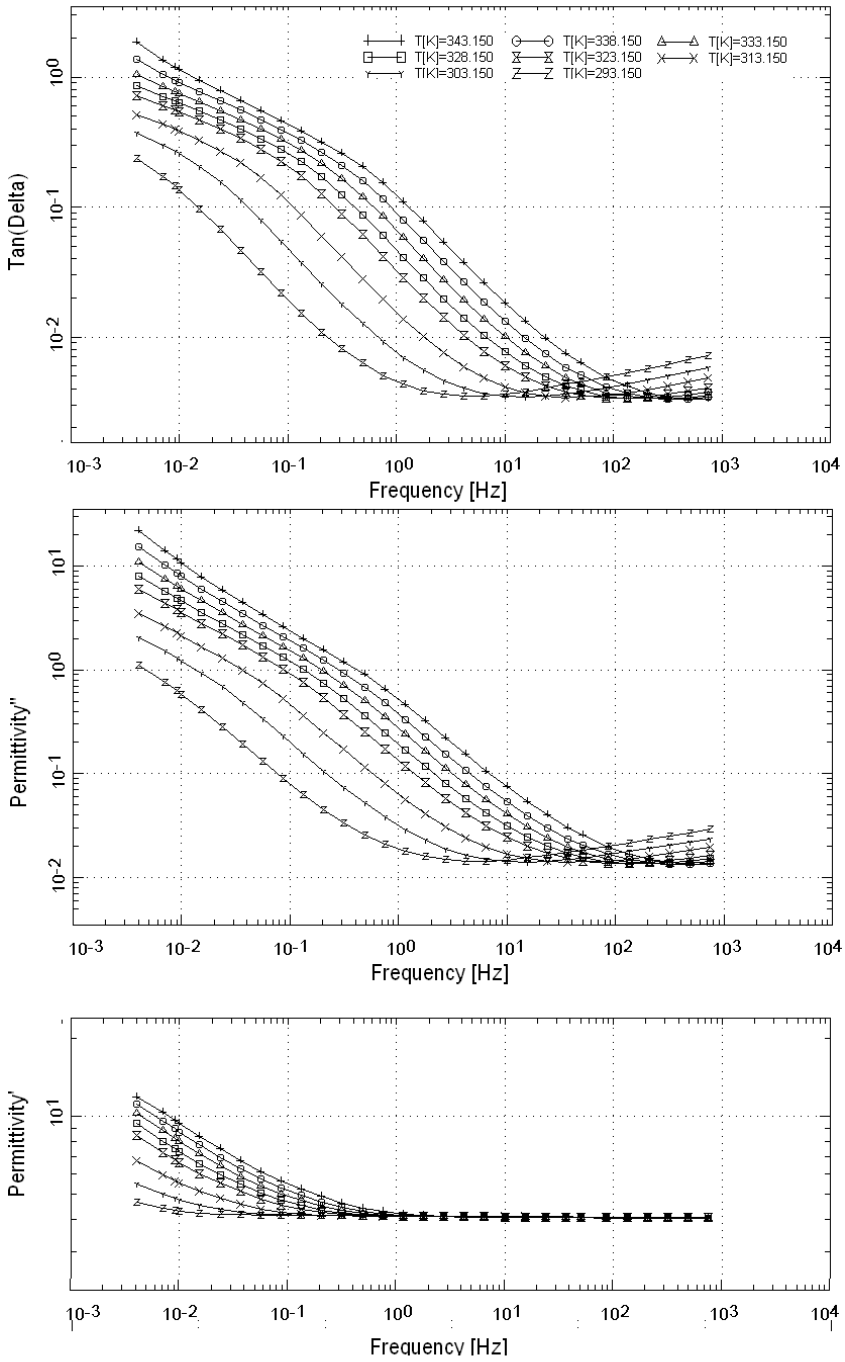


***Figure A.4.*** *Dielectric spectroscopy result for sample thermally aged for 1320 hours, Stage D*

# Prominent Loss Peaks:

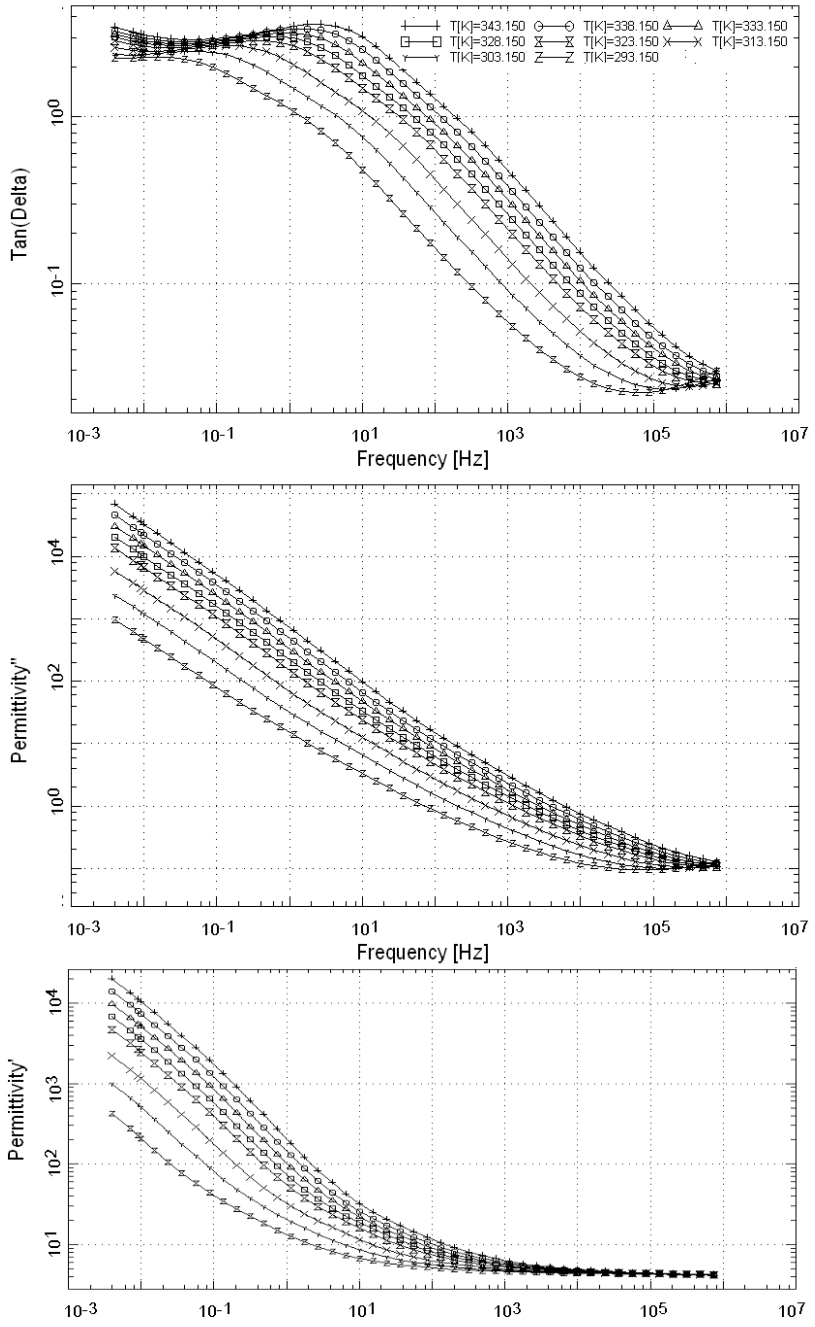


***Figure A.5.*** *Dielectric spectroscopy result for sample A, Stage D*

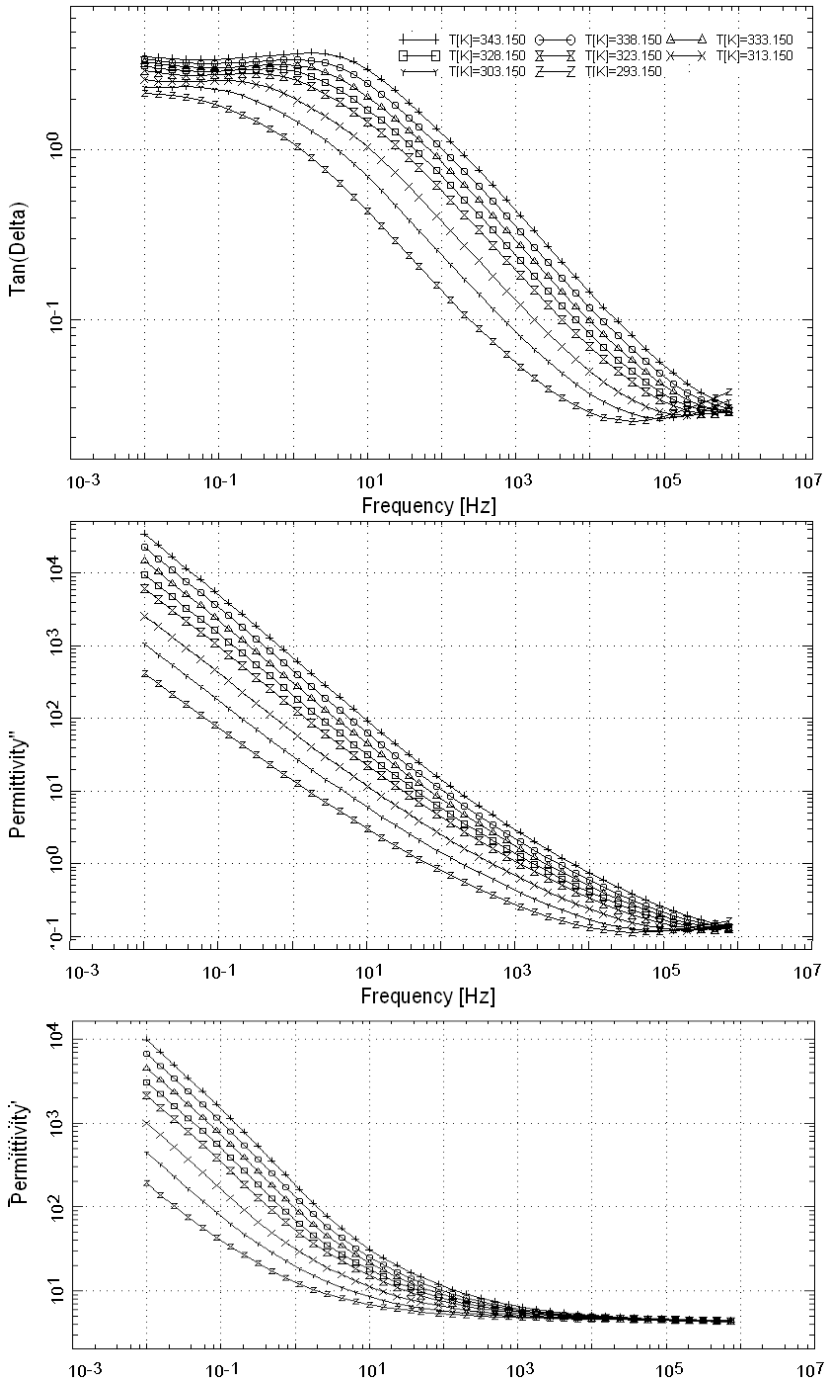


***Figure A.6.*** *Dielectric spectroscopy result for sample B, Stage D*

# References


**[1]** **ABB, "HVDC, efficient power transmission", ABB Power Systems.**

**[2]** **J. Graham et al., "Power System Interconnections using HVDC Links", ABB Brazil, ABB Sweden.**

**[3]** **M. Salah Khalil, "International Research and development trends and problems of HVDC cables with polymeric insulation", IEEE Elec. Ins. Mag., vol. 13, No. 6, 1997.**

**[4]** **M.P. Bahram, "Overview of HVDC transmission", Pow. Sys. Conf. and Exp., pp. 18-23, 2006.**

**[5]** **"High Voltage Direct Current transmission - proven technology for power transmission", Siemens.**

**[6]** **W. Litzenberger, "Advances in HVDC Technology as applied to the Pacific HVDC Intertie", IEEE Trans. and Dist. Conf. and Exp, pp. 1-4, 2008.**

**[7]** **S. Maruyama et al., "Development of a 500kV DC XLPE Cable System", Furukawa review, No. 25, 2004.**

**[8]** **M. Jeroense, "Charges and Discharges in HVDC Cables", PhD-thesis, Delft University of Technology, 1997.**

**[9]** **F.H. Kreuger, "Industrial High DC Voltage", Delft University Press, 1995.**

**[10]** **R. Bodega, "Space charge accumulation in polymeric high voltage dc cable systems", PhD-thesis, Delft University of Technology, 2006.**

**[11]** **B. Alijagic - Jonuz, "Dielectric properties and space charge dynamics of dc insulating materials", PhD-Thesis Delft University of Technology, 2007.**

**[12]** **F. N. Lim, R.J. Fleming, R.D. Naybour, "Space charge accumulation in power cable XLPE insultaion", IEEE Trans. on Diel. and Elec. Ins., Vol. 6, Iss. 3, pp. 273 -381, 1999.**

**[13]** **T.L. Hanley et al., "A general review of polymeric insulation for use in HVDC cables", IEEE Elec. Ins. Mag., Vol. 19, Iss. 1, pp. 13-14, 2003.**

**[14]** **F.H.Kreuger, "Industrial High Voltage 2", Delft University Press, 1992.**

**[15]** **E.Gulski et al., "Knowledge rules support for CBM of power cable circuits", CIGRE, 2002.**

**[16]** **J. Smith, E. Gulski, "Advanced condition assessment of high voltage power cables", IEEE, Proc. of Int. Symp. on Elec. Ins. Mat., Vol. 3, pp. 869-872, 2005.**

**[17]** **J. Elovaara et al., "PD measurements as a tool in upgrading the transmission capacity of the Fenno-Skan HVDC cable", CIGRE 21-203, 2000.**

**[18]** **CIGRE WG 21, "Recommendations for tests of power transmission DC cables for a rated voltage up to 800kV", Electra 189, 2000.**

**[19]** **G. Evenset, "The Breakdown Mechanism of HVDC Mass Impregnated Cables", CIGRE WG 21, Session 303, 2000.**

**[20]** **A. Helgeson, "Dielectric properties of machine insulation studied with dielectric response", PhD-thesis, Kungl Tekniska Hogskolan, Sweden 1997.**

**[21]** **S.M. Gubanski et al., "Dielectric response methods for diagnostics of power transformers", CIGRE, TF D1.01.09, 2002.**

**[22]** **A.K. Jonscher, "Dielectric relaxation in solids", J. Phys. D: Appl. Phys. 32 R57-R70, 1999.**

**[23]** **J. Einfeldt et al., "Molecular interpretation of the main relaxations found in dielectric spectra of cellulose – experimental arguments", University of Rostock, Germany, 2003.**

**[24]** **A. Rachocki et al., "Dielectric relaxation in cellulose and its derivatives", Proc. Int. meeting on radio and microwave spectroscopy, 2005.**

**[25]** **"Report of the World Commission on Environment and Development", United Nations, 1987.**

**[26]** **"Global installed wind power capacity (MW)", Global Wind Energy Council ,2008**

**[27]** **B. Quak, "Information strategy for decision support in maintaining high voltage infrastructures", PhD-thesis, Delft University of Technology, 2007.**

**[29]** **G. Hjalmarsson et al., "After-service analysis of the 32-year-old HVDC cable Gotland 1", CIGRE, Proc. of the 34th Session, Vol. 1, pp.21-302, 1993.**

**[30]** **I.Vancer et al., "A survey of the reliability of HVDC systems throughout the world during 2003 - 2004", CIGRE, B4.04, 2006.**

**[31]** ***High-voltage test techniques - Partial discharge measurements*, IEC 60270 Ed. 3.0 b, 2000.**

**[32]** **F. Wester, "Condition assessment of power cables using partial discharge diagnosis at damped AC voltages", PhD-thesis, Delft University of Technology, 2004.**

**[33]** **H. Kent, G. Bucea, "Distributed Temperature Sensing of high voltage cables – case studies from Sydney, Australia", CIGRE session, 1992.**

**[34]** **Agilent Technologies, *Distributed Temperature System***

**[35]** **J.E. Skog et al. , "The NorNed HVDC cable link – A power transmission highway between Norway and The Netherlands", ABB, Nexans, Statnett.**

**[36]** **P.Chen, B.Xu, J.Li, "A Traveling Wave Based Fault Locating System for HVDC Transmission Lines", IEEE, Int. Conf. on Power Sys. Tech., pp. 1- 4, 2006.**

**[37] G. T. Kohman, "Cellulose as an insulating material,Kohman", Ind. Eng. Chem., 31 (7), pp 807–817, 1939.**

**[38] T.A. Prevost, T.V. Oommen, "Cellulose Insulation in oil-filled power transformers", IEEE, Volume 22, Issue 1, Jan.-Feb. 2006 .**

**[39] ABB High Voltage Cables. AB, Sweden ,"Baltic Cable AB", Nobelvagen, Malmo, Sweden.**

**[40] A. Rachocki, E. Markiewicz, "Dielectric Relaxation in Cellulose and its derivatives", Acta Physica Polonica A, vol. 108, Issue 07, p.137**

**[41] Task Force D1.01.10, "Ageing of cellulose in mineral-oil insulated transformers", CIGRE, Electra, Numb 234, pages 50-59, 2007.**

**[42] I. Fofana, "Ageing of transformer insulating materials under selective conditions", European Transactions on Electrical Power, 2006.**

**[43] T.K Saha, "Investigations of temperature effects on the DR measurements of transformer oil-paper Insulation System", IEEE Trans. on Pow. Del., Vol. 23 Iss. 1, pp. 253-250, 2008.**

**[44] Tsuge, Kenji; Wada, Yasaku, "Effect of sorbed water on Dielectric Dispersion of Cellulose at low frequencies", Journal of the Physical Society of Japan, Volume 17, Issue 1, pp. 156, 1962.**

**[45] Ingebrigtsen, S. Dahlund, M. Hansen, W. Linhjell, D. Lundgaard, L.E., "Solubility of carboxylic acids in paper (kraft)-oil insulation systems", IEEE CEIDP Ann. Rep. on Elec. Ins and Diel. Phen., 2004.**

**[46] Kachler, A.J.; Hohlein, I., "Aging of cellulose at transformer service temperatures. Part 1: Influence of type of oil and air on the degree of polymerization of pressboard, dissolved gases, and furanic compounds in oil", IEEE Elec. Ins. Mag., Vol. 21, Iss. 2, pp. 15-21, 2005.**

**[47] Prevost, T.A.; Oommen, T.V, "Cellulose Insulation in Oil-Filled Power Transformers: Part 1 – History and Devlopment.", IEEE Elec. Ins. Mag., Vol. 21, Iss. 1, pp. 28-35, 2003.**

**[48] Lessard, M.C.; Van Nifterik, L.; Penneau, J.F.; Grob, R.; Masse, M , "Physiochemical characterization of the thermal ageing of insulating paper in power transformers" Conf. Rec. on the IEEE Int. Symp. on Elec. Ins, Vol.2, pp. 553 -537, 1996.**

**[49] A. M. Emsley and G. C. Stevens "Kinetics and mechanisms of the low temperature degradation of cellulose", Cellulose journal, 1994.**

**[50] Soares et al., "Low temperature thermal degradation of cellulosic insulating paper in air and transformer oil.", Polymer Int'l, 2001.**

**[51] H. Ding D. Wang, "On the degradation evolution equations of cellulose" cellulose 2008 [52] R.J. Heywood et al., "Life assessment of cable paper using slow thermal ramp methods", Thermochimica Acta, Volume 332, Issue 2, 19 July 1999, Pages 189-195**

**[53]** **Task Force D1.01.10, "Ageing of cellulose in mineral-oil insulated transformers", CIGRE, ELECTRA, Numb. 234, pages 50-59, 2007.**

**[54]** **A. K. Jonscher, "Review Article: Dielectric Relaxation in Solids", journal of applied Physics, 1999.**

**[55]** **A.M. Emsley, G. C. Stevens, "Review: Kinetics and mechanisms of the low-temperature degradation of cellulose", Cellulose, 1994.**

**[56]** **A. Shkolnik, "Determination of water content in transformer insulation", Proc. of 2002 14th IEEE Int. Conf. on Diel. Liq., pp. 337-340, 2002.**

**[57]** **J. Gielniak et al., "Dielectric responses of new and aged transformer pressboard in dry and wet states", IEEE, Proc. of Int. Symp. on Elec. Ins., Mat., Vol. 2, pp. 386-389, 2005.**

**[58]** **Y. Du et al.,"Moisture equilibrium in transformer paper-oil systems", Elec. Ins. Mag., Vol. 15, Iss.1, pp. 11-20, 1999.**

**[59]** **J. Einfeldt et al.,"Molecular interpretation of the main relaxations found in dielectric spectra of cellulose – experimental arguments", Cellulose 2, 2004.**

**[60]** **S. Cherukupalli at al., "Condition assessment of distribution PILC cables from electrical, chemical, and dielectric measurements", IEEE Elec. Ins. Mag., Vol. 20, Iss. 12. pp. 6-12, 2004.**

**[61]** **A.Rachocki et al., "Dielectric relaxation in cellulose and its derivatives", Proceedings International meeting on radio and microwave spectroscopy, 2005.**

**[62]** **Linhjell, D.; Hestad, O.L.; Gafvert, U.; Lundgaard, L.E "Dielectric Response of oil-impregnated cellulose from 0.1mHz to 3MHz" IEEE Int. Conf. on Diel. Liq, pp. 227-280, 2005.**

**[63]** **Y. Du M. Zahn "Moisture and temperature effects on the dielectric spectrum of transformer board", Electrical insulation and dielectric phenomena conference, 2002.**

**[64]** **Linhjell, D.; Gafvert, U.; Lundgaard, L.E, "Dielectric reponse of oil-impregnated paper insulation: variation with humidity and ageing level", IEEE Elec. Ins. and Diel. Phen, pp. 162-266, 2005.**

**[65]** **V. M. Montsinger, "Loading Transformers by Temperature", AIEE Trans., Vol. 32, 1930.**

**[66]** **W. Kuhn et al, "Hydrolysis of polysaccharides", Ber. 63, 1510, 1930.**

**[67]** **A. Ekamstam, "The behavior of cellulose in mineral acid solutions: Kinetics study of the decomposition of cellulose in acid solution", Ber. 69,553, 1939**

**[68]** **A. Jurlewicz, K. Weron, "A General Probabilistic approach to the Universal Relaxation Response of Complex Systems" Proc. SPIE, 3181, pp. 11-18, 1997.**

**[69]** **R. Neimanis, R.Eriksson, "Diagnosis of moisture in oil/paper distribution cables-part1: estimation of moisture content using frequency-domain spectroscopy", IEEE Pow. Eng. Rev., Vol. 22, Iss. 9, 2002.**

**[70]** **R. NEimanis, R.Eriksson, T. K. Saha, "Determination of moisture content in mass impregnated cable insulation using low frequency dielectric spectroscopy", IEEE Pow. Eng. Soc. Summer Meeting, Vol. 1, pp. 463-469, 2000.**

**[71]** **J. Einfeld, "Polymerdynamics of cellulose and other polysaccharides in solid state-secondary dielectric relaxation processes", Progress in Polymer Science Volume 26, Issue 9, Pages 1419-1472, 2001.**

**[72]** **E.Scholz, "Karl Fischer coulometry - the cathode reaction" Riedel-de Hahn A.G., Postfach, D-30926 Seelze, Germany.**

**[73]** ***Karl Fischer Titration basics,* EMD Chemical.**

**[74]** **Manual: Metrohm, 756/831 KF Coulometer Instructions**

**[75]** **V. Sokolov, "Moisture equilibrium and moisture migration within transformer insulation systems", CIGRE, WG A2.03, 1998.**

**[76]** **R.Neimanis, R.Eriksson, R.Papazyan, "Diagnosis of Moisture in il/Paper Distribution Cables—Part II: Water Penetration in Cable nsulation–Experiment and Modeling", IEEE Trans. on Pow. Del., Vol. 19. Iss. 1, pp. 15-20, 2004.**

**[77]** **Werelius, "Power Cable Diagnostics by Dielectric Spectroscopy", IEEE Pow. Eng. Soc. Winter Meeting, Vol. 3, pp. 1599-1603, 2000.**

**[78]** **Gubanski et al., "Methods for diagnostics of power transformers", CIGRE, TF D1.01.09, 2000.**

**[79]** **Lars E. Lundgaard, "Aging of Oil-Impregnated Paper in Power Transformers" IEEE Trans. on Pow. Del., Vol. 9, Iss. 1, pp. 230-239, 2004.**

**[80]** **` Review: Kinetics and mechanisms of the low-temperature degradation of cellulose A. M. EMSLEY, 1994.**

**[81]** **H. Ding D. Wang, "On the degradation evolution equations of cellulose" Cellulose, 2008.**

**[82]** **A.M. Emsley et al., "Degradation of cellulosic insulation in power transformers. Part 3:effects of oxygen and water on ageing in oil" IEE Proc. – Sc. Tech. and Meas. 2000, Vol. 147, Iss. 3, pp. 115-119, 2000.**

## Acknowledgements

**I would especially like to thank my supervisor dr. Morshuis for his enthusiasm and commitment to this thesis project. He always made time to discuss my work and for this I am grateful.**

**Furthermore, I would like to thank the rest of the staff at HCPS. A special note of thanks must go to Mr. Naagen, ing. Van Nes and Mr. van der Graff with whom I had daily contact. The jovial atmospehere around the laboratory made it a pleasure to complete my graduation project there.**

**Also, I would like to thank Mr. Cichecki for advice he gave me and Mr. Andritsch for the many times he helped me with test equipment. To those mentioned and to the remainder of the staff, I wish you all success in your future endeavors.**